Evaluation of Stress in Concrete using Ultrasonic Waves

A Thesis

presented to

the Faculty of the Graduate School

at the University of Missouri-Columbia

In Partial Fulfillment

of the Requirements for the Degree

Master of Science

---

by

Damien Stone

Dr. Sarah Orton, Thesis Supervisor

December 2018

The undersigned, appointed by the dean of the Graduate School, have examined the Thesis entitled

EVALUATION OF STRESS IN CONCRETE
USING ULTRASOINC WAVES

presented by Damien Stone,

a candidate for the degree of Master of Science
and hereby certify that, in their opinion, it is worthy of acceptance

_____

Professor Sarah Orton

_____

Professor Glenn Washer

_____

Professor Ahmed Sherif El-Gizawy

Dedication

I would like to dedicate this thesis to my parents. My father, Ryan was the sole reason I found interest in Civil Engineering by working construction with him as a young kid. He still helps me to look at the bigger picture in both my career and my life. My mother, Sammi whose continuous love and guidance are with me in whatever I pursue. She is the sole reason that I continued my education and have finished this thesis. Thank you and I love you both very much.

Acknowledgements

This work would never have been possible without the guidance and the many hours spent looking over the data had it not been for my advisor and mentor, Associate Professor Sarah Orton in the Civil Engineering department. It is because of her I found this topic interesting as an undergraduate while doing honors research. And from there I continued to further develop this topic into this thesis. I can't thank you enough for all your work and knowledge you've shared with me during my time at Mizzou. I would also like to thank Professor Glenn Washer in the Civil Engineering department for his knowledge of ultrasonic testing and further reviewing of the test data because without his help this thesis would not have been possible. I also want to thank him for allowing the use of his ultrasonic equipment. I want to thank Ahmed Al-Zuheriy, candidate of Doctor of Science in Civil Engineering, for helping on this topic while I was an undergraduate and graduate. If it wasn't for Ahmed and his kindness to always answer any questions and teach me to use the ultrasonic equipment, then I wouldn't have enjoyed pursuing this topic. Another student I would like to thank is Menghao Wu, candidate of Bachelor of Science in Civil Engineering, for helping conduct additional ultrasonic testing during the summer and fall semesters. A small thank you goes to all my friends who have encouraged me to never give up and always strive to achieve my goals as a student.

Table of Contents

Acknowledgements ii

List of Figures vi

List of Tables x

Abstract xi

Chapter 1 Introduction 1

1.1 Objectives 1

1.2 Scope of work 1

1.2.1 Application 2

1.3 Motivational Example 2

Chapter 2 Background 6

2.1 Existing Nondestructive Testing methods 6

2.1.1 Penetration method 6

2.1.2 Schmidt Rebound Hammer Method 9

2.1.3 Pull-Out-Test method 12

2.1.4 Radiographic method 14

2.1.5 Impact echo 16

2.1.6 Ultrasonic Pulse Velocity 18

2.2 Ultrasonic background 28

2.2.1 Acoustoelastic Effect 30

2.3 Previous research in ultrasonic stress determination in concrete 33

2.3.1 Schumacher, Chen, Ozturk, and Attoh-Okine (2013) 37
2.3.2 Shokouhi, Zoëga, and Wiggenhauser (2010) 38
2.3.3 Shah, Ribakov, and Zhang (2013) 40
2.3.4 Hazif and Schumacher (2018) 42
Chapter 3 Procedure 44
3.1 Ultrasonic equipment 44
3.1.1 Oscilloscope 45
3.1.2 Transducers 46
3.1.3 Pulser-receiver 48
3.1.4 Specimen frame 49
3.1.5 Specimens 50
3.1.6 Loading levels 53
3.2 Laboratory testing 54
3.2.1 Reference specimens 55
3.2.2 Pulser-receiver settings 57
3.2.3 Oscilloscope settings 59
3.2.4 Transducer setup 60
Chapter 4 Results 63
4.1 Laboratory testing 63
4.1.1 Wave velocity 65

4.1.2 Time of Flight 66

4.1.3 Frequency harmonics 69

4.2 Overall concrete condition 73

4.2.1 Concrete quality 74

4.2.2 Strength determination 74

Chapter 5 Conclusions 75

5.1 Time of Flight (TOF) 75

5.2 Frequency harmonics 76

5.3 Concrete quality 76

5.4 Concrete strength 77

5.5 Future Research 77

References 78

Appendix A: Wave form data A-1

Appendix B: Frequency plots B-1

List of Figures

Figure 1-1 Proposed pedestrian bridge design [1] 4
Figure 1-2 Full collapse of the main bridge segment [1] 4
Figure 1-3 Cracking of truss member 11 after bridge placement [1] 5
Figure 1-4 Cracking two before bridge collapse [2] 5
Figure 2-1 Windsor probe equipment [4] 7
Figure 2-2 ASTM requirement for penetration testing in reinforced concrete [4] 8
Figure 2-3 Steel rod probe profile in concrete [4] 8
Figure 2-4 Internal operation of Schmidt Rebound Hammer [6] 10
Figure 2-5 ASTM representation of released hammer to measure rebound value [6] 11
Figure 2-6 Drilled pull out test method [7] 13
Figure 2-7 Gamma ray passing through voided regions [9] 15
Figure 2-8 Two methods that comply with ASTM (A) measures time required for P-wave to travel between transducers and (B) measures frequency which the P-wave is reflected between the parallel (opposite) surfaces [11] 17
Figure 2-9 Transmitter and receiver sensor alignment paths [12] 19
Figure 2-10 Cross section of (A) vertical crack depth approximation and cross section of (B) horizontal crack depth approximation [16] 27
Figure 2-11 P, S, and R-wave behavior in homogenous material 29
Figure 2-12 Ultrasonic Waves in a homogenous medium [22] 30
Figure 2-13 Lillamand, Chaix, Ploix, and Garnier transducer layout and axis of study [25] 32
Figure 2-14 Wave transform with shear transducers both in the parallel (23) and perpendicular (21) direction to applied stress [22] 38
Figure 2-15 Surface velocities for loading and unloading [23] 40
Figure 2-16 FFT analysis with w/c of 0.4 at (a) 0% damage and (e) 80% damage [27] 41
Figure 2-17 Waveform plot (a) with zoomed windows for TOF (b) and coda wave (c) analysis [28] 43
Figure 2-18 MSC vs normal stress (a) P1 λ=66 mm (2.61 in), (b) P1 λ=36 mm (1.41 in), and (C) P2, λ=36 mm (1.41 in) [28] 43
Figure 3-1 Overall setup of ultrasonic testing equipment 45

Figure 3-2 Hewlett Packard oscilloscope 46
Figure 3-3 Pressure wave transducers used for testing [21] 47
Figure 3-4 Panametrics pulser-receiver 49
Figure 3-5 PVC polymer material to hold transducers on concrete surface 50
Figure 3-6 Stress and strain of Batch 1 51
Figure 3-7 Stress and strain of Batch 2 51
Figure 3-8 Stress and strain of Batch 3 52
Figure 3-9 Concrete specimens [21] 53
Figure 3-10 Wet specimen being soaked for 3 weeks 53
Figure 3-11 Loading and unloading stages 54
Figure 3-12 Data acquisition for lab testing [22] 55
Figure 3-13 Polypropylene plastic specimen for wave velocity reference (D=2.5, H=4) 56
Figure 3-14 Steel cylinder specimen for wave velocity reference (D=6, H=4) 56
Figure 3-15 FFT of waveform through steel sample (100 kHz transducer, 250 kHz receiver) 57
Figure 3-16 Data acquisition setup 60
Figure 3-17 Depiction of single transducer use [14] 61
Figure 4-1 Ultrasonic wave depicting P and S-wave initiation (a), compression wave traveling faster than shear, (c) compression wave beginning refraction, and compression fully refracted back to source (d) [22] 64
Figure 4-2 Change in TOF on wet 8 specimen (a) and wet 9 specimen (b) at 400V 68
Figure 4-3 Change in TOF on wet 8 specimen (a) and wet 9 specimen (b) at 900V 69
Figure 4-4 Specimen 8 amplitude change at different loading level 400V 72
Figure 4-5 Specimen 9 amplitude change at different loading level 400V 72
Figure 4-6 Specimen 9 amplitude change at different loading level 900V 73
Figure A-1 Specimen 8 wet 400V A-1
Figure A-3 Specimen 8 wet 900V A-2
Figure A-4 Specimen 9 wet 900V A-2
Figure A-5 Unloaded polypropylene reference specimen with 200V amplitude A-3
Figure A-6 Unloaded steel reference specimen with 200V amplitude A-3
Figure A-7 Specimen 1 unloaded waveform with 200V amplitude A-4
Figure A-8 Specimen 1 1oaded waveform with 200V amplitude A-4

Figure A-9 Specimen 1 unloaded waveform with 400V amplitude A-5
Figure A-10 Specimen 1 loaded waveform with 400V amplitude A-5
Figure A-11 Specimen 2 unloaded waveform with 200V amplitude A-6
Figure A-12 Specimen 2 1oaded waveform with 200V amplitude A-6
Figure A-13 Specimen 2 unloaded waveform with 400V amplitude A-7
Figure A-14 Specimen 2 loaded waveform with 400V amplitude A-7
Figure A-15 Specimen 3 unloaded waveform with 200V amplitude A-8
Figure A-16 Specimen 3 1oaded waveform with 200V amplitude A-8
Figure A-17 Specimen 3 unloaded waveform with 400V amplitude A-9
Figure A-18 Specimen 3 loaded waveform with 400V amplitude A-9
Figure A-19 Specimen 4 unloaded waveform with 200V amplitude A-10
Figure A-20 Specimen 4 1oaded waveform with 200V amplitude A-10
Figure A-21 Specimen 4 unloaded waveform with 400V amplitude A-11
Figure A-22 Specimen 4 loaded waveform with 400V amplitude A-11
Figure A-23 Specimen 5 unloaded waveform with 200V amplitude A-12
Figure A-24 Specimen 5 1oaded waveform with 200V amplitude A-12
Figure A-25 Specimen 5 unloaded waveform with 400V amplitude A-13
Figure A-26 Specimen 5 loaded waveform with 400V amplitude A-13
Figure A-27 Specimen 6 unloaded waveform with 200V amplitude A-14
Figure A-28 Specimen 6 1oaded waveform with 200V amplitude A-14
Figure A-29 Specimen 6 unloaded waveform with 400V amplitude A-15
Figure A-30 Specimen 6 loaded waveform with 400V amplitude A-15
Figure B-1 Specimen 7 wet 900V B-1
Figure B-2 Specimen 8 wet 400V B-1
Figure B-3 Specimen 9 wet 400V B-2
Figure B-4 Specimen 8 wet 900V B-2
Figure B-5 Specimen 9 wet 900V B-3
Figure B-6 Unloaded steel reference specimen 200V B-3
Figure B-7 Unloaded polypropylene reference specimen 200V B-4
Figure B-8 Specimen 1 200V unloaded amplitude vs frequency B-4
Figure B-9 Specimen 1 200V loaded amplitude vs frequency B-5

Figure B-10 Specimen 1 400V unloaded amplitude vs frequency B-5
Figure B-11 Specimen 1 400V loaded amplitude vs frequency B-6
Figure B-12 Specimen 2 200V unloaded amplitude vs frequency B-6
Figure B-13 Specimen 2 Mix 3 200V loaded amplitude vs frequency..... B-7
Figure B-14 Specimen 2 400V unloaded amplitude vs frequency B-7
Figure B-15 Specimen 2 400V loaded amplitude vs frequency B-8
Figure B-16 Specimen 3 200V unloaded amplitude vs frequency B-8
Figure B-17 Specimen 3 200V loaded amplitude vs frequency B-9
Figure B-18 Specimen 3 400V unloaded amplitude vs frequency B-9
Figure B-19 Specimen 3 400V loaded amplitude vs frequency B-10
Figure B-20 Specimen 4 200V unloaded amplitude vs frequency B-10
Figure B-21 Specimen 4 200V loaded amplitude vs frequency B-11
Figure B-22 Specimen 4 400V unloaded amplitude vs frequency B-11
Figure B-23 Specimen 4 400V loaded amplitude vs frequency B-12
Figure B-24 Specimen 5 200V unloaded amplitude vs frequency B-12
Figure B-25 Specimen 5 200V loaded amplitude vs frequency B-13
Figure B-26 Specimen 5 400V unloaded amplitude vs frequency B-13
Figure B-27 Specimen 5 400V loaded amplitude vs frequency B-14

List of Tables

Table 2-1 Direct and semi-direct velocity rating comparison to concrete quality 22
Table 2-2 Indirect velocity rating comparison to concrete quality 22
Table 2-3 Temperature effect on ultrasonic pulse velocity 23
Table 2-4 Reported research pulse velocity limits 23
Table 2-5 Comparison of ultrasonic versus dynamic modulus [18] 25
Table 2-6 Ultrasonic wave types [20] 28
Table 4-1 Prism reference name 64
Table 4-2 Wave velocity from unloaded wet specimens 65
Table 4-3 Wave velocity from loaded wet specimens 66
Table 4-4 Specimen 8 400V amplitude difference 70
Table 4-5 Specimen 9 400V amplitude difference 71
Table 4-6 Specimen 9 900V amplitude difference 71
Table 4-7 Strength calculation using Jones P-wave velocity equation 74

Abstract

This research investigates the use of ultrasonic waves to evaluate the stress and damage in concrete. Tests were conducted on 6 in. x 6 in. x 12 in. plain concrete specimens (f ’c = 6,000psi) at different loading stages that include 20, 40, 60, and 80% of the concrete compressive strength. Unloading at each stage was also recorded to evaluate the damage in the concrete structure. Use of higher amplitude waves were used to trigger nonlinear ultrasonic behavior. Various voltage amplitudes were used in this research at various loading stages, which included 200, 400, and 900V. The data showed a difference in wave velocity (time of flight), amplitudes, and frequency components. The time of flight (TOF) increased in a linear fashion with increased damage (previous load level). However, load on the specimen (at low level of load) decreased the time of flight readings. The amplitudes of higher frequency harmonics of waveforms decreased with damage and load level. However, both the slope of the TOFs and harmonic amplitudes with load level were not the same for the specimens tested making determination of a constant to evaluate stress in concrete difficult.

Chapter 1 Introduction

This chapter will help to describe the objectives of this research project and possible applications.

1.1 Objectives

The goal of this research is to further understand the behavior of ultrasonic waves traveling through for non-reinforced concrete elements. The objective of the research is to determine which wave characteristics can be related to the load level (stress) or damage (caused by micro-cracking due to previous loading) in the concrete such that evaluation of stress and damage can be conducted in the field. The wave characteristics analyzed include:

- Changes in TOF readings with load level (stress) in the concrete member
- Changes in TOF readings with damage in the concrete member
- Changes in amplitudes of higher harmonics in frequency spectra of the waveform with load level (stress) in the concrete member
- Changes in amplitudes of higher harmonics in frequency spectra with damage in the concrete member

1.2 Scope of work

The scope of the topic is to understand the behavior of ultrasonic waves in the concrete at different loading and un-loading levels. The loading levels consist of zero, twenty, forty, sixty, and eighty percent of the compressive strength. The unloading levels consist of a return to zero load after a previous load level. This will allow investigation

into the changes in wave characteristics caused by damage due to micro-cracking from the previous load level. Ultrasonic evaluation of the concrete is accomplished by using an ultrasonic transducer and receiver connected an oscilloscope to record wave amplitude versus time data. The data is analyzed to determine changes in the TOF and frequency spectra amplitudes with loading level and damage in the concrete.

1.2.1 Application

Analysis of ultrasonic wave's characteristics in concrete can be used for inspection of buildings, parking structures, and bridges. If a technique could be developed that could relate the wave characteristics to the actual state of stress that the element was under or the damage level in the concrete (previous level of stress), then information from structural evaluations could provide definitive data on the condition of the structure. These data could be used to support decision making regarding retrofit and repair of damaged structures.

1.3 Motivational Example

A possible example of where ultrasonic stress data could be valuable is the collapse of the Florida International University walkway. On March 15th, 2018 at 1:30 PM the pedestrian bridge over the US 41 (Tamiami Trail/8th Street) at the Florida International University collapsed resulting in six fatalities merely five days after placement on March 10th by the Munilla Construction Management company [1]. The proposed design and aftermath of the collapse are pictured in Figure 1-1and Figure 1-2.

The purpose of this pedestrian bridge was to connect the university campus to the neighboring city of Sweetwater, where many students and faculty members had residency. The two-span post tensioned cable pedestrian bridge, with a main span of 174 feet, began

construction in late 2017 for the design traffic of 5,000 ~ 6,000 pedestrians to safely cross over the 7-lane highway [1].

Preliminary inspection after on-site fabrication revealed a macro crack along with other micro cracks in a critical truss member connecting into the deck. After the collapse of the bridge, three independent engineers examined the photos, records, and design drawings where the cracking occurred, and they all agreed that the crack was a big concern for the structure. Refer to Error! Reference source not found.Error! Reference source not found. for the direction and sizing of the crack.

Speculations arose for plausible causes of the cracking, which included overstressing wire strands, improper material construction, inadequate loading from the gantry cranes while moving the bridge into place. Continuing structural investigation is being conducted by FDOT, State Transportation officials, and other private investigators to determine the cause/s for the catastrophic failure. Current explanation for the cause of the collapse is based on the design truss member No. 11, which was found to be under-designed and not strong enough to withstand loading from the dead weight of the bridge itself [1].

Figure 1-1 Proposed pedestrian bridge design [1]

Figure 1-2 Full collapse of the main bridge segment [1]

Use of ultrasonic testing that could evaluate the stress level or damage in the concrete could have identified the over load in the truss member, possible defects, or damage in the concrete. With this knowledge, the post-tensioning operation could have been halted and the bridge repaired prior to the collapse.

Figure 1-3 Cracking of truss member 11 after bridge placement [1]

Figure 1-4 Cracking two before bridge collapse [2]

Chapter 2 Background

Physical inspection of concrete on the surface doesn't guarantee the internal condition will also match. As a result, NDT has become more important for inspections of concrete materials. Over the years many different methods have been developed and are used to evaluate the concrete condition. This chapter will help to define the different types of NDT that have been used for crack detection or strength evaluation of concrete.

2.1 Existing Nondestructive Testing methods

Current methods for NDT in concrete include some invasive measurements, while other tests only negligibly disturb the surface of the concrete. These methods include: Penetration resistance method, Schmidt rebound hammer method, Pull out test method, Radiographic method, Impact echo, and Ultrasonic pulse velocity. All of these methods are currently used for research and current practice uses.

2.1.1 Penetration method

Penetration testing, also known as probe testing, is a gun that requires a small powder cartridge (32 caliber) to shoot a steel rod into the concrete [2]. Data measurement from the test are based on the remaining length of steel rod that is protruding out of the concrete surface, which is measured electronically. The use of this method is to measure the compressive strength of concrete in the localized area of interest. In some circumstances the penetration method is used on a damaged or spalling area for evaluation,

or the testing can be completed on a normal area routinely for inspection purposes. The testing equipment for the penetration method is list in Figure 2-1.

Figure 2-1 Windsor probe equipment [3]

For accurate measurements and proper procedures, the penetrating method uses the American Society for Testing and Materials (ASTM) C803 or C803M standard [3]. The required equipment for following ASTM standards is properly labeled in Figure 2-1 are as follows. The probes, labelled as C, are the specific hardened alloy steel rods that are shot into the concrete surface. When the power driver or gun is used, labelled A, to fire the rods into the surface. Once the rod has penetrated the surface the template is removed, and a gauge plate is threaded onto the rod for a level depth measurement, labelled D. The electronic measuring device, labelled as B, measures precise depth and reports the value which is then correlated with Windsor Probe strength figures or tables [4].

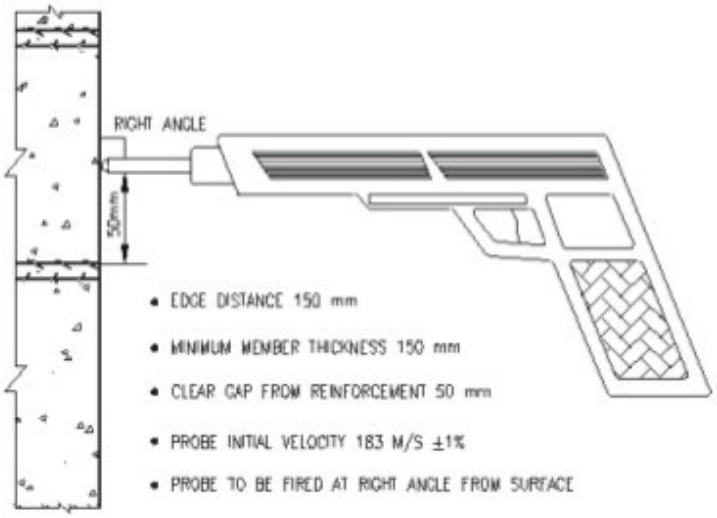

Figure 2-2 ASTM requirement for penetration testing in reinforced concrete [3]

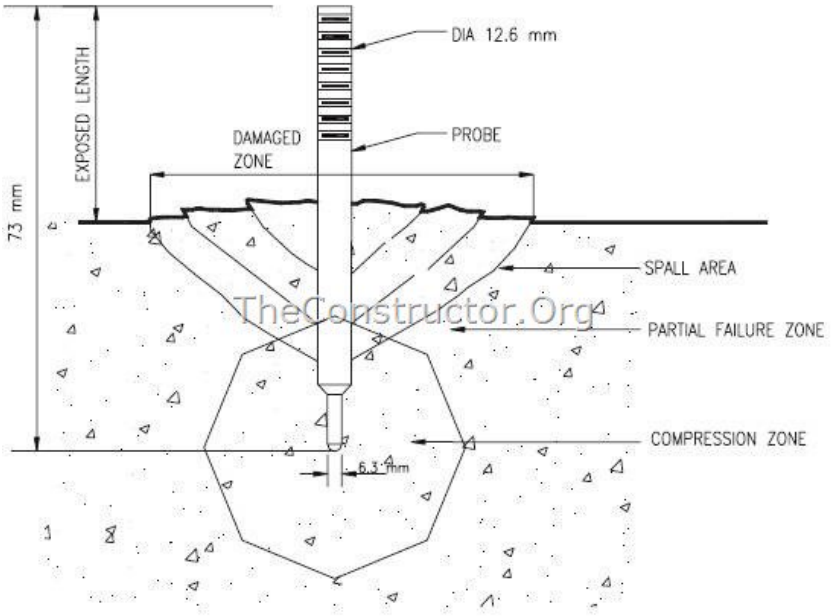

Figure 2-3 Steel rod probe profile in concrete [3]

Based on the testing, there are some advantages and limitations for using this NDT method. The advantages of this method include:

- Simple setup, cost effective, requires little maintenance, durable equipment and requires little training or experience to use [2].

The disadvantages of the penetration method include:

- Explosion hazard if proper charge isn't used, measures compressive strength near the surface, requires frequent calibration, leaves remaining void in concrete and may result in additional cracking/spalling in the area [2].

2.1.2 Schmidt Rebound Hammer Method

The Schmidt Rebound Hammer, also known as Swiss Rebound Hammer, consists of a steel rod attached to a spring which is all housed inside a tube frame. Data collected by a technician is achieved by pressing the front plunger against a smooth surface, then the steel weight will compress the spring to a certain length. When the spring reaches the max limit, it will let the weight inside slide to rebound on the surface. After all the previous steps have occurred the value, from 0 to 100, on the rebound chart is recorded. The number recorded from the chart is then correlated to a line graph to estimate the compressive strength of concrete [2]. This testing is also assessing the compressive strength in a localized area of interest, whether the area is damaged or not. A detailed diagram depicting the rebound hammer, pictured in Figure 2-4, shows each internal component that will record the rebound number.

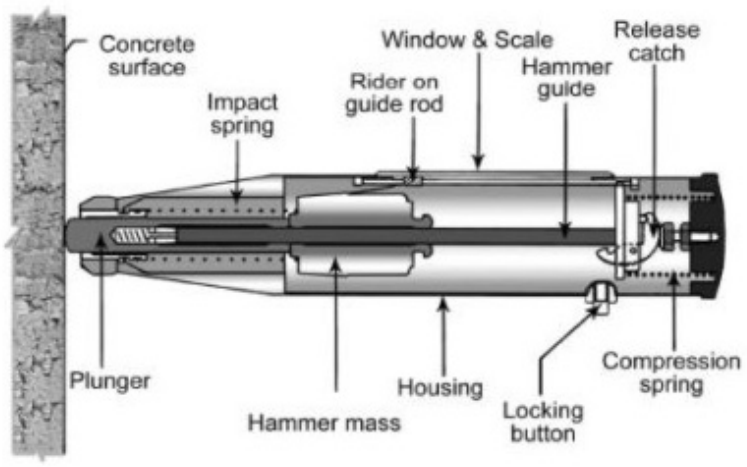

Figure 2-4 Internal operation of Schmidt Rebound Hammer [5]

To comply with standard procedures and record adequate measurements, the Schmidt Rebound Hammer method uses the ASTM C805 or C805M standard for proper testing [5]. ASTM has many requirements when testing on surface conditions for rebound numbers. When testing an individual should avoid damaged areas, such as scaling or honeycombs, and test on a smooth finished area that hasn't been broom finished. If such areas can't be used, then the surface must be sanded until smooth and flat. At each location, a desired 10 readings should be taken if readings are off by six units, then discard that specific reading. Lastly, concrete should not be tested if surface temperature is less than or equal to 32 degree Fahrenheit because rebound values will be much larger.

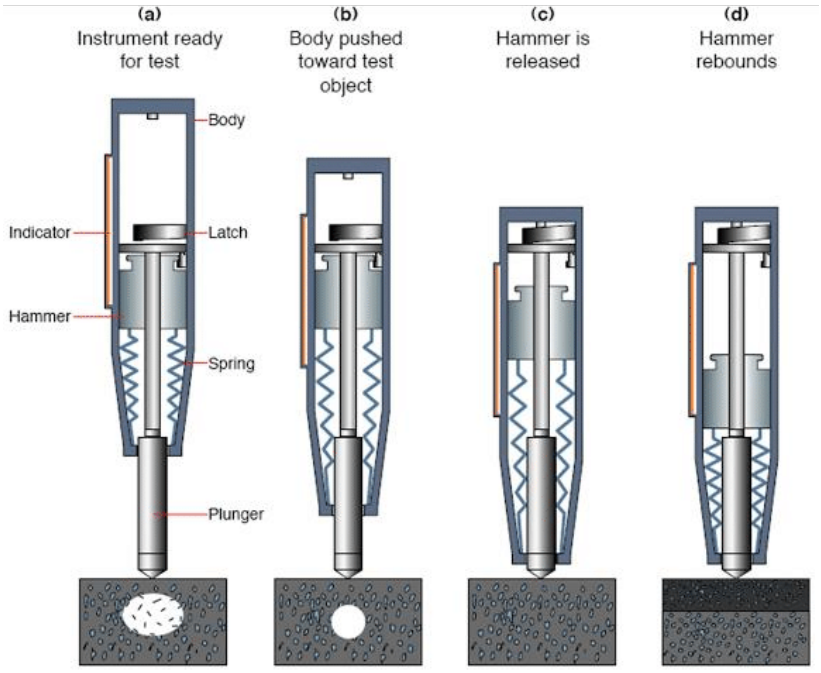

Figure 2-5 ASTM representation of released hammer to measure rebound value [5]

The Schmidt Rebound Hammer also has its advantages and disadvantages for testing. The disadvantages of this method include:

- Smooth surface condition, inaccurate for thin concrete elements, high concrete moisture content leads to inaccurate data, equipment can cost $1,000 or more, aggregate types may skew rebound values, and measures compressive strength on the surface [2].

The advantages of this testing include:

- Simple to use, fast data collection, and little training needed to operate the device [2].

2.1.3 Pull-Out-Test method

The Pull-Out-Test, also referred to as cast-in-place pull out, is a simple testing procedure that involves pulling a steel rod out of the concrete to estimate the compressive strength of the concrete. The steel rod, with an enlarged bottom plate, is placed while the concrete is still workable and allowed to bond together. The tool used to pull the rod is usually a hollowed ram that is hand operated. The tension data collected from the test is divided by the conical area of the pull out region and is compared to the design compressive strength. The two values are divided to create a ratio roughly from 0.1 to 0.3 [2]. Once the ratio is concluded, a comparison is used from graphs or tables to determine a current compressive value of the concrete.

To comply with standard procedures and record adequate measurements, the Pull-Out-Test method uses the ASTM C900 or C900M standard for proper testing [6]. Pull-Out-Test may also be completed after the concrete has set and hardened by drilling and creating a grooved section, stages of the test can be seen in Figure 2-6.

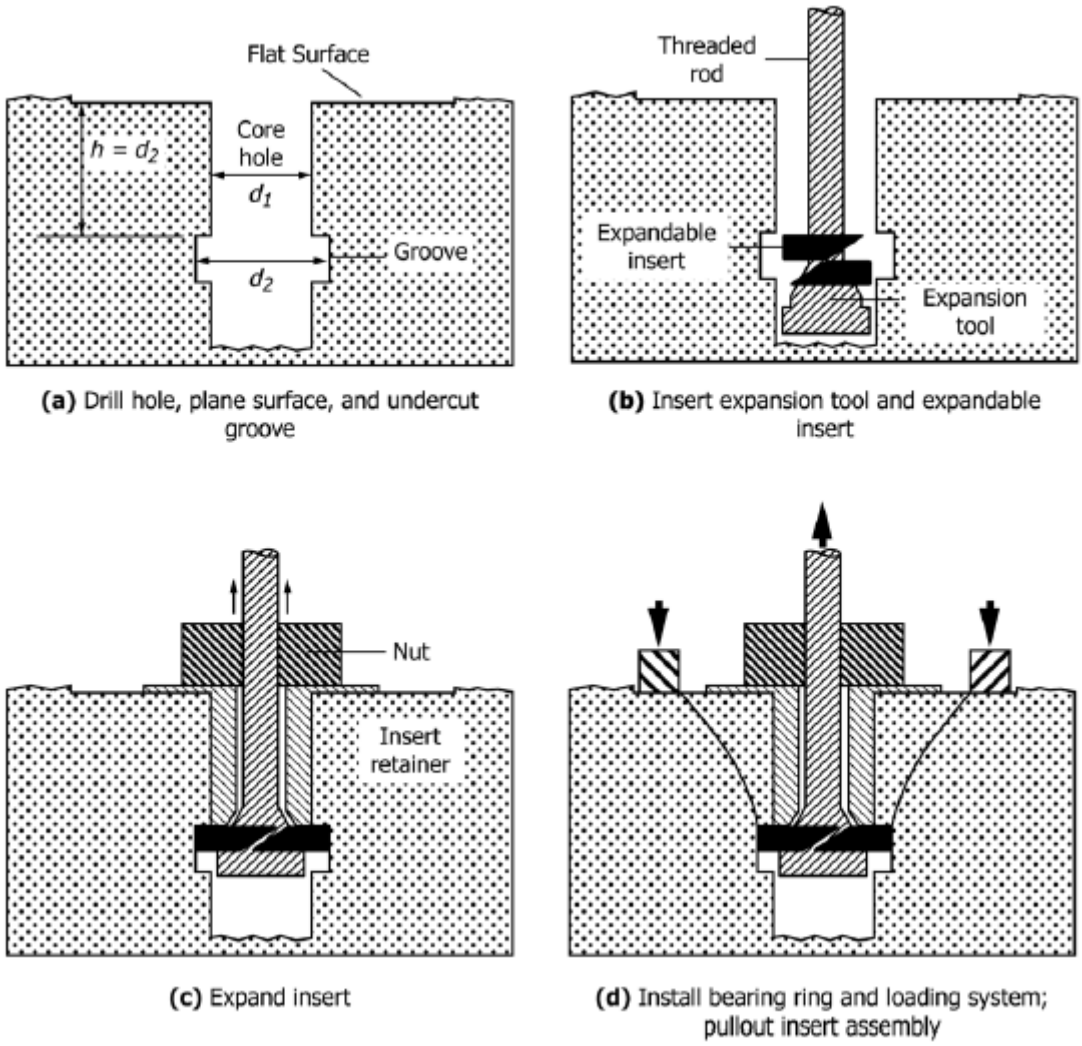

Figure 2-6 Drilled pull out test method [6]

The surface conditions for this test must also be smooth and not on a broom finish, if no smooth surface can be located, then sanding or grinding of the area is acceptable. When all procedures are completed, and the test has resulted in a max load value on the pressure gauge the stress in the concrete is found by using an empirical equation within the ASTM standard. The equation relates the load over the conical area of the pulled out section, which is then multiplied with the angle produced by the conical shape.

The disadvantages of this method include:

- Destructive test compared to the other nondestructive methods, varying expense cost for tests $1,000 to $6,000, spalling or removal of conical area in concrete, scheduling where to place the rods while concrete is being poured [2].

The advantages of this testing include:

- Testing internal or surface strength, measures strength by comparison of shear and tensile forces, and the coefficient of variation correlated to compressive strengths are 0.97 to 0.99 [2].

2.1.4 Radiographic method

Radiography, typically, incorporates the use of gamma ray or x-rays. This method utilizes radiation that passes through the member. The intensity is reduced according to the thickness, density and absorption characteristics of the materials within the member. The quantity of radiation passing through the member is recorded on X-ray film. [7]. Sources to create the gamma radiation vary but common elements are Iridium 192, Cesium 137, and Cobalt 60. Determination of voids, cracks, or other anomalies are achieved by placing a photographic detector film beneath or opposite side of the gamma ray source. Any imperfection in the concrete is printed out on the film, for example a crack somewhere in the concrete will show up as a black or light outline on the film. Whereas, if the gamma ray crossed a piece of rebar the film would display a lighter blackened outline because the rays attenuate more through steel than voids. A simple diagram depicting the gamma rays passing through a voided area within the concrete can be seen in Figure 2-7.

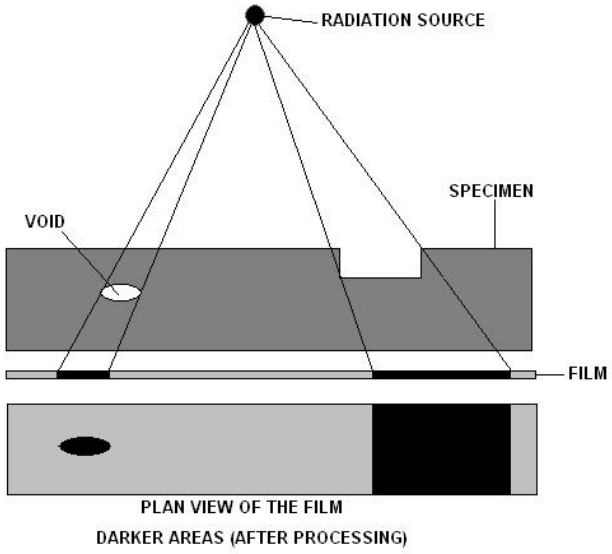

Figure 2-7 Gamma ray passing through voided regions [8]

To comply with standard procedures and record adequate measurements, the radiographic method uses the ASTM E94 or E94M standard for proper testing [8]. This type of testing requires that both sides of the concrete be accessed, so typically only walls or slabs are inspected with this method. Surface conditions are not a big concern for this radiography testing. The imaging camera, or the point where gamma rays are expelled, is above the concrete surface area known as the focus to object distance. On the other side of the concrete is where the radiographic film is placed along with a metallic or aluminum foil to catch/ limit the back scatter of the radiation. ASTM requires that a metallic plate, usually lead is, placed over top of the area of interest with an ID number or location number [8]. After some time, the image is printed on the film of any possible defects and will be further investigated.

The advantages of this method include:

- Locating delamination's in the concrete as well as rebar layout, portable setup, and good accuracy [7].

The disadvantages of this method include:

- Hazardous exposure to the possible radiation, well-trained and highly qualified technician, varying cost with the different use of isotope Cobalt 60, Iridium 192, and Cesium 137 [7].

2.1.5 Impact echo

This method is analyzed by producing a stress induced wave into the concrete. To accomplish this testing a transducer or mechanical impact device creates the stress wave. As the wave travels through concrete it can be reflected by any cracks, voids, honeycombing, or reinforcement. There are two possible setups to use for this type of inspection work. The first setup uses a transducer and mechanical hammer device to determine these delaminations. This option may be used with a computer or other acquisition device to record and save testing data. The second additional option uses an impact scanning device that rolls along the concrete surface to inspect more area in less time [9].

To comply with standard procedures and record adequate measurements, the Acoustic impact method uses the ASTM C1383 or C1383M for proper testing [10]. The standard has two distinct methods for measuring P-wave velocity in concrete specimens. The first method, entails measuring the time it takes for the P-wave generated to travel

between two transducers that are positioned at a known distance apart along the surface of the concrete. The second method requires measurement of the frequency which the P-wave impact is reflected between the parallel surfaces of a concrete. Surface preparation is required for this testing because sound waves can't travel effectively through if the transducer doesn't have full contact with the surface. Spacing of transducers and the distance where the impact is introduced is detailed in Figure 2-8.

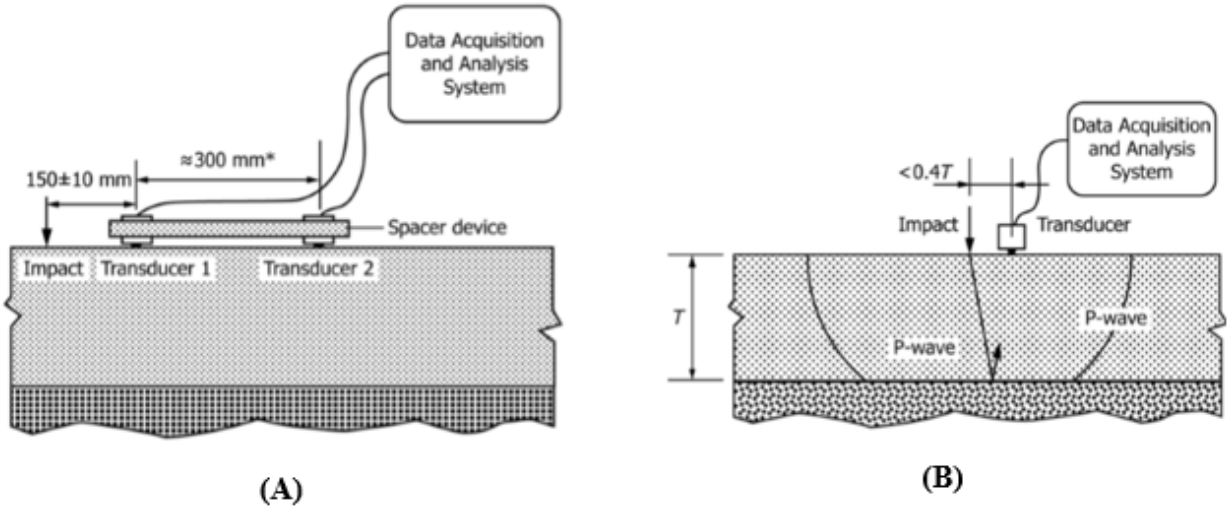

Figure 2-8 Two methods that comply with ASTM (A) measures time required for P-wave to travel between transducers and (B) measures frequency which the P-wave is reflected between the parallel (opposite) surfaces [10]

The advantages of this method include:

- Easily transported to any site for investigation, accuracy is good, and if scanner is used this saves time on inspections [9].

The disadvantages of this method include:

- Requires a skilled technician or experience, cost for equipment, not accurate for small concrete elements [9].

2.1.6 Ultrasonic Pulse Velocity

This method has been the most universally accepted testing procedure in both the field, as well as in research development for over 40 years. This method works by creating an ultrasonic sound wave in the concrete material and measuring how long the time that the wave took to travel from one transducer to another. Depending on the density and the elastic properties of the concrete, velocity waves can vary. While using this testing method, geometry properties of the concrete are considered negligible, so whether testing a specimen in the short or long direction assuming the concrete is isotropic in all directions the sound wave should travel the same speed [2]. When this ultrasonic wave comes across any discontinuity, the wave will take more time to travel around the impurity, which tell the technician the condition of the concrete is not as good. If this discontinuity is large enough, such as a crack, the wave will not pass through the concrete material at all. This method has also been used to estimate the compressive strength of the concrete by using the penetrating velocity, but after attempts it's not as reliable as using the velocity rating to determine the condition of the concrete. Different transducer orientations can be seen in Figure 2-9.

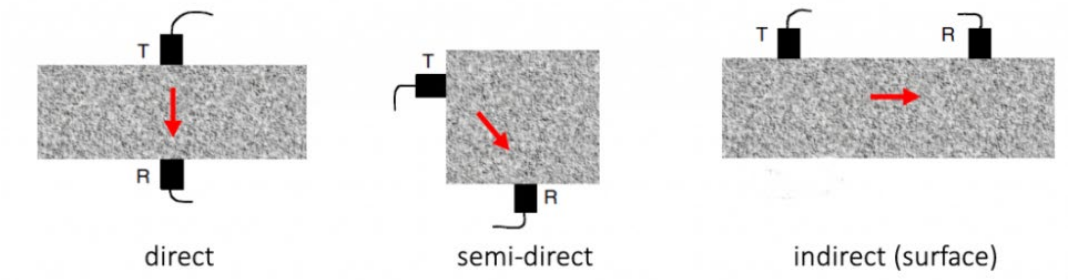

Figure 2-9 Transmitter and receiver sensor alignment paths [11]

Ultrasonic Pulse Velocity is conducted using two transducers, typically piezoelectric transducers, which are in direct contact. This type of contact means both transducers are on opposite sides of the piece of structural concrete. Some cases require other transducer orientations because all faces of the concrete are not available. An indirect orientation would mean only one face is available to perform testing on, such as a bridge deck. A semi-direct orientation has more than one face exposed to place the transducers on, an example of this would be used on an abutment. Both types of testing may produce inaccuracies, so if possible, use the direct orientation for best results, and refer to

Figure 2-9 for transducer orientation. The transducers produce the ultrasonic waves by exciting the crystals within them with an electric voltage from a trigger unit. From this action the transducer will cause a vibration that will travel into the material at the rated amplitude. When travelling through concrete the wave will encounter different types of material that may slow the velocity or not allow the wave to travel through the concrete. Cracks, aggregate, or air voids can be the causes that can disrupt the wave. Steel is considered homogenous when compared to concrete, so the wave will travel through faster, when testing a reinforced specimen consideration should be taken to orient the transducers away from the area with rebar.

To comply with standard procedures and record adequate measurements, the Acoustic impact method uses the American Society for Testing and Materials (ASTM) C597 or C597M standard for proper testing [11]. This standard requires that when conducting test on a concrete specimen that the smallest dimension should be greater than the wavelength. For example, if a transmitting frequency is at 100 kHz with a calculated wave velocity of 10,000 $\frac{\mathrm{m}}{\mathrm{s}}$ then the minimum thickness of the specimen should be 0.1 m to collect the refracted compression wave. ASTM notes that accurate data has been collected from minimum size of 2 in (50 mm) to maximum size of 50 in (15 m). Present in the apparatus a transmitting transducer shall have a resonant frequency in the range from 20 from 100 kHz.

The advantages of this method include:

- Reliable testing data determine the smallest impurities or defects in concrete, equipment can be easily portable, and wave penetration through deep sections of concrete [2].

The disadvantages of this method include:

- Surface conditions must be smooth, surface temperature below freezing, concrete moisture content can vary data, and reinforcement can cause an increase in wave velocity [2].

2.1.6.1 Concrete condition

With the determination of the ultrasonic pulse velocity, an individual can assess the overall quality of concrete in an area of interest. This inspection method usually will inspect

damaged, or deteriorating, areas because inspecting the non-damaged areas would not be cost effective. The direct orientation of transducers will yield a more accurate representation of the quality, but the Construction Diagnostic Centre (CDC) Company have developed tables depicting any configuration of transducer along with different grades of concrete. See Table 2-1 and Table 2-2 for reference [12]. There are many influences that may vary the accuracy of the ultrasonic pulse velocity. The impact of moisture content, aggregate type, water-to-cement ratio, reinforcement, and path length all have a direct effect on the ultrasonic waves in concrete. The CDC reports that early aged concrete can increase the pulse velocity by 2 ~ 10%. The influence of water-to-cement ratio can fluctuate the pulse velocity by the percentage change in the concrete strength. The CDC reports that steel has a pulse velocity around 19,300 ft/s (5.9 km/s) so depending on the orientation of the rebar it may have an impact. Concrete with rebar oriented parallel to the transducer face will vary the pulse velocity by 5 ~ 20%. The rebar with a perpendicular alignment can vary the pulse velocity by 1 ~ 5% [12]. If possible, it would be ideal to test concrete in a less reinforced area to collect accurate sets of data and to determine velocity of the wave the calculation follows:

$$V = \frac{L}{t} \qquad \text{Equation 2-1}$$

Where,

V = velocity $\frac{ft}{s}$ or $\frac{km}{s}$
L = distance between the transducers
t = time when the ultrasonic wave is read by the receiving transducer

2.1.6.1.1 Concrete quality

CDC is a consulting and construction material testing facility that specializes in non-destructive testing. Based on different types concrete design strengths, the company has been able to identify the quality of the concrete based on pulse velocities. Direct and semi-direct transducer orientation values are located in Table 2-1 and indirect orientation values are located in Table 2-2 [13].

Table 2-1 Direct and semi-direct velocity rating comparison to concrete quality

Gradation of Quality of concrete (as per CDC) - Direct & Semi Direct velocity, km/s			
Quality of concrete	Grade of concrete (MPa)		
	20 to 25	30 to 35	> 40
Excellent	More than 4.400	More than 4.600	More than 4.900
Good	3.750 to 4.400	3.900 to 4.600	4.150 to 4.900
Medium	3.400 to 3.750	3.600 to 3.900	3.800 to 4.150
Poor	Less than 3.400	Less than 3.600	Less than 3.800

Table 2-2 Indirect velocity rating comparison to concrete quality

Gradation of Quality of concrete (as per CDC) - Direct & Semi Direct velocity km/s			
Quality of concrete	Grade of concrete (MPa)		
	20 to 25	30 to 35	> 40
Excellent	More than 3.900	More than 4.100	More than 4.400
Good	3.250 to 3.900	3.400 to 4.100	3.650 to 4.400
Medium	2.900 to 3.250	3.100 to 3.400	3.300 to 3.650
Poor	Less than 2.900	Less than 3.100	Less than 3.300

Researchers have also reported temperature effects and varied ultrasonic pulse velocities. A Material Engineer, Kaushal Kishore, reports a temperature variation in both air dry and saturated concrete is evident. Table 2-3 indicates both Fahrenheit and Celsius

degree changes [14]. Malhotra reported to the ACI Monograph, his research velocities that correlated to the quality assessment of concrete in Table 2-4 [15]. Leslie and Chessman conclude pulse velocity values with the limit on excellent and very poor conditions, also labelled in Table 2-4 [16].

Table 2-3 Temperature effect on ultrasonic pulse velocity

Temperature		Correlation to the measured pulse velocity	
		Air dried concrete	Water saturated concrete
˚F	˚C	%	%
140	60	5	4
104	40	2	1.7
68	20	0	0
32	0	-0.5	-1
24.8	-4	-1.5	-7.5

Table 2-4 Reported research pulse velocity limits

Quality	Pulse Velocity	
	Malhotra, ft/s (km/s)	Leslie and Chessman, ft/s (km/s)
Excellent	> 15092 (4.6)	–
Good	12139 to 15092 (3.7 to 4.6)	> 16404 (5.0)
Fair/Medium	9843 to 12139 (3.0 to 3.7)	13123 to 16404 (4.0 to 5.0)
Poor	6890 to 9843 (2.1 to 3.0)	9843 to 13123 (3.0 to 4.0)
Very poor	< 6890 (2.1)	–

2.1.6.2.1 Concrete Strength

The strength determination is similar to the conditional assessment of concrete quality that uses the pulse velocity to correlate a quality rating. With the use of Jones Equation 2-2 through Equation 2-4 [17]. By the use of the equation, it is possible to solve in reverse to find the modulus, then by using the proper modulus equations from ACI 318 the strength in concrete can be concluded.

$$V_P = \sqrt{\frac{E(1-v)}{\rho(1+v)(1-2v)}} \quad \text{Equation 2-2}$$

$$V_S = \sqrt{\frac{E(1-v)}{2\rho(1+v)}} \quad \text{Equation 2-3}$$

$$V_R = \frac{0.87+1.12v}{1+v}\sqrt{\frac{E}{\rho} * \frac{1}{2(1+v)}} \quad \text{Equation 2-4}$$

Where,

E = Modulus of elasticity, psi (MPa)
v = poisons ratio for concrete 0.1 ~ 0.2
ρ = density of concrete $\frac{lb}{ft^3}$ ($\frac{kg}{m^3}$)

Based on a study conducted by Lee and Oh [18] to test reinforced concrete slabs, as well as prestressed slabs. Three slabs were tested with one being reinforced and the other prestressed, all having different spacing. Their reinforcement are as follows, transverse and longitudinal 13 mm diameter reinforcements with 560 mm spacing at 20 and 230 mm depths, respectively. Prestressed slab 2 and slab 3 in the x and y ways, respectively. Five 12.7 mm diameter strands with 350 mm spacing were applied in each direction [18]. In their research no transducer was applied parallel to the rebar because, like in Section

2.1.6.1.1 , this increases the pulse velocity which can over-estimate the present stress level. In their conclusion, measuring all three P, S, and R-waves the error estimates with the three slabs remained less than 13% [18]. Tabulated values can be seen in Table 2-5.

Table 2-5 Comparison of ultrasonic versus dynamic modulus [18]

Measurement	Slab	Ultrasonic test			Static test			Error
		Avg m/s	Edu* (GPa)	ν	fck** (Mpa)	E_c (GPa)	E_d (GPa)	
P-wave	S1	3285	22.80	0.16	14.84	17.68	21.30	7.01%
	S2	3367	23.96	0.16	14.84	17.68	21.30	12.46%
	S3	3362	23.88	0.16	14.84	17.68	21.30	12.09%
S-wave	S1	1910	22.67	0.16	14.84	17.68	21.30	6.43%
	S2	1960	23.87	0.16	14.84	17.68	21.30	12.07%
	S3	1950	23.63	0.16	14.84	17.68	21.30	10.93%
R-wave	S1	1880	22.55	0.16	14.84	17.68	21.30	5.86%
	S2	1934	23.87	0.16	14.84	17.68	21.30	12.06%
	S3	1918	23.46	0.16	14.84	17.68	21.30	10.15%

Edu*: dynamic modulus by ultrasonic test, fck**: 28-day compressive strength.

2.1.6.3 Crack depth/size

For some inspections, the goal is to determine if any internal defects or possibly determine how serve a crack might be within the concrete. To do so, a technician would setup the transducers in an indirect formation to observe any vertical and horizontal cracking. Based on concrete beam experiments conducted by Kumar and Santhanam, they were able to use equations to estimate the depth of a vertical and horizontal crack. For the determination of a vertical crack depth both transducers must be equally spaced from the crack, recommended “x” spacing should be 6 ~ 8 in. (150 ~ 200 mm) to satisfy Equation 2-5. The same spacing of “x” applies for the horizontal crack determination depth in Equation 2-6. Malhorta is credited for developing both equation for crack depth and size [15]. Both equations can be seen below.

$$h = \frac{x}{T_2}(T_1^2 - T_2^2)^2$$ Equation 2-5

$$y = 0.5\sqrt{V^2(T^2 - x^2)}$$ Equation 2-6

The vertical equation uses two different times within the equation where T_1 is characterized as the transmit time that it takes to get around the crack when using S-wave analysis, whereas T_2 is described as the transmit time along the surface of the concrete without any defects. To denote that the path length must be equal between T_1 and where T_2. To ensure that the crack is vertical from the surface a technician should have both traducers placed equally apart and begin to spread each transducer one at a time. If the TOF decreases, then it is evident that the crack angles in the direction of the transducer that was recently moved.

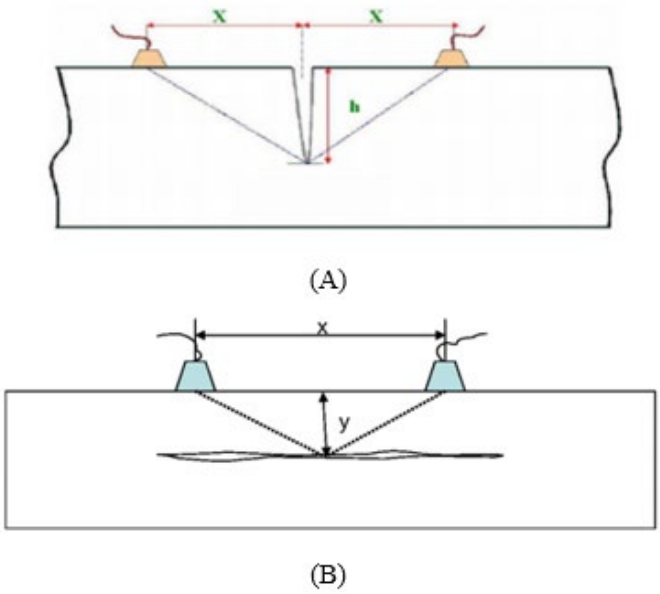

Figure 2-10 Cross section of (A) vertical crack depth approximation and cross section of (B) horizontal crack depth approximation [15]

Based on Kumar and Santhanam's study, they prefabricated the beams to have a horizontal void, to imitate a crack, at various depths in the four beams tested. Depths of each beam can be found in the paper. Some conclusions drawn from the testing showed that if the transducers are placed 4 ~ 8 in (100 ~ 200 mm) apart that this yields that best accuracy for the determination of crack depths. For example, beam 4 had a void placed at 75 cm from the surface and between the 100, 150, and 200 mm spacing, the estimated depth was 61.78, 80.08, and 85.58 cm. The error estimation at those transducer spacing's are as follows, 17.6, 6.8, and 14.1% [19]. These numbers can be wide-ranging depending on the elastic properties and density of the concrete.

2.2 Ultrasonic background

Ultrasonic waves travel at a frequency higher than that of human hearing (typically above 20 kHz). There are three main types of waves: P or compression waves, S or shear waves, and R or surface waves. Each wave type is described in Table 2-6. The travel of the waves through a homogenous medium is shown in Figure 2-12. However, concrete is not homogenous. The aggregate particles and micro-cracking in the concrete can create discontinuities that will disrupt the wave path and velocity. This research is attempting to determine which wave characteristics (after it has travelled through the concrete) can be used to evaluate the stress level or damage in the concrete.

Table 2-6 Ultrasonic wave types [20]

Dilatational Waves	Distortional Waves	Rayleigh Waves
Compression Waves	Shear Waves	Surface Waves
P - Waves	S - Waves	R- Waves
Parallel to particle motion	Perpendicular to particle motion	Propagates along surface of solid
Associated with normal stresses	Associated with shearing stresses	Particle motion is retrograde elliptical
Can propagates in all type of media	Can propagates only in media with shear stiffness, that is solid	–
11500 to 14800 ft/s (3.5 to 4.5 km/s)	6900 to 8900 ft/s (2.1 to 2.7 km/s)	5900 to 8200 ft/s (1.8 to 2.5 km/s)

Lee and Oh [18] discuss how the waves propagate through an elastic stress-free solid material, which is pictured in Figure 2-11. With concrete being non-homogenous, waves will behave very different due to varying aggregate size, air voids, and other possible defects.

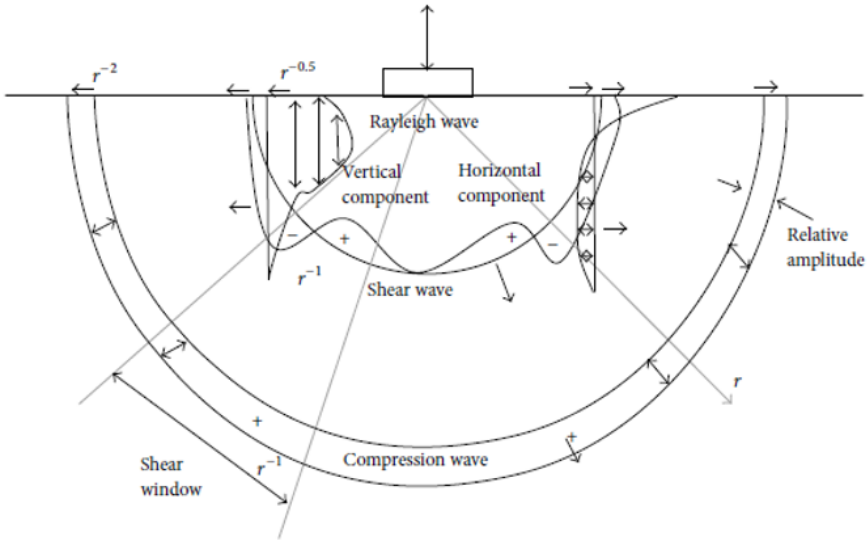

Figure 2-11 P, S, and R-wave behavior in homogenous material [18]

Lee and Oh report the velocity of P-waves can range between 11500 to 14800 $\frac{\text{ft}}{\text{s}}$ (3.5 to 4.5 $\frac{\text{km}}{\text{s}}$) for good quality concrete. A study conducted by Graff (1975) proved that the velocity of the S-wave is 60% of the P-wave velocity. While the P and S-wave have a limited velocity range, the R-wave velocity can range from 5900 to 8200 $\frac{\text{ft}}{\text{s}}$ (1.8 to 2.5 $\frac{\text{km}}{\text{s}}$).

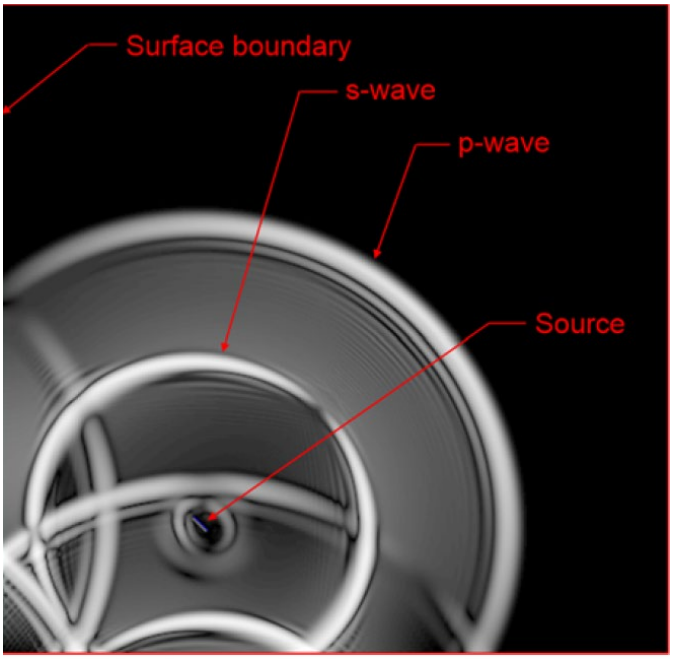

Figure 2-12 Ultrasonic Waves in a homogenous medium [21]

2.2.1 Acoustoelastic Effect

The idea of acoustoelasticity originated in 1953 by the authors of Hughes and Kelly, which branched from Murnaghan's rules of nonlinear elasticity. The summary of this effect states that changes in the elastic wave velocities due to the state of stress in a material exhibiting a nonlinear elastic behavior [22]. To understand how Hughes and Kelly arrived at this theory suggests going back to when Murnaghan presented the third order elastic constants (ℓ, m, and n) in 1951 [23]. In which, he added to Lamé's second order coefficients known as (λ and μ). After coalescing all those, Hughes and Kelly created empirical equations to compare stress in a homogenous isotropic material and ultrasonic wave pulse velocity. The result of Hughes and Kelly work can be seen in Equation 2-7 through Equation 2-12.

Lillamand, Chaix, Ploix, and Garnier [24] conducted an experiment on concrete in uni-axial compression to see the possible effect of studying acoustoelasticity in multiple axes (x, y, and z). Figure 2-13 depicts the layout of their 500 kHz transducers for the research. In this experiment they tested concrete cylinders, with a strength of 6500 ~ 7000 psi (45 ~ 50 MPa), using both longitudinal and shear waves to analyze the behavior. Although their equations, Hughes & Kelly [25], differ by use of variable subscripts, they remain the same overall. Based on the research, Lillamand [24] found that the concrete 1) displays a sensitive acoustoelastic behavior 2) ultrasonic global wave velocity increase proportionally to the absolute value of mean stress 3) longitudinal waves on axis one are five times as sensitive as longitudinal waves in both axis one & two, and transverse waves are three times as sensitive as transverse waves on axis one, or transverse waves in both 2 & 3 axes [24].

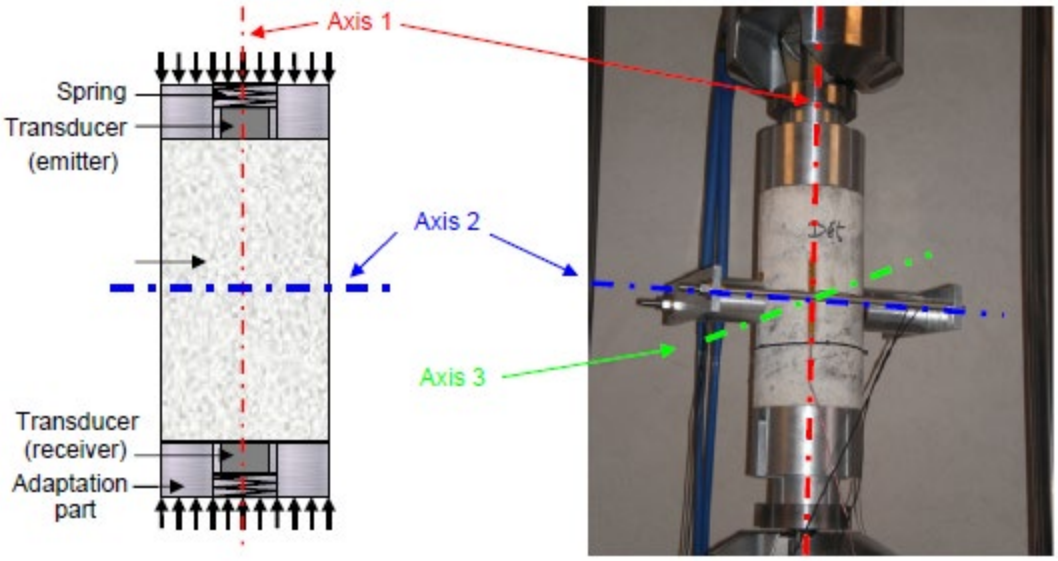

Figure 2-13 Lillamand, Chaix, Ploix, and Garnier transducer layout and axis of study [24]

$$V = V_o * (1 + K * \sigma) \qquad \text{Equation 2-7}$$

$$\rho_o v_{11}^2 = \lambda + 2\mu - \frac{\sigma_{11}}{3K}\left[2\ell + \lambda + \frac{\lambda+\mu}{\mu}(4m + 4\lambda + 10\mu)\right] \qquad \text{Equation 2-8}$$

$$\rho_o v_{12}^2 = \rho_o V_{13}^2 = \mu - \frac{\sigma_{11}}{3K}\left[m + \frac{\lambda n}{4\mu} + 4\lambda + 4\mu\right] \qquad \text{Equation 2-9}$$

$$\rho_o v_{22}^2 = \lambda + 2\mu - \frac{\sigma_{11}}{3K}\left[2\ell - \frac{2\lambda}{\mu}(m + \lambda + 2\mu)\right] \qquad \text{Equation 2-10}$$

$$\rho_o v_{21}^2 = \mu - \frac{\sigma_{11}}{3K}\left[m + \frac{\lambda n}{4\mu} + \lambda + 2\mu\right] \qquad \text{Equation 2-11}$$

$$\rho_o v_{23}^2 = \mu - \frac{\sigma_{11}}{3K}\left[m - \frac{\lambda+\mu}{2\mu}n - 2\lambda\right] \qquad \text{Equation 2-12}$$

Where,

$\lambda = \frac{vE}{(1+v)(1-2v)}$

$\mu = \frac{E}{2(1+v)}$

$\ell = \frac{\lambda}{1-2v}\left[\frac{1-v}{v}L_{22} + \frac{2}{1+v}(L_{21} + vL_{23}) + 2v\right]$

$m = 2(\lambda + \mu)\left[\frac{v}{1+v}L_{23} + \frac{1}{1+v}L_{21} + 2v - 1\right]$

$n = \frac{4\mu}{1+v}[L_{21} - L_{23} - 1 - v]$

Compressibility modulus, $K = \lambda + \frac{2\mu}{3}$

Longitudinal velocity in multiple axis, $v_{11,12}$

Shear velocity in multiple axis, $c_{21,22,23}$

Applied normal applied stress, σ_{11}

Density of concrete, ρ_o

2.3 Previous research in ultrasonic stress determination in concrete

Past efforts have been made to study the effects of ultrasonic testing in concrete to determine TOF changes, correlation of wave velocity to stress, how micro/macro cracking can affect the harmonics, and many other aspects. While concrete is not homogenous, research has sought to quantify a reliable and replicating method that inspectors can use for field inspections of damaged or routine analysis of concrete structures.

The concept of a method to measure stress in concrete is based on the idea that materials exhibit physical changes under stress. As explained in the previous section, acoustic waves propagate at a certain velocity depending on the elastic properties of a material (i.e., density, modulus of elasticity, Poisson's ratio, and other elastic constants). However, when a material is strained (or stressed), the velocity of an acoustic wave is

altered because the atoms are displaced from the equilibrium position, increasing atomic energy and causing interatomic forces to develop. The acoustoelastic effect expresses variations in the elastic properties of the material resulting from applied strains through the effect on the velocity of an acoustic waves (Lozev et al. 1996). The relationship between stress and velocity is most readily observed when stresses are applied to a material in which the change in applied stress from an initial stress state can be measured (Santos and Bray 2002). However, concrete is a heterogeneous, anisotropic material that exhibits nonlinear stress-strain behavior. The acoustic waves can be scattered and reflected by the aggregate particles in the concrete. Furthermore, as stress levels increase, irreversible micro cracking occurs in the concrete which can further disrupt the acoustic signal. These properties make the application of simple acoustoelastic theories much more difficult. The nonlinearity can be quantified by realizing that micro cracking that occurs at higher stress levels results in anisotropy of the wave velocities and depending on the wave length will result in a reduction of the wave velocity. However, the stress history of the concrete can be difficult to quantify. If the material has been stressed above its elastic limit (only 30% to 45% of the peak strength) then there will be irreversible micro cracking in the hardened cement paste. Even if the stress is removed the presence of the micro-cracks can still alter the wave velocity. There has been some limited previous research that investigates possible acoustical methods to directly determine the level of stress in concrete. Chaix et al. (2008) found that the pressure wave in the loading direction and the shear wave polarized in the loading direction were the most sensitive to the applied load. However, it was only shown for elastic stresses and the variation was weak and would be difficult to measure in situ. Zhang et al. (2012), Larose and Hall (2009) evaluated the use of coda (end of temporal

signal) analysis which has been used successfully in geophysics. Larose and Hall (2009) found that this method can accurately predict concrete compressive stress to an accuracy of 100kPa, however only within the elastic stress range (stress less than 20% peak compressive stress). Zhang et al. (2012) used the method to accurately predict the tensile stress in concrete. Schumacher et al. (2013) found a correlation between time of flight measurements of the shear waves polarized parallel and perpendicular to the uniaxial stress the stress in the concrete, but the method did not work well in previously loaded specimens. Shokouhi et al. (2010) studied the variation of sonic surface wave velocities and found that the sonic wave velocities are stress dependent.

Other researchers recommended to use the nonlinear ultrasonic approach to get more accurate results through using multiple pulse and harmonic waves. The use of two pulse sources at different frequencies enables the wave interactions to be analyzed to determine nonlinear components that vary proportionally with applied stress and material nonlinearity. This type of noncollinear wave-mixing to analyze nonlinear characteristics of materials has been successfully applied to asphalt concrete (McGovern et al. 2015). Another possible technique uses a harmonic input signal to evaluate the resonant frequency of the concrete sample. This technique has been applied to measure the change in elastic modulus due to concrete deterioration but has not been applied to stress measurement. For example, nonlinear ultrasonic parameters have been applied to investigate the level of damage in concrete (Shah and Ribakov 2009, Shah et al. 2013). In this approach, harmonic generation in the material is studied by inducing a large amplitude ultrasonic wave of amplitude A_1 and frequency ω_1 on one side of the specimen. If the amplitude of this wave is sufficiently large, the received waveform on the other side of the specimen will contain

harmonics of the induced wave with amplitudes A_2 and frequency $2\omega_1$, A_3 and frequency $3\omega_1$, and so on. The harmonics are generated from nonlinear interactions with the material that increase as damage increases. Recently, Ongpeng et al. (2016, 2017) studied the effect of the loading pattern on the generation of higher harmonics on concrete specimens with two W/C ratios. They found that the third harmonic amplitude more sensitive to single loading pattern than the second harmonic amplitude for both w/c ratios, while the inverse happened under multiple loading/unloading pattern. In their second study, they demonstrated a comparison study between mortar and normal concrete with different sizes of aggregate under two levels of damages (total and incremental) by using the nonlinear ultrasonic technique.

Some of the previous studies focused on only acoustoelastic effects and others have been applied to investigate the level of damage in concrete under the change in elastic modulus due to concrete deterioration. Thus, to overcome the limitations found in previous studies, the synergy of these different approaches will be studied to develop a new approach for stress measurement in concrete in this research.

Clearly, while the theory is simple – there is some physical manifestation of stress in concrete - the application - how to actually measure and quantify that manifestation – is extremely difficult. The methods presented in the previous research show promise but are far from being implementable and are not applicable for all ranges of stress. The purpose of this research is to evaluate, improve, and determine new methods that will lead to accurate direct stress measurement in concrete and a fundamental transformation in the field of structural evaluation. Detailed review of some specific key research is described next.

2.3.1 Schumacher, Chen, Ozturk, and Attoh-Okine (2013)

The first paper to look at was produced from the University of Delaware University Transportation Center. Their study was to better understand how non-homogenous materials affects a stress wave, and also to develop rapid assessment tools for structural elements and extreme events. To accomplish testing 6 in. x 12 in. cylinders, 6 in. x 6 in. x 12 in. block, and 6 in. x 6 in. x 21 in. block were used in this paper. The cylinders and blocks consisted of have a compressive strength of 3,000 psi. The type of transducers used in this experiment consisted of polarized shear waves that propagated parallel to the applied stress and perpendicular directions. Once data was collected, they compared the differences between the behaviors.

The conclusion of this research found that the shear waves behaved very different in two opposite directions, which can be seen in Figure 2-14. When taking a closer look at the waveform the TOF is slightly increased in the perpendicular direction (21) compared to the parallel direction. After their MATLAB program measured from the initiated signal to the positive peak of the received signal, they calculated a TOF for each loading level, normalized TOF ratio, and applied stress ratio between the different loadings. In the comparison they found before 40% of the applied stress ratio the TOF had a slight decrease, but after 40% the trend increase exponentially [21]. Another comparison of normalized TOF ratio and applied stress showed a linear trend up to about 90% of the compressive strength, here the concrete was considered failed and caused this drastic increase in the data. They also concluded that acoustoelasticity primarily governs the behavior during lower stress, within the elastic region approximately below 30 ~ 40% of ultimate strength. Concurrently, prior research suggests that preexisting micro-cracks may be closing during

the early portion of the curve until the stress creates more micro-cracks that grow larger until they develop into macro-cracks [21].

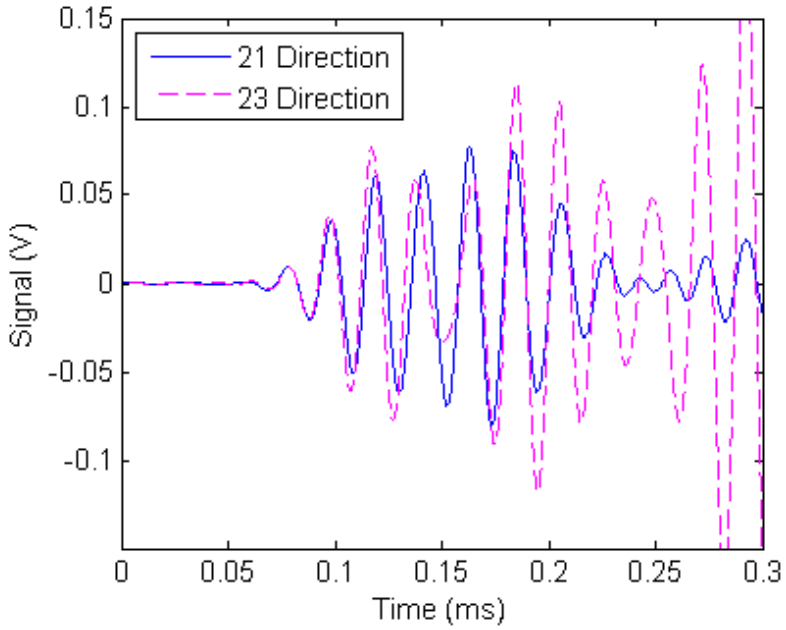

Figure 2-14 Wave transform with shear transducers both in the parallel (23) and perpendicular (21) direction to applied stress [21]

2.3.2 Shokouhi, Zoëga, and Wiggenhauser (2010)

"Nondestructive Investigation of Stress-Induced Damage in Concrete" also investigates stress wave velocity from using the acoustic/impact emission method. They found that the linear behavior of the concrete was predominately controlled by the acoustoelastic theory, which allowed them to use surface wave velocity equations. Details of the prisms used are dimensions of 0.2 m x 0.2 m x 0.6 m with a w/c ratio of 0.55, which resulted in a strength of 4,000 psi. The course of this study used loading increments of 50 kN and unloading stages of 100 kN to see the damaging effects based on wave velocities.

During those loadings stages a minimum of 36 measurements were recorded to ensure reliability and repeatability.

After the data was established the researchers found a linear increase in relative velocity change from fully unloaded until after a stress level of 10 MPa. Once after 10 MPa a slight change in slope is seen due to the presence of micro or possible macro cracking in the structure. Once after 20 MPa the velocity is evidently decreasing from developing macro cracking [22]. The result of the testing is presented in Figure 2-15, which should the behavior of 9 loading cycles. The surface wave velocity measurements of both loading and unloading phases are shown from cycle 2 to 9. The red arrows indicate the average velocity change at the stress-free state before and after the addition of load in each of the cycles. The second y-axis indicates the level of loading as a percentage of the final load at failure. Loading stage 6 has shown a large difference between the loaded and unload wave velocities which is conclusion with the amount of damage present. Loading stage 8 has the most significant change in wave velocity as most of the concrete has experienced macro cracking in the structure. The team concluded that the surface wave velocities measured parallel to the loading on one side of a prismatic specimen undergoing uniaxial compression are highly stress dependent and the velocity stress relationship follows a general multiphase trend. Moreover, the velocity-stress relationship preserves the signature of the loading history of the specimen. By measuring the velocities during unloading phases of load cycles, when no additional damage occurs (according to Kaiser Effect), one can separate the effect of stress and damage on the measured velocities [22].

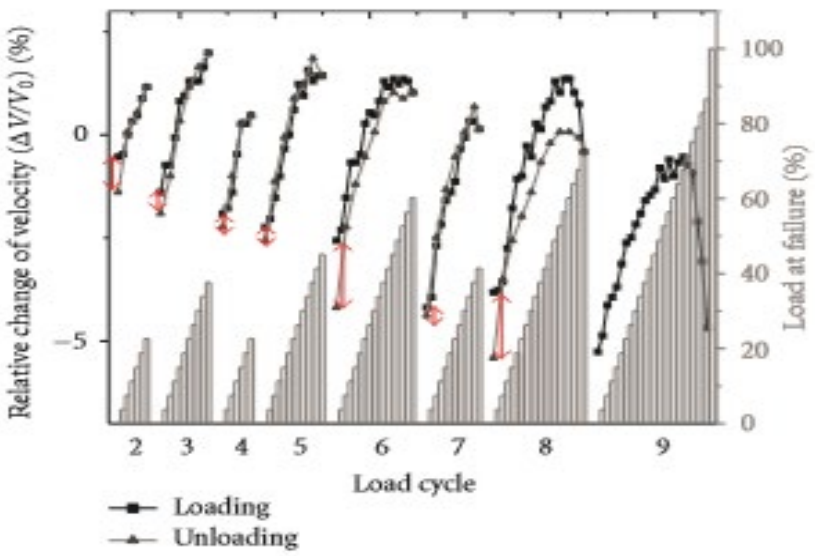

Figure 2-15 Surface velocities for loading and unloading [22]

2.3.3 Shah, Ribakov, and Zhang (2013)

This research effort was to understand the efficiency and sensitivity of linear and non-linear ultrasonics to identify micro and macro defects in concrete. The concrete tested had various w/c ratios at 0.4, 0.5, and 0.6 to see possible defects in ultrasonic behavior during loading and unloading stages. The compressive strengths were determined by 100 mm x 200 mm cylinders in the same order of w/c ratios that follow 56, 45, and 38 MPa. The sizes of the cubes used in the research measured 150 mm each side. To see vertical micro or macro cracking while recording ultrasonic data, the team orientated the pulse waves to be perpendicular to the applied stress. This decision was made because transducers that emit parallel waves would possibly miss detecting any cracking, which was important for the non-linear analysis in this research.

Varying voltage levels were used to see how the specimens behaved under axial compression and to show the change in amplitudes with the increasing frequency harmonics. Shah, Ribakov, and Zhang found that the single attenuation increases with respect to the increased level of damage in concrete. Also, they reported a damage level of 80% of the approximate changes in the pulse attenuation at fundamental, second, and third harmonic frequencies compared to the baseline values were estimated as 37%, 50%, and 59% for w/c equals 0.50 and 52%, 67%, and 78% for w/c equals 0.60 [26]. In their final conclusion the relationship of the change in amplitude versus ratio of loading and ultimate strength showed a clear linear decrease due to the increasing damage present in the concrete. To see the concluded effect of increased loading and damage on the concrete cubes, review Figure 2-16 for the change in amplitude heights at the various harmonics.

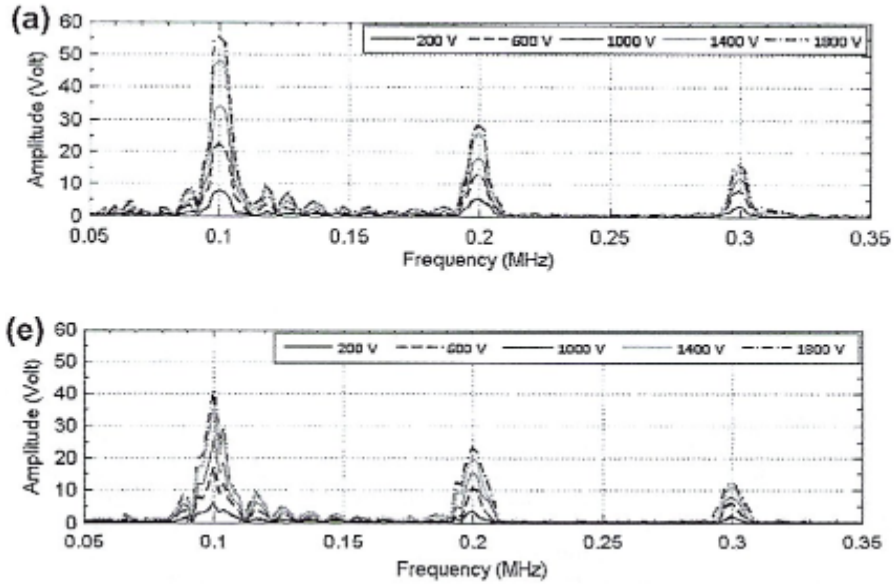

Figure 2-16 FFT analysis with w/c of 0.4 at (a) 0% damage and (e) 80% damage [26]

2.3.4 Hazif and Schumacher (2018)

The final paper discusses Monitoring of Stresses in concrete using the Ultrasonic Coda Wave Comparison Technique (CWC). This explains with the use of the highly sensitive diffuse portion of the recorded ultrasonic waveform (coda wave portion) it is able to detect any change in velocity. Additionally, changes in the applied stress were used to correlate any changes observed in the ultrasonic waveform which were assessed using the magnitude-squared coherence (MSC) method. The project took place first in the laboratory on 6 in. x 12 in. cylinders using a single transducer for a pitching and catching method of data recording. Further testing was completed using 6 in. x 6 in. x 21 in. prisms with a direct transducer setup and constant loading rate of 35 $\frac{\text{lb}}{\text{s}}$. After collecting laboratory data, Hazif and Schumacher transitioned the testing to the I-84 bridge near Echo, Oregon to test on the slab, columns, and prestressed concrete girders.

Based on the loading and unloading of the concrete prisms Hazif and Schumacher found that using their CWC technique it is possible to detect the changes in the internal stress of the concrete. The results of the first prism (P1) show that the sensitivity of the MSC (λ) values were influenced by the wavelength, which is a function of pulse frequency assuming a p-wave velocity of 3,600 m/s (141,000 in/s). The pulse with the smaller wavelength was more sensitive to changes in interior stress than the larger wavelength, as shown in Figure 2-17. When the applied load increased from 10 to 40% of the ultimate stress, the MSC (λ) decreased from 0.88 to 0.6 for λ = 36 mm (1.41 in), where the decrease for λ = 66 mm (2.62 in) was from 0.88 to 0.85. Moreover, the R^2 of the linear fit for the results of the MSC (λ) for the shorter wavelength was higher [27]. What the researchers

found when testing on the girders of the bridge was the MSC values dropped due to the vibrations when the service loading truck stopped. The MSC values show a linear relationship with the applied stress, up to a specific limit which depends on several variables but can be assumed to be at least 50% of ultimate stress [27]. Furthermore, their CWC method was able to correlate the internal stresses extremely well when compared to their computer generated structural analysis.

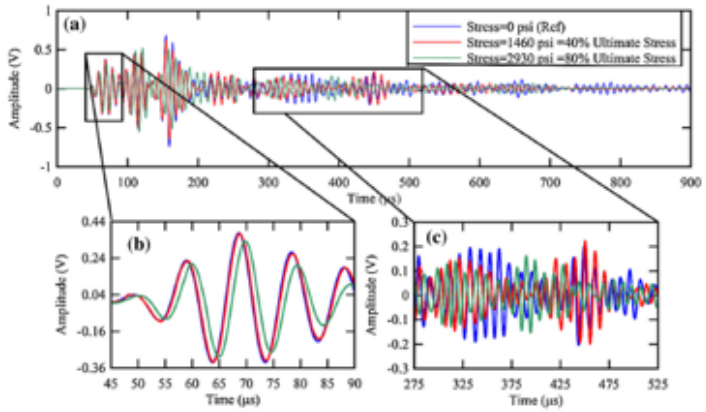

Figure 2-17 Waveform plot (a) with zoomed windows for TOF (b) and coda wave (c) analysis [27]

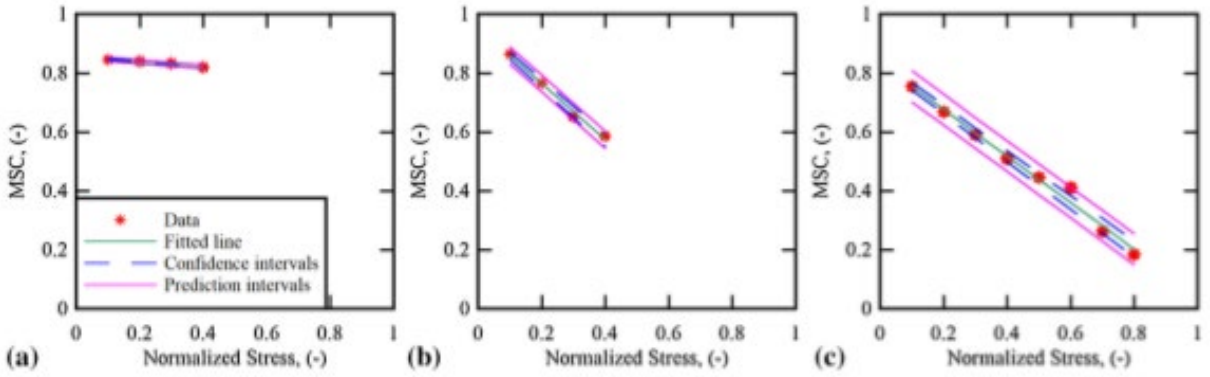

Figure 2-18 MSC vs normal stress (a) P1 λ=66 mm (2.61 in), (b) P1 λ=36 mm (1.41 in), and (C) P2, λ=36 mm (1.41 in) [27]

Chapter 3 Procedure

The procedure and experimental setup is described in this chapter. Much of this research was conducted in a laboratory to replicate consistent data. During this study assessment of the TOF and higher harmonic amplitudes was used to see any small changes within the structure of the concrete. This also helped to identify the stress applied to the concrete or the previous damage from a prior load. By seeing these defects in the TOFs and higher harmonic amplitudes, a more precise evaluation can be used to determine the state of the concrete.

3.1 Ultrasonic equipment

The overall setup of this NDE testing can be seen in Figure 3-1. With this setup the waveform data was transferred from the oscilloscope to a desktop computer for quick analysis of both TOF and FFT analysis. A smaller aspect of the setup required the use of a three quarter inch steel plate to allow full transfer of load from the Forney axial machine onto the concrete prism surface. Also, to note in the setup is a commercially available oscilloscope that was able to produce accurate measurements throughout this study. The use of the ultrasonic equipment will be discussed more in detail in subsequent sections. For this reason, specific settings, adjustments, and other important factors will be addressed in point.

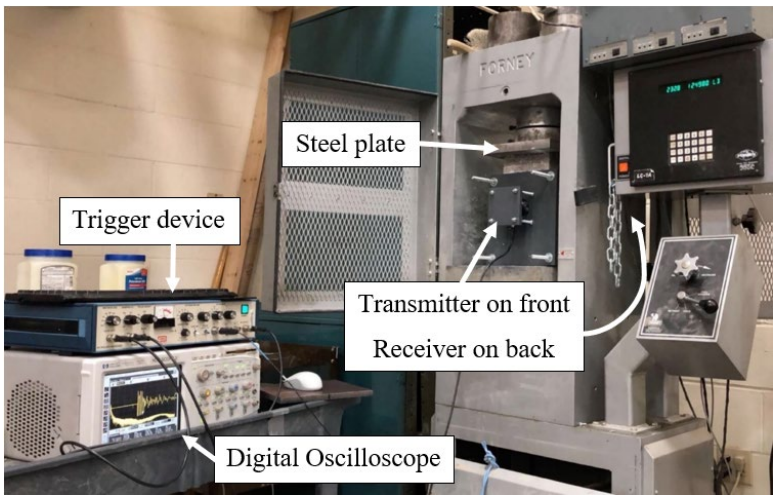

Figure 3-1 Overall setup of ultrasonic testing equipment

3.1.1 Oscilloscope

The oscilloscope was a Hewlett Packard Infinium 54815A model displayed in Figure 3-2. This oscilloscope has 4 channel connections to allow multiple receivers or transmitting transducers. Has a maximum bandwidth of up to 500 MHz and allows a sampling rate of up to a 1 GSa/s sampling rate, and superior probing bandwidths of up to 4 GHz. There are multiple trigger settings that include glitch, pattern, state, and delay by time/events, setup/hold time, transition and video. It also has built in programs to calculate fast Fourier transforms (FFT) and has the ability to produce measurement statistics [28]. Pictured below, in Figure 3-2, is the oscilloscope used in throughout the ultrasonic testing.

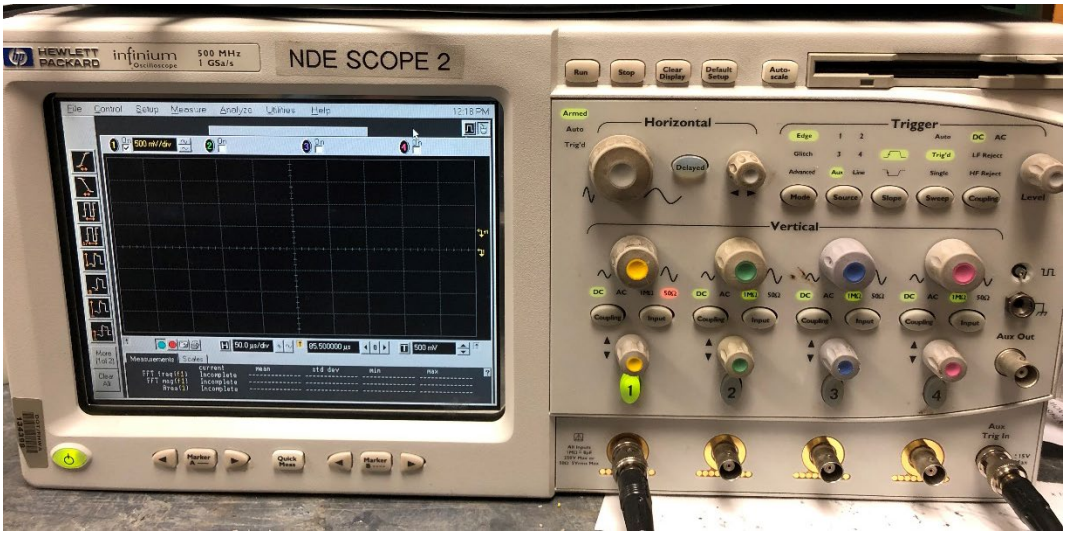

Figure 3-2 Hewlett Packard oscilloscope

The weight of this machine is roughly 20 ~ 30 lbs. with dimensions of 1.5 ft. x 2 ft. Depending on the sampling rate or specified number of data points to collect, the collection of data can require a lot of time. With the limited amount of hard drive space, ~5 MB, on the oscilloscope it would make in field inspections very lengthy between transferring data from the floppy disk to a laptop. Possible future modification would be needed to make this a portable system or to purchase a smaller oscilloscope would be ideal.

3.1.2 Transducers

The various compression wave transducers were used in this research to see how the effects of TOF, amplitude, frequency, and amount of damage. These transducers operate by the piezoelectric crystals inside that change shape and size when a voltage is applied by a triggering system. The AC trigger voltage makes the crystals oscillate at a specific frequency and help to produce an ultrasonic sound. As a result, the piezoelectric materials can generate a wave when a voltage is applied to the transducer. While some

testing systems use separate transmitter and receivers, or other systems use a combination of both functions in a single piezoelectric transceiver. Each of the transducers are Olympus manufactured. The 1.5-inch diameter main transmitter is a 100 kHz right angle transducer that are capable of withstanding a 900V amplitude for this type of testing. The secondary receiving transducers are the straight 250 kHz and right-angle microdot 500 kHz models. The 250 kHz model was used in the beginning of the research to better understand the behavior of the waveform, as well as FFT frequency plotting. The additional 500 kHz transducer was incorporated to see a finite change in the waveform and FFT analyses at higher frequencies. Figure 3-3 shows all three transducers used for this study.

Figure 3-3 Pressure wave transducers used for testing [20]

Coupling of the transducers was not required for this study but consideration was taken to use coupling to ensure high quality data was captured. Previous testing was not conclusive when using the "pitch and catch" method where only one transducer is used on the concrete specimen. Contact of the transducers influences the ultrasonic data greatly. If

the contact is not level, surface is rough, or if the application of petroleum jelly is limited then amplitude, frequency, and TOF data will be inaccurate.

3.1.3 Pulser-receiver

For the ultrasonic wave to be transmitted, a pulser device is required to have in the testing setup so that a waveform can be generated. The Panametrics High Voltage Pulser-Receiver model 5058PR has various settings that allow a technician to have a tailored interface. The system has adjustable pulse heights at 100V, 200V, 400V, 900V, or various custom voltages. Some features of this pulser-receiver include high gain & low noise broadband (10 MHz) receiver, pulse-echo and thru-transmission modes, high isolation (80 dB) in thru-transmission mode, 60 dB RF gain, additional 30 dB gain available from internal auxiliary preamplifier, receiver attenuation range of 0 dB to 80 dB in 1 dB steps, 1 dB vernier for fine adjustment, switch option for high pass and low pass filters, PRF rate switch selectable from 20 Hz to 2 kHz. Controls permit either discrete, calibrated settings, or continuous adjustment [29].

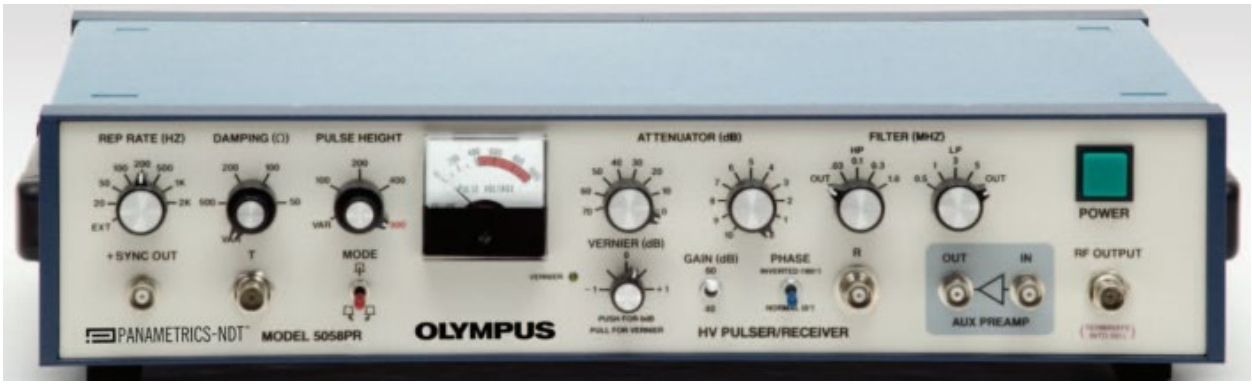

Figure 3-4 Panametrics pulser-receiver

An important feature of this pulser-receiver is the ability to use pulse-echo and thru-transmission modes. For example, the pulse-echo mode allows the single use of a transducer to act as the transmitting and receiving device. Throughout the testing on the reference specimens and the concrete prisms the pulse-echo mode was deemed to have sporadic data. As a result, this form of testing was not used as extensively, but was used more for the selection of ultrasonic test settings.

3.1.4 Specimen frame

Initial ultrasonic testing did not include this polymer frame setup to hold the transducers in place. Instead, plastic ties were wrapped around the concrete prisms to secure them to the surface. As a result, this led to varying waveform and FFT data which was not conclusive to correlate the stress in the concrete. The two main functions of the new testing frame were to secure the transducers to the surface of the concrete prisms and to keep the transducers in the middle region of the prism. This frame can ensure the transducers had full contact to the surface with small springs pressing them against the sides. The springs on each side of the frame can be seen in Figure 3-5. While some

specimens had possible internal defects or a large aggregate near the surface this required moving the frame and transducers around until the oscilloscope displayed an acceptable amplitude. After the area with the greatest amplitude was found the two large plates were tightened to each surface and the transducers were applied.

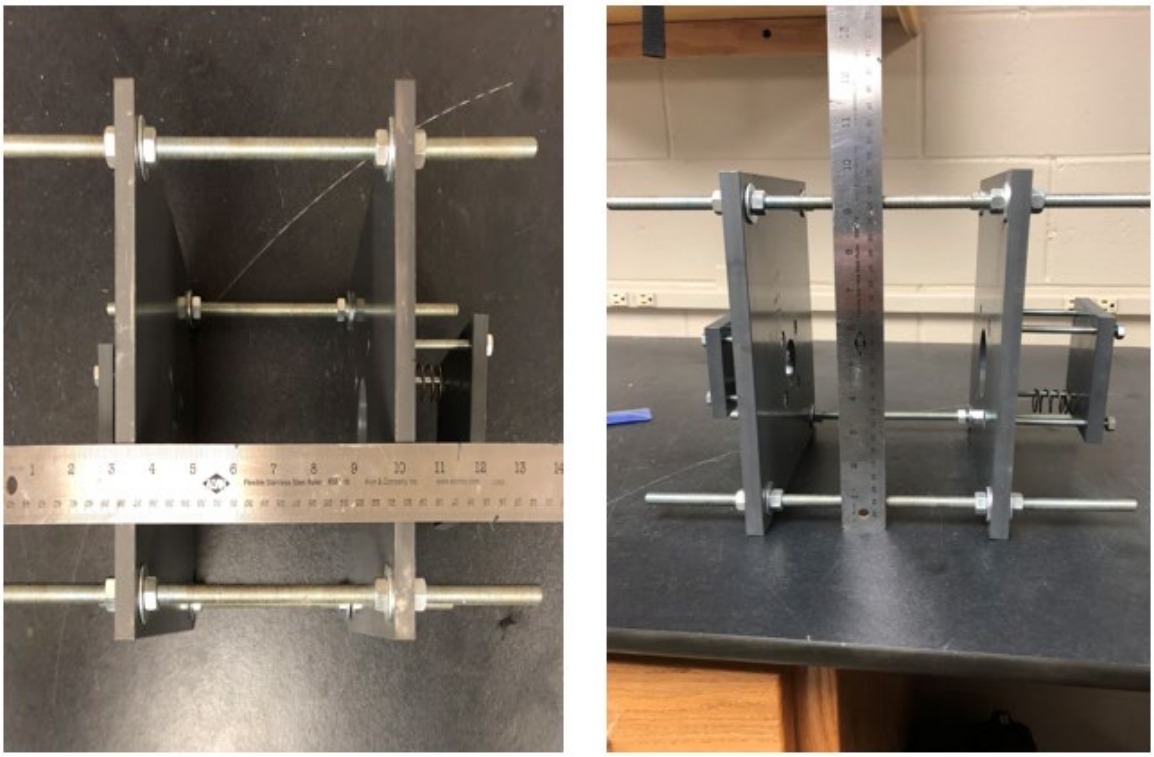

Figure 3-5 PVC polymer material to hold transducers on concrete surface

3.1.5 Specimens

A standard concrete mixture (max aggregate size 3/4 in. w/c ~ 0.4, f'_c ~ 6,000 psi), was chosen for this study. To test the strength and ductility of the concrete, three cylinders were cast from each of three concrete batches were tested. Figure 3-6, Figure 3-7, and Figure 3-8 shows the behavior of each batch and confirm that the strength of the concrete was on average 6,000 psi.

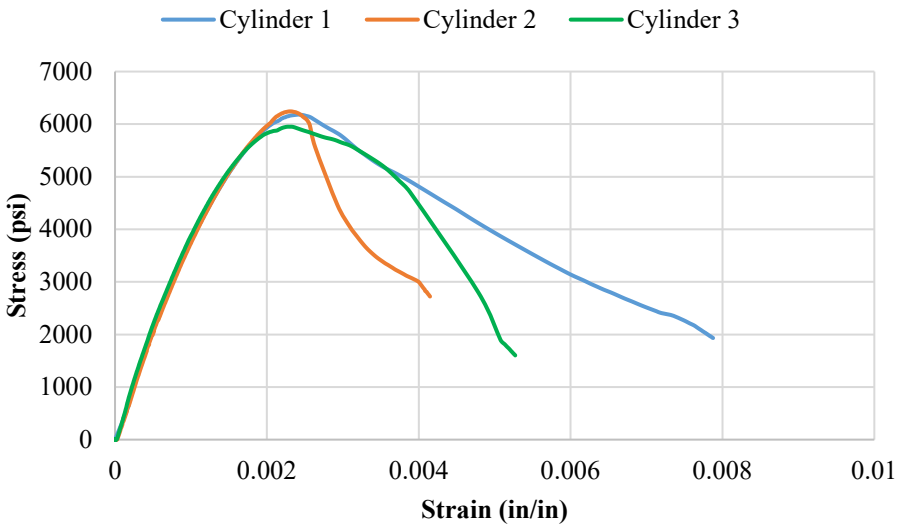

Figure 3-6 Stress and strain of Batch 1

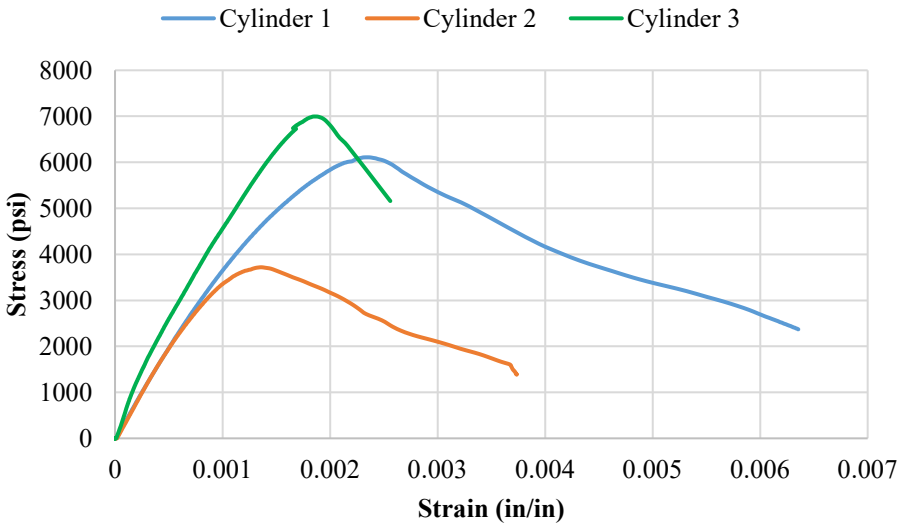

Figure 3-7 Stress and strain of Batch 2

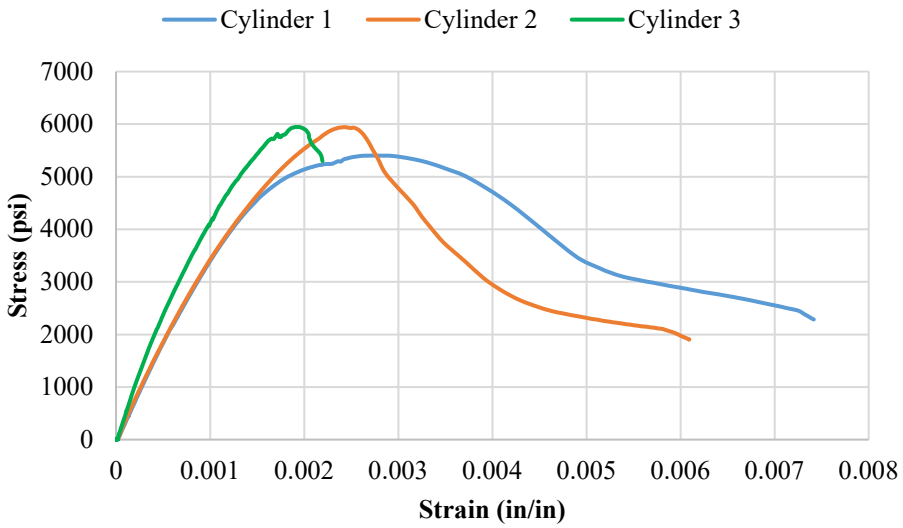

Figure 3-8 Stress and strain of Batch 3

As mentioned earlier there were two different concrete conditions tested to see the possible effects from the ultrasonic testing. After the first test series had been completed on the smaller dry specimen and the data was analyzed, the decision to resize and saturate the prisms were tasked for the next phase. The secondary concrete prisms had been fully cured since May of 2017. Before testing began the caps of the prisms needed to be fully level to ensure no eccentric loading would occur and cause the concrete to fail prematurely. Once this task had been completed a sulfur cap was added to eliminate any other possible flaws with trimming the ends. The prism sides were also ground to be smooth to allow full contact of the transducers. To ensure the concrete would fully be saturated the specimens were submerged for over three weeks as pictured in Figure 3-10 Wet specimen being soaked for 3 weeks. During the day of testing the specimens were removed from the water and the sides were patted dry so there would be no water damage to the transducers.

Figure 3-9 Concrete specimens [20]

Figure 3-10 Wet specimen being soaked for 3 weeks

3.1.6 Loading levels

The initial loading levels for the first test series included nine different stages. These stages ranged from fully unloaded to approximately 50% of the compressive

strength, with loading increments of 6,000 lbs. at each stage [20]. These testing levels did not allow the research to see more of the non-linear behavior in the concrete as the loading stages had stopped during the early parts of it. Also associated with the loading stages, this did not include unloading stages to record data to review damaging effects in the concrete.

When the first sequence testing was completed, the second series was conducted with increased loading stages to see this non-linear effect in the. The new loading stages also had 9 different cases to record at. These ranged from fully unloaded to 80% of the compressive strength unloaded. Illustrated below is a physical representation of the new loading stages for the second testing series. The arrows show the sequence of the loading stages.

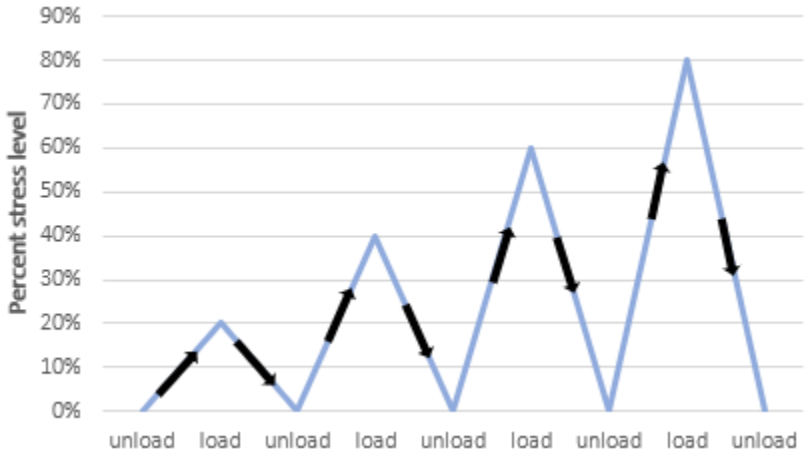

Figure 3-11 Loading and unloading stages

3.2 Laboratory testing

Since no setup or device configuration allowed for in-field testing, all previous and current ultrasonic testing was conducted within a temperature controlled laboratory. A simple diagram of the current testing setup is display in Figure 3-12.

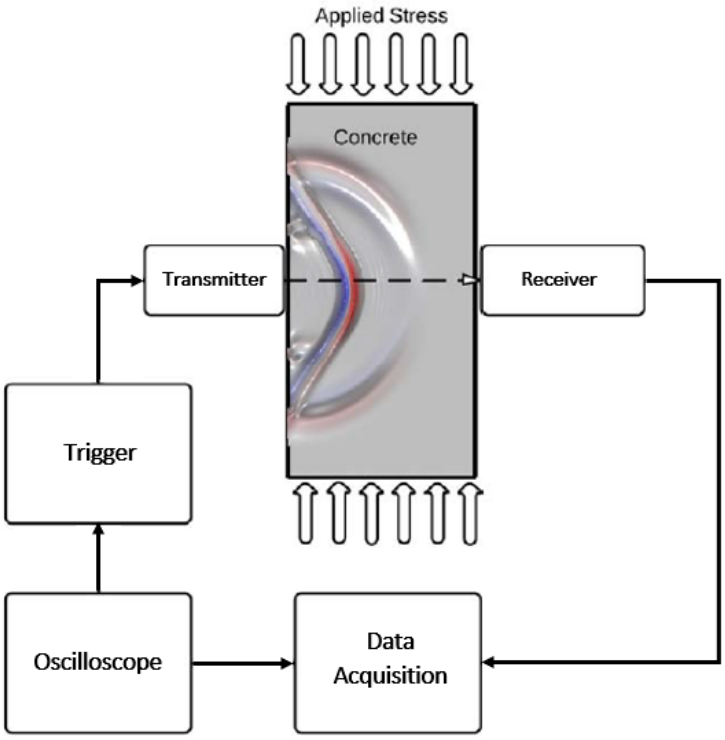

Figure 3-12 Data acquisition for lab testing [21]

3.2.1 Reference specimens

To ensure the ultrasonic wave equipment was working or calibrated properly two reference specimens were chosen to test on before testing on the concrete specimens. These chosen specimens were both a four in block of polypropylene plastic and a mild steel. By the standards of ASTM both specimens are thick enough to collect the refracted compression wave. The known velocities of each specimen were found from the Olympus material sound velocities section. The polypropylene should have a velocity near 96,850 $\frac{\text{in}}{\text{s}}$ $\left(2{,}460\ \frac{\text{m}}{\text{s}}\right)$ and the mild steel was rated to have a velocity of 230,315 $\frac{\text{in}}{\text{s}}$ $\left(5{,}850\ \frac{\text{m}}{\text{s}}\right)$ [30]. The specimens are pictured in both Figure 3-13 and Figure 3-14.

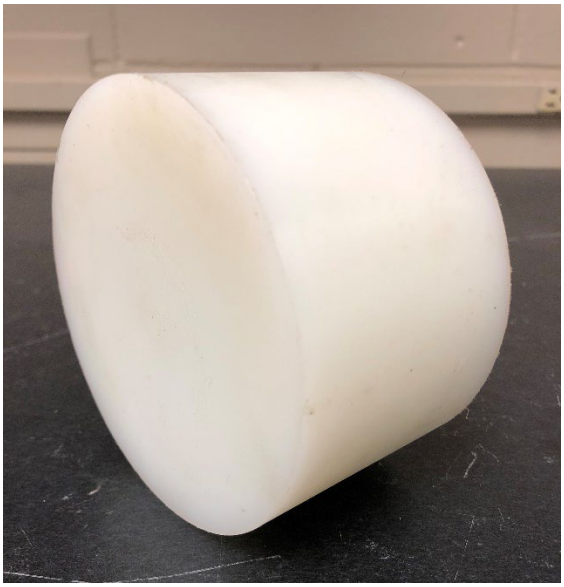

Figure 3-13 Polypropylene plastic specimen for wave velocity reference (D=2.5, H=4)

Figure 3-14 Steel cylinder specimen for wave velocity reference (D=6, H=4)

When testing on both specimens the calculated wave velocity in the polypropylene was concluded to be 145,985 $\frac{\text{in}}{\text{s}}$ and the steel had a velocity of 228,571 $\frac{\text{in}}{\text{s}}$. The possible reason for the difference in wave velocity for the polymer specimen could be a result of

the higher density. Olympus reports other materials that have high densities result in faster wave velocities. Figure 3-15 shows the FFT of the signal through the steel sample with a 100 kHz transducer and 250 kHz receiver.

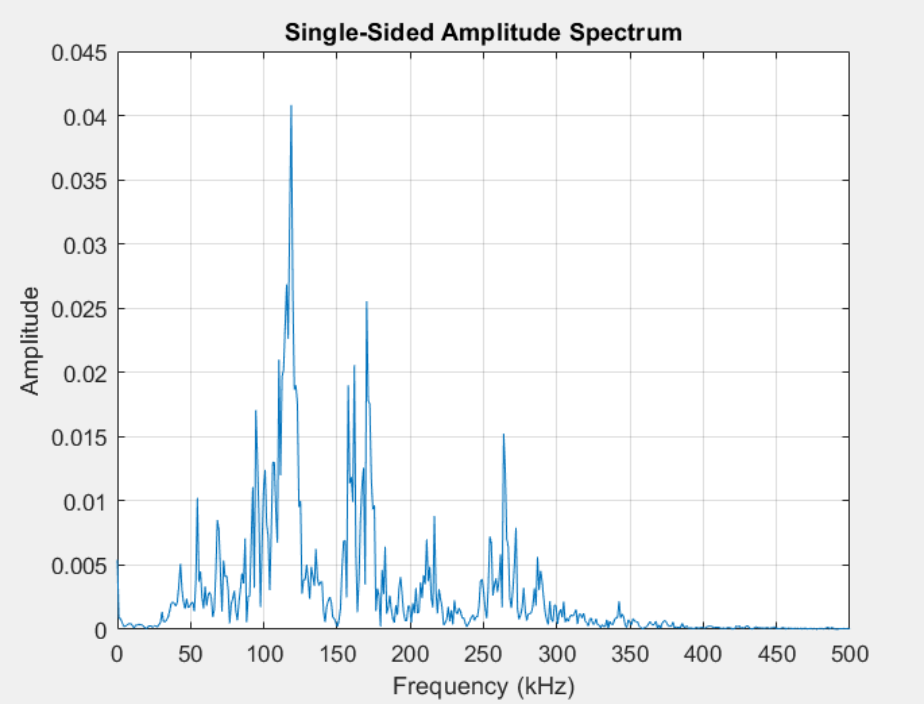

Figure 3-15 FFT of waveform through steel sample (100 kHz transducer, 250 kHz receiver)

3.2.2 Pulser-receiver settings

The repetition rate on the device determines the number of pulses that is transmitted by the device. When the testing of the dry specimens were conducted this setting was adjusted at 200 Hz, where the max setting is 2,000 Hz. After multiple tests the resulting repetition rate that showed consistent results was set at 20 Hz.

The dampening resistance settings also needed adjustment throughout the entire testing series. This setting entails controlling a resistor that modifies the shape of the

outgoing waveform to the oscilloscope. If the damping was set to a lower value this resulted in increases pulse damping and improves near surface resolution. And if damping was increased, then reduces pulse damping and improves penetration in the material [31]. Having the highest setting at 500 Ω allowed penetration through the dense concrete element.

Some testing setups use a single transducer that acts as the transmitting and receiving unit. Primarily the testing used in this research was with two transducers, the testing mode did not need to be changed unless a single transducer was used to compare waveform data with the dual system. This setting is depicted in Figure 3-4 as the red switch under the pulse height.

The gain settings on the trigger device allowed an increase in amplitude in the concrete. This setting was used at 40 dB in the testing since a good smooth surface area was always used, so the need for increased amplitude was not required.

Attenuation on the trigger device is used to cause the ultrasonic wave to decay as it propagates through the concrete [31]. In the early stages of testing series two there was not a lot of signal passing through the concrete, so this adjustment was set to completely zero to fully allow the wave to travel through the prism.

The smaller setting, Vernier allowed the control of the width of the waves to be recorded in the waveform. The pulse widths in the waveforms were easy to distinguish so this setting was left on zero to not increase or decrease the widths of the waves.

Low pass (LP) filter is categorized as being able to clean the noise up in the ultrasonic wave. If lower frequencies are being used, then it's possible to increase this

setting to improve the signal to noise ratio of the waves by filtering out the higher frequencies [31]. Since the transducers were producing adequate frequencies the setting was adjusted to off.

High pass (HP) filter is the opposite of the LP filter setting. If high frequencies are used in the testing, it's possible to filter out the lower frequency that can be scattering the ultrasonic waves in the concrete. Again, the transducers operated effortlessly with the setting switched to off.

3.2.3 Oscilloscope settings

During early assessment of the data collected from the oscilloscope there were issues of the data being clipped or shortened. Within the acquisition setup menu there were options to increase the amount of data points to include in the waveform, or by using the automatic setting which would adjust depending on the amount of sampling rate and volts per division. The numerical number for volts per division, which can be seen in Figure 3-16, was kept constant through the wet specimens testing. Another issue with early testing on the prisms was the data was being smoothed too much and was hard to see fine differences between TOF and changes in harmonics. Initially the averaging setting was kept at 16 samples and when changed to 8 there was a clearer difference in the data. After reducing this to the current setting of 4 the data produces much clear points where the TOF can be seen and where points have a defined peak in the FFT analysis.

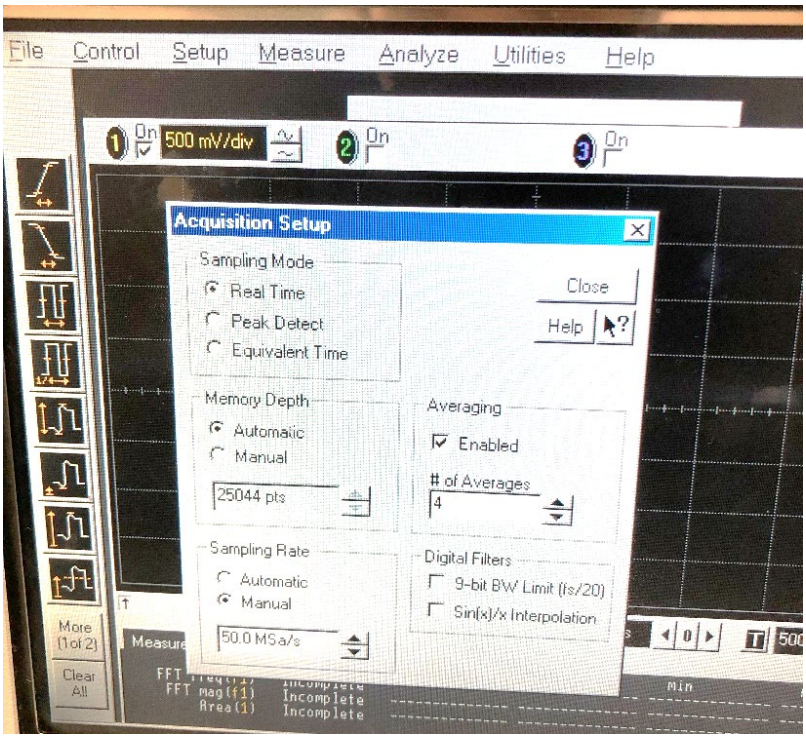

Figure 3-16 Data acquisition setup

3.2.4 Transducer setup

As mentioned in previous sections this study predominantly used the direct transducer configuration due to the accurate data produced, whereas the single transducer resulted in slightly skewed data. Each description of single and dual transducer use will be further explained in the following sub sections.

3.2.4.1 Single

Often this single transducer is referred to as the pitching and catching method. This means that the transducer can emit an ultrasonic wave and also at the same time receive that wave when it refracts back. A depiction of this action can be seen in Figure 3-17. There hasn't been considerable research completed with just using one transducer to relate

velocities, TOF, or frequency harmonics to in-situ stress or quality determination of concrete. This use of a single transducer may be used to identify if there is a defect below the surface but not quantify the size or possibly how deep it may be. Another possible use is to determine the thickness of a concrete member. A big motive for using this setup is if only one side of the concrete is exposed during an inspection.

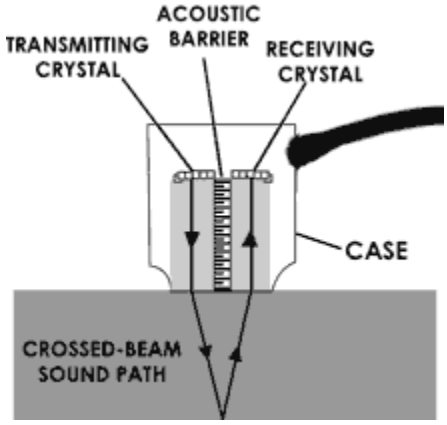

Figure 3-17 Depiction of single transducer use [13]

3.2.4.2 Dual

A depiction of the few orientations that are possible to use with dual transducers can be found in Figure 2-9. Depending on the type of testing that is being conducted, each orientation of the transducers has its own benefits. If concrete is heavily reinforced, then the semi direct layout could be a good option to determine the wave velocity or in-situ stress. For example, on a square column that has a at least two surfaces exposed by 90 degrees. The indirect configuration isn't used as often but can be used in the assessment of crack depths that were discussed in Section 2.1.6.3 Crack depth/size. Most of this research

used the dual mode with the 100 kHz transducer sending the ultrasonic waves and either the 250 kHz or 500 kHz receiving the waves.

Chapter 4 Results

The results found from this testing will evaluate wave characteristics at different levels of load and damage (previous load level). The data will be analyzed to determine the changes in TOF and changes in amplitude of higher harmonics in the frequency spectra. Furthermore, from the calculated velocity a determination of the quality rating of concrete as well as current strength in the concrete is concluded.

4.1 Laboratory testing

The testing in this research was able to determine the velocity of the ultrasonic wave by measuring the distance required for the wave to travel and analyzing when the first signal is read by the receiving transducer. A MATLAB program was used to numerically determine multiple TOF for each of the loading stages. This was accomplished by measuring the distance from the zero time to the time at which the amplitude is greater than or equal to 0.8V. Lastly, the FFT analysis was also used in the same MATLAB program to generate the plots as well as looking closer into the data to see the changes of loading on the concrete at each of the different harmonic levels. Detailed discussion is given on each Specimen 8 and 9 wet tested specimens as these specimens yielded the best results.

Table 4-1 Prism reference name

Name	Mix #	Condition
Specimen 1	1	Dry
Specimen 2	2	Dry
Specimen 3	3	Dry
Specimen 4	1	Dry
Specimen 5	2	Dry
Specimen 6	3	Dry
Specimen 7	1	Wet
Specimen 8	2	Wet
Specimen 9	3	Wet

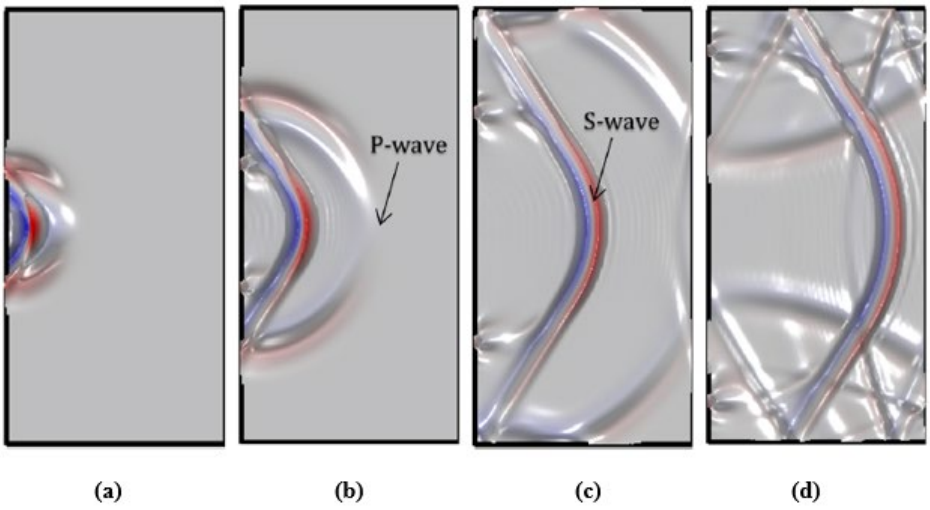

Figure 4-1 Ultrasonic wave depicting P and S-wave initiation (a), compression wave traveling faster than shear, (c) compression wave beginning refraction, and compression fully refracted back to source (d) [21]

The waveforms for specimen 8 and 9 tests are given Appendix A. Within Appendix A: Wave form data, the changes in amplitude versus time can also be seen between the dry and wet specimens.

4.1.1 Wave velocity

The known dimension between the transducers was the same as the measured geometry dimension, which was 6 inches. When all the waveforms from specimens 7 through 9 were input into the MATLAB program the resulting TOF were calculated and then averaged for each different pulse height. Presented in Table 4-2 and Table 4-3 are the time at which the signal is received at 0.8V.

Table 4-2 Wave velocity from unloaded wet specimens

	400 V				900 V			
Stress level	t (s)	v (in/s)	v (ft/s)	v (km/s)	t (s)	v (in/s)	v (ft/s)	v (km/s)
0%	3.465E-05	173,160	14,430	4.398	3.392E-05	176,887	14,741	4.493
20%	3.485E-05	172,166	14,347	4.373	3.410E-05	175,953	14,663	4.469
40%	3.495E-05	171,674	14,306	4.361	3.420E-05	175,439	14,620	4.456
60%	3.515E-05	170,697	14,225	4.336	3.449E-05	173,963	14,497	4.419
80%	3.544E-05	169,300	14,108	4.300	3.478E-05	172,513	14,376	4.382

Table 4-3 Wave velocity from loaded wet specimens

	400 V				900 V			
Stress level	t (s)	v (in/s)	v (ft/s)	v (km/s)	t (s)	v (in/s)	v (ft/s)	v (km/s)
0%	3.465E-05	173,160	14,430	4.398	3.415E-05	175,695	14,641	4.463
20%	3.464E-05	173,210	14,434	4.400	3.415E-05	175,695	14,641	4.463
40%	3.464E-05	173,210	14,434	4.400	3.416E-05	175,644	14,637	4.461
60%	3.475E-05	172,662	14,388	4.386	3.423E-05	175,285	14,607	4.452
80%	3.495E-05	171,674	14,306	4.361	3.445E-05	174,165	14,514	4.424

Due to missing some data points, particularly in specimen 8 at the 900V measurement the averaged numbers were taken as the values determined in specimen 9 at the 900V rating. Overall, the velocities changed very little even at the highest level of stress. The greatest difference between the velocities is at the 60 and 80 percent in the unloaded case, approximately 0.83% difference. After reviewing Table 4-2 and Table 4-3, the loaded cases have a velocity higher than that of the unloaded cases. Excluding the zero stress level, the average difference between each loading case is close to 37 $\frac{\text{ft}}{\text{s}}$.

4.1.2 Time of Flight

Previously stated in the last section a MATLAB program determined the time required for the transmitting wave to be received by the opposite transducer. The voltage the program recorded the TOF at was when the voltage was greater than or equal to 0.8V. Clearly shown in Figure 4-2 and Figure 4-3 is the graphical representation that shows the increase in TOF with load level and damage.

The TOF readings for the unloaded specimens (load level is 0, however previous load level applied causing possible damage in the concrete) is fairly linear. This indicates that the TOF increases as the micro-cracking caused by the previous load slows down the ultrasonic wave in the concrete as expected. It is surprising that there is a difference even with a 20% f ’c previous load as this load level is generally considered to be well within the elastic range of the concrete. These readings show that damage from previous loading will affect the wave velocity and impact the stress measurement. Furthermore, the slope of the unloaded TOF readings with previous load level is different between the two specimens. The slope of specimen 8 is 40% less than that of specimen 9. This difference in two specimens of the same concrete would make it difficult to use the TOF as a way to determine the stress level or damage in the concrete.

The loaded TOF show a slight decrease in the TOF from 0 to the 40 percent stress level, excluding specimen 9 at the 900V rating. It is expected that under load the TOF will decrease as the particles are pushed closer together and the wave velocities increase. At a low level of load, the effect of the load (decreasing the TOF) is greater than the effect of the damage due to micro-cracking in the concrete causing the decrease in TOF at low levels of load. At higher levels of load the damage effect becomes greater and the overall TOF increases. This result indicates that any ultrasonic method based on TOF will have to account for the damage due to previous loading in the concrete because that effect can be greater than the effect of the load itself.

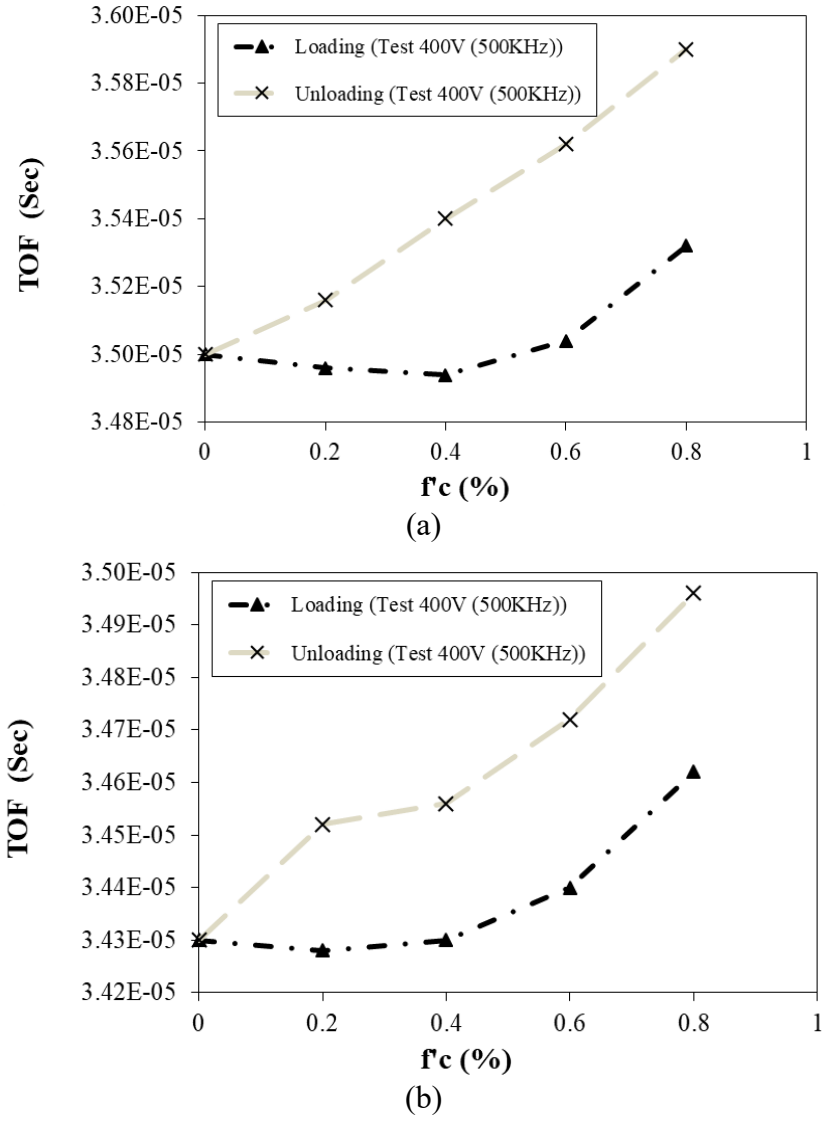

Figure 4-2 Change in TOF on wet 8 specimen (a) and wet 9 specimen (b) at 400V

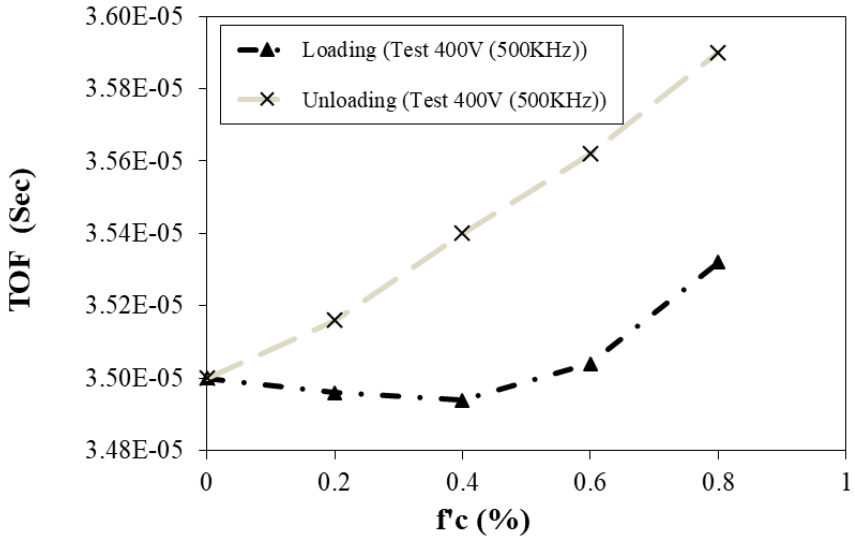

(a)

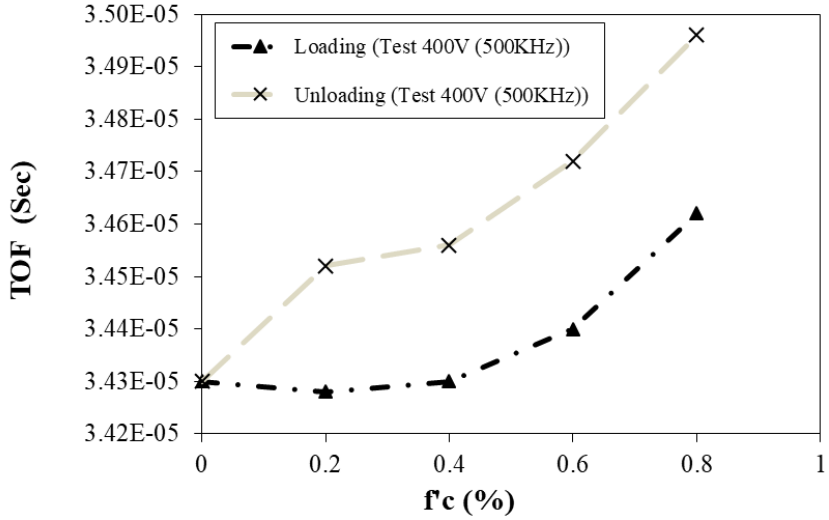

(b)

Figure 4-3 Change in TOF on wet 8 specimen (a) and wet 9 specimen (b) at 900V

4.1.3 Frequency harmonics

The fast Fourier transform is a method that converts the time domain to a frequency. The FFT analysis showed the largest peak at the transmitted frequency of 100 kHz. Higher harmonics occurred at around 150 kHz and 250 kHz. Although these are not the exact harmonic (one would expect the next harmonic to be at 200 kHz) the difference can be due

to the transducer is transmitting a pulse not a wave and the harmonic of the transmitted wave is not precisely clean. Furthermore, the receiver is centered on a 500 kHz frequency that can even further distort the wave. Figure 3-15 shows a wave transmitted through the steel reference specimen that confirms this anomaly.

For each harmonic the amplitude is recorded in Table 4-4 to Table 4-6. The "A" positions are correlated at the specific frequencies that are labelled in the tables. A plot of the amplitude with load level is shown in Figure A-1 to Figure A-4. After analyzing the data in the three specimens it is evident that the behavior between the amplitude heights and stress level is nearly linearly decreasing.

Table 4-4 Specimen 8 400V amplitude difference

400V (500KHz)					
Loaded	A2 @ 150KHz	A3 @ 250KHz	Unloaded	A2 @ 150KHz	A3 @ 250KHz
0	0.0834	0.02389	0	0.0834	0.02389
20%	0.08385	0.02242	20%	0.08364	0.02297
40%	0.08112	0.02347	40%	0.0786	0.02143
60%	0.08092	0.02243	60%	0.07628	0.01917
80%	0.07788	0.01955	80%	0.07434	0.01656

Table 4-5 Specimen 9 400V amplitude difference

400V (500KHz)					
Loaded	A2 @ 150KHz	A3 @ 250KHz	Unloaded	A2 @ 150KHz	A3 @ 250KHz
0	0.0834	0.02389	0	0.0834	0.02389
20%	0.08385	0.02242	20%	0.08364	0.02297
40%	0.08112	0.02347	40%	0.0786	0.02143
60%	0.08092	0.02243	60%	0.07628	0.01917
80%	0.07788	0.01955	80%	0.07434	0.01656

Table 4-6 Specimen 9 900V amplitude difference

900V (500KHz)					
Loaded	A2 @ 200KHz	A3 @ 250KHz	Unloaded	A2 @ 200KHz	A3 @ 250KHz
0	0.07182	0.02141	0	0.07182	0.02141
20%	0.05742	0.0248	20%	0.06624	0.02003
40%	0.0455	0.02218	40%	0.05997	0.01775
60%	0.03836	0.02214	60%	0.04455	0.02147
80%	0.03088	0.02241	80%	0.03166	0.02349

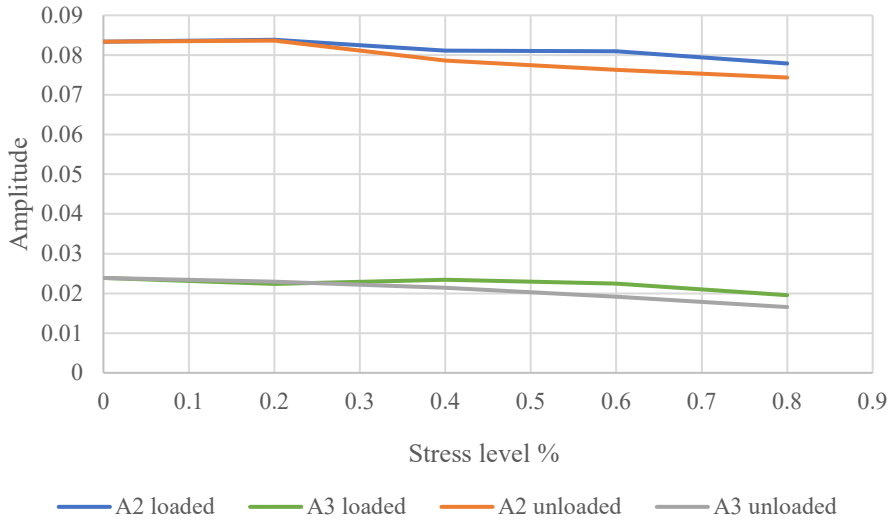

Figure 4-4 Specimen 8 amplitude change at different loading level 400V

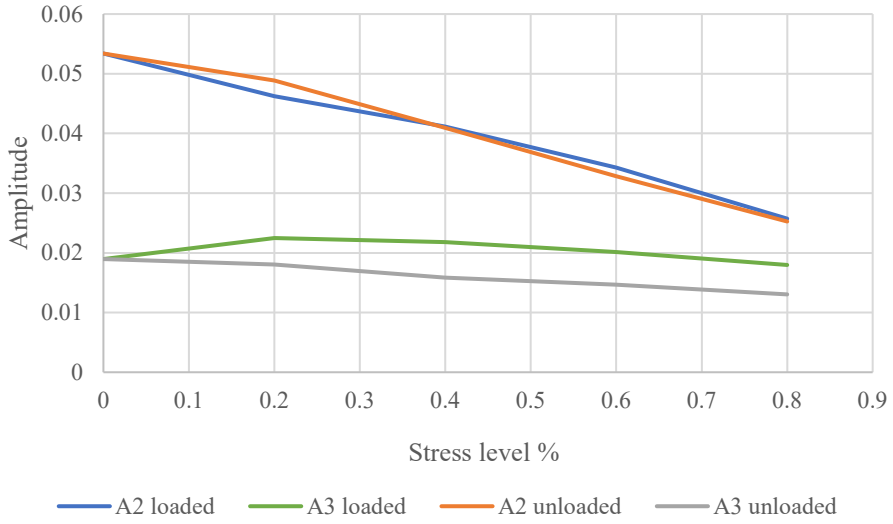

Figure 4-5 Specimen 9 amplitude change at different loading level 400V

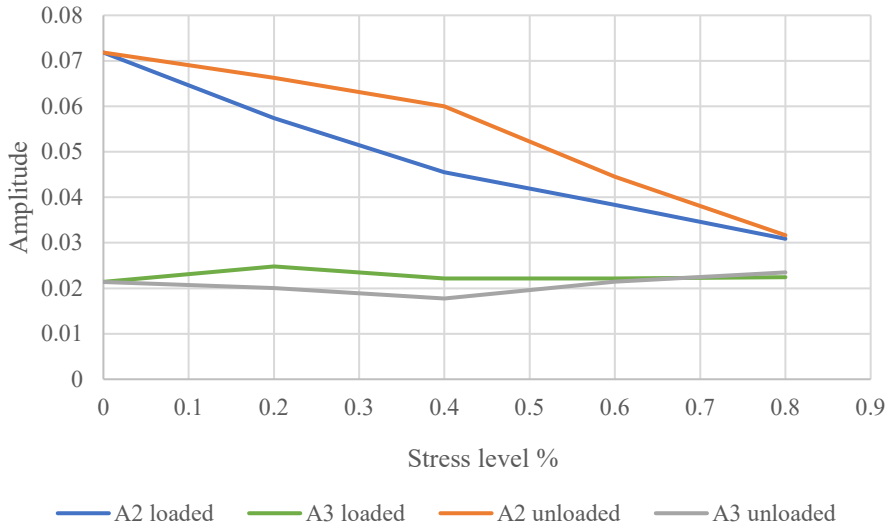

Figure 4-6 Specimen 9 amplitude change at different loading level 900V

When reviewing Specimen 9 at 400 and 900V rating, there is a clear behavior of the linear decrease as seen in the second harmonic. While the third harmonic change is not very different in any of the three cases due to the resulting macro cracking that has made both the loading and unloading nearly equal. To quantify the changes between the specimens the 900V rating amplitude in the 3rd harmonic did not decrease as much as the 400V rating. Also to note, the slope of specimen 9 400V at position A2 was 80% greater than specimen 8 400V at position A2. From this data acquisition it is evident that it may be difficult to determine the stress with greater difference between the amplitude readings.

4.2 Overall concrete condition

An overall assessment of the concrete can be made using results of previous research and the wave velocities determined in this testing.

4.2.1 Concrete quality

Based on the ultrasonic wave velocities presented in Sections 2.1.6.1.1 and 4.1.1 Wave velocity and data from Table 2-4. Wave velocity can be used estimate the overall quality of the concrete. For the wave velocities in 4.1.1 the concrete quality is "Good" with reference to Malhotra's study and "Fair/ Medium" with Leslie and Chessman's research.

4.2.2 Strength determination

With the use of Equation 2-2 from Jones's report on pressure wave velocity determination, Section 2.1.6.2.1 , and the assumption of a Poisson's ratio of 0.15 and density of concrete to be 145 $\frac{\text{lb}}{\text{ft}^3}$ $\left(2300\ \frac{\text{kg}}{\text{m}^3}\right)$, there is a reasonable estimation of the strength of concrete at each loading stage.

Table 4-7 highlights the summary of the compressive strength for specimen 9 at the individual loading stage in the prism. The determined compressive strengths are close to the measured compressive strength of 6,000 psi and after the increase in load there is an evident decrease strength. Furthermore, the reduction in compressive strength demonstrates the damage from the previous loading in the concrete.

Table 4-7 Strength calculation using Jones P-wave velocity equation

Loading	Vp (ft/s)	Vp (km/s)	E (MPa)	f 'c (MPa)	f 'c (psi)
0	14,741	4.493	43,973	42.98	6,233
20%	14,663	4.469	43,509	42.07	6,102
40%	14,620	4.456	43,254	41.58	6,031
60%	14,497	4.419	42,530	40.20	5,831
80%	14,376	4.382	41,823	38.88	5,638

Chapter 5 Conclusions

The objective of this research was to determine which wave characteristics can be related to the load level (stress) or damage (caused by micro-cracking due to previous loading) in the concrete such that evaluation of stress and damage can be conducted in the field. This chapter will give the conclusions from the series of experimental tests using ultrasonic waves in concrete. Future work that can be performed to help continue this research will also be discussed.

5.1 Time of Flight (TOF)

The increasing TOF readings for the damaged (unloaded) specimens indicates that the TOF increases as the micro-cracking caused by the previous load slows down the ultrasonic wave in the concrete, as expected. It is surprising that there is a difference in TOF even with a 20 percent f'_c previous load as this load level is generally considered to be well within the elastic range of the concrete. At a low level of load, the effect of the load (decreasing the TOF) is greater than the effect of the damage due to micro-cracking in the concrete causing the decrease in TOF at low levels of load. At higher levels of load the damage effect becomes greater and the overall TOF increases. The change in TOF due to previous damages is as great at the change in TOF due to the compressive load. Therefore, damage from previous loading will affect the wave velocity and impact the stress measurement. This result indicates that any ultrasonic method based on TOF will have to account for the damage due to previous loading in the concrete because that effect can be greater than the effect of the load itself.

Furthermore, the slope of the unloaded TOF readings with previous load level is different between the specimens. This difference in the specimens of the same concrete would make it difficult to use the TOF as a way to determine the stress level or damage in the concrete.

5.2 Frequency harmonics

The amplitude of higher harmonics in the frequency spectra of the waveform is generally decreasing with increasing stress level and damage. There is a strong linear decrease as seen in the second harmonic. However, the third harmonic change is not as clearly distinguishable. Furthermore, the slope of specimen 9 was 80% greater than specimen 8. Because of the significantly different trend in two specimens of the same concrete, it may be difficult to determine the stress or damage level with only the amplitude readings.

5.3 Concrete quality

Based on the ultrasonic wave velocities that are presented in Table 4-2 and Table 4-3 past research was used to assess the quality of the concrete. The faster the pulse velocity is, the higher the density of the concrete. As a result of having a high density in concrete this correlates to a better and strong concrete. To demonstrate the quality of the concrete, the calculated velocities in Section 4.1.1 Wave velocity proved that the quality was “Good” with reference to Malhotra’s study. And resulted in the “Fair/ Medium” condition as the assumption with Leslie and Chessman’s research.

5.4 Concrete strength

Using the wave velocities, the strength of the concrete was estimated at each loading stage [18]. The determined compressive strengths are close to the measured compressive strength of 6,000 psi. As the load increases there is an apparent decrease in strength. The reduction in compressive strength demonstrates the damage from the previous loading in the concrete.

5.5 Future Research

To help ensure this type of testing can be repeatable and reliable there needs to be further testing of plain concrete. Additional testing of specimens may yield information in the variability of the data such that a repeatable link to the stress or damage can be determined. Eventually testing of actual reinforced concrete members and field testing will verify the suitability of the method. Only two methods were able to quantify the ultrasonic testing results. Additional analysis techniques such as the waveform energy or coda wave analysis may yield better results. Finally, analysis of ultrasonic waves in concrete could be used in the investigation of fire damaged concrete.

References

[1] A. Viglucci, N. Nehamas and J. Staletovich, "Cracks where FIU bridge buckled may have signaled 'imminent failure'," Miami Herald, 7 May 2018. [Online]. Available: https://www.miamiherald.com/news/local/community/miami-dade/article210449384.html.

[2] J. R. Clifton and N. J. Carino, "Nondestructive Evaluation Methods for Quality Acceptance of Installed Building Materials," *National Bureau of Standards,* vol. 87, no. 5, pp. 407 - 438, 29 July 1982.

[3] ASTM, "Standard Test Method for Penetration Resistance of Hardened Concrete," 2017. [Online]. Available: https://www.astm.org/Standards/C803.htm.

[4] J. Industries, "Probe Strength Table," 2016. [Online]. Available: http://www.ndtjames.com/v/vspfiles/templates/james10/images/Windsor/Windsor_Probe_Strength_Tables.pdf.

[5] ASTM, "Standard Test Method for Rebound Number of Hardened Concrete," 2013. [Online]. Available: https://www.astm.org/Standards/C805.htm.

[6] ASTM, "Standard Test Method for Pullout Strength of Hardened Concrete," 2015. [Online]. Available: https://www.astm.org/Standards/C900.htm.

[7] "Guidebook on non-destructive testing of concrete structures," Wagramer Strasse 5, Vienna, 2002.

[8] ASTM, "Standard Guide for Radiographic Examination Using Industrial Radiographic Film," 2017. [Online]. Available: https://www.astm.org/Standards/E94.htm.

[9] M. J. Sansalone and W. B. Streett, "The Impact-Echo Method," 1998. [Online]. Available: https://www.ndt.net/article/0298/streett/streett.htm.

[10] ASTM, "Standard Test Method for Measuring the P-Wave Speed and the Thickness of Concrete Plates Using the Impact-Echo Method," 2015. [Online]. Available: https://www.astm.org/Standards/C1383.htm.

[11] ASTM, "Standard Test Method for Pulse Velocity Through Concrete," 2016. [Online]. Available: https://www.astm.org/Standards/C597.htm.

[12] "ULTRASONIC PULSE VELOCITY TEST," 2018. [Online]. Available: http://www.ndtconcrete.com/ultrasonic-pulse-velocity-test.html.

[13] "Ultrasoinc Pulse Velocity Test," 2018. [Online]. Available: http://www.ndtconcrete.com/ultrasonic-pulse-velocity-test.html.

[14] K. Kishore, "Ultrasonic testing in concrete," 2017. [Online]. Available: https://www.engineeringcivil.com/ultrasonic-testing-of-concrete.html.

[15] V. M. Malhotra, Testing hardened concrete: Nondestructive methods ACI, vol. Vol. 9, Iowa State University Press, 1976.

[16] J. R. Leslie and W. J. Cheesman, "An ultrasonic Method of Studying deterioration and cracking of concrete structures," *ACI,* vol. Vol. 46, no. No. 1, pp. 17 - 36, September 1949.

[17] R. Jones, Non-Destructive Testing of Concrete, London: Cambridge University Press, 1962.

[18] Y. H. Lee and T. Oh, "The Measurement of P-, S-, and R-Wave Velocities to Evaluate the Condition of Reinforced and Prestressed Concrete Slabs," *Advances in Materials Science and Engineering,* vol. 2016, no. 1548215, pp. 1 - 15, 2016.

[19] M. Santhanam and S. A. Kumar, "Detection of Concrete Damage Using Ultrasonic Pulse Velocity Method," *National Seminar on Non-Destructive Evaluation,* pp. 301 - 308, 2006.

[20] A. S. Al-Zuheriy, "Ultrasonic Measurement of Stress in Steel and Concrete," Columbia, MO, 2018.

[21] T. Schumacher, A. Chen, S. Ozturk and N. Attoh-Okine, "Development of Rapid Assessment Tools for Structural Parts after Extreme Events ," 2013.

[22] P. Shokouhi, A. Zoëga and H. Wiggenhauser, "Nondestructive Investigation of Stress-Induced Damage in Concrete," *Advances in Civil Engineering,* vol. 2010, no. 740189, 2010.

[23] F. D. Murnaghan, Finite Deformation of an Elastic Solid, John Wiley & Sons, 1951, p. 140.

[24] I. Lillamand, J.-F. Chaix, M.-A. Ploix and V. Garnier, "Acoustoelastic effect in concrete material under uni-axial compressive loading," *NDT&E International,* vol. 43, pp. 655 - 660, 2009.

[25] D. S. Hughes and J. L. Kelly, "Second-Order Elastic Deformation of Solids," *Physcial Review,* vol. 92, no. 5, pp. 1145 - 1149, 1953.

[26] A. A. Shah, Y. Ribakov and C. Zhang, "Efficiency and sensitivity of linear and non-linear ultrasonics to identifying micro and macro-scale defects in concrete," *Elsevier,* vol. Material and Design, no. 50, pp. 905 - 916, 2013.

[27] A. Hafiz and T. Schumacher, "Monitoring o fStresses in Concrete Using Ultrasonic Coda Wave Comparison Technique," *Journal of Nondestructive Evaluation,* pp. 37 - 73, 2018.

[28] Agilent Technologies, "AGILENT/HP 54815A Datasheet," Agilent Technologies, 2001.

[29] "Model 5058PR High Voltage Pulser-Receiver," Olympus, 2009.

[30] Olympus, "Material Sound Velocities," 2018. [Online]. Available: https://www.olympus-ims.com/en/ndt-tutorials/thickness-gage/appendices-velocities/.

[31] "Pulser-Receivers," 2018. [Online]. Available: https://www.nde-ed.org/EducationResources/CommunityCollege/Ultrasonics/EquipmentTrans/pulserreceivers.htm.

[32] N. Nehmaas, A. Viglucci and M. O. Madan, "Cracks in FIU bridge grew to ‘shocking’ size days before collapse, new photos show," 9 August 2018. [Online]. Available: https://www.miamiherald.com/news/local/community/miami-dade/article216388430.html.

Appendix A: Wave form data

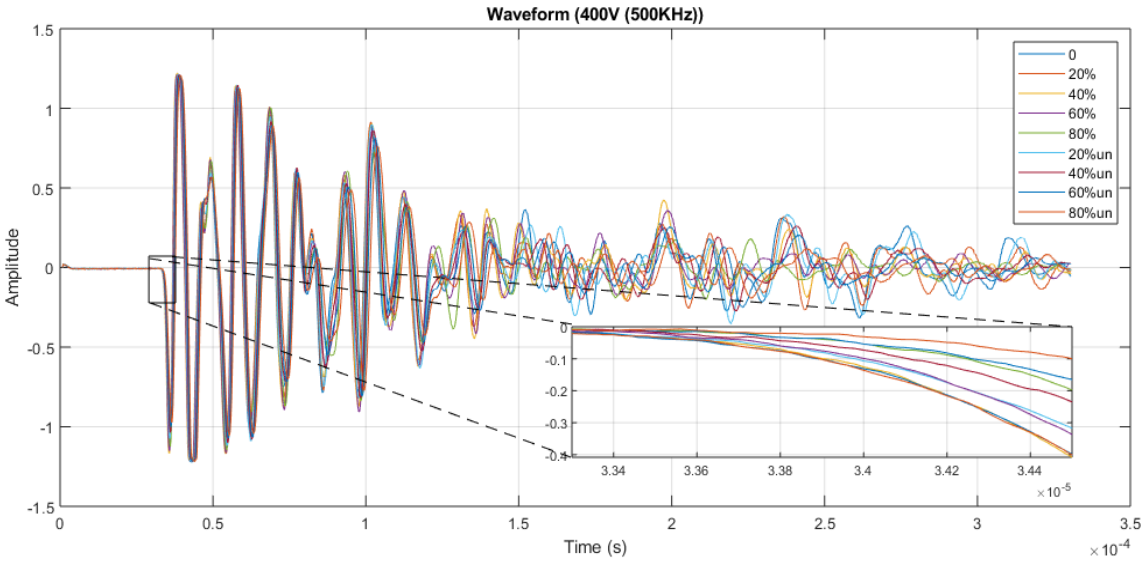

Figure A-1 Specimen 8 wet 400V

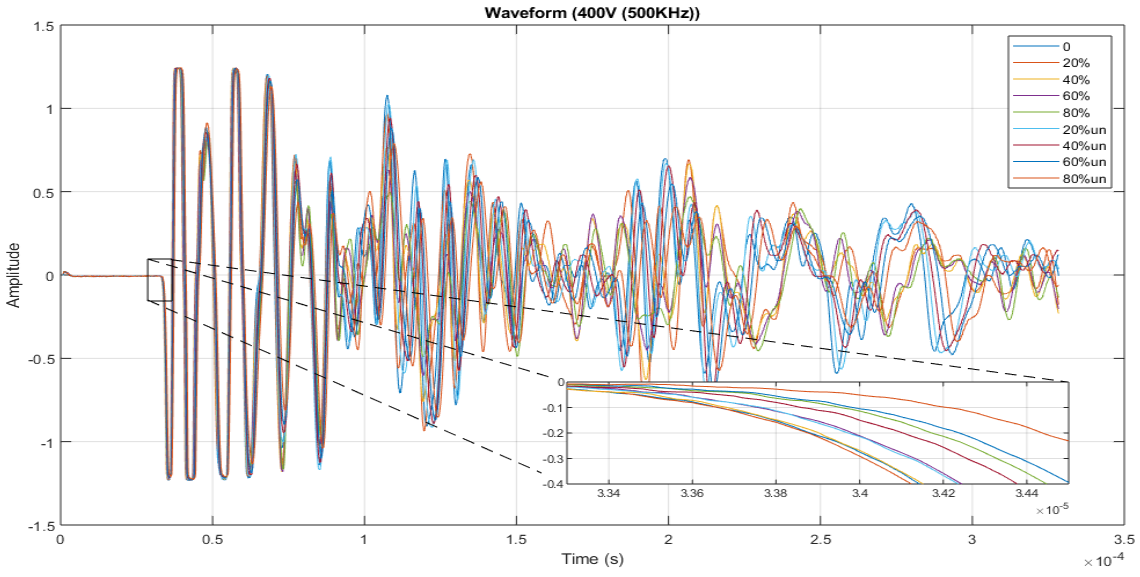

Figure A-2 Specimen 9 wet 400V

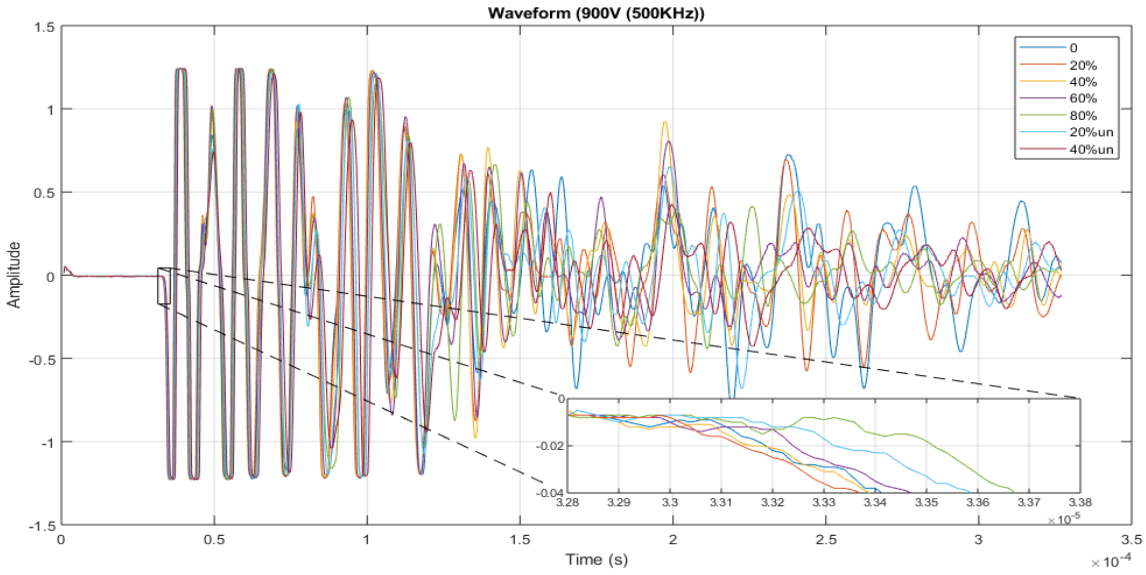

Figure A-2 Specimen 8 wet 900V

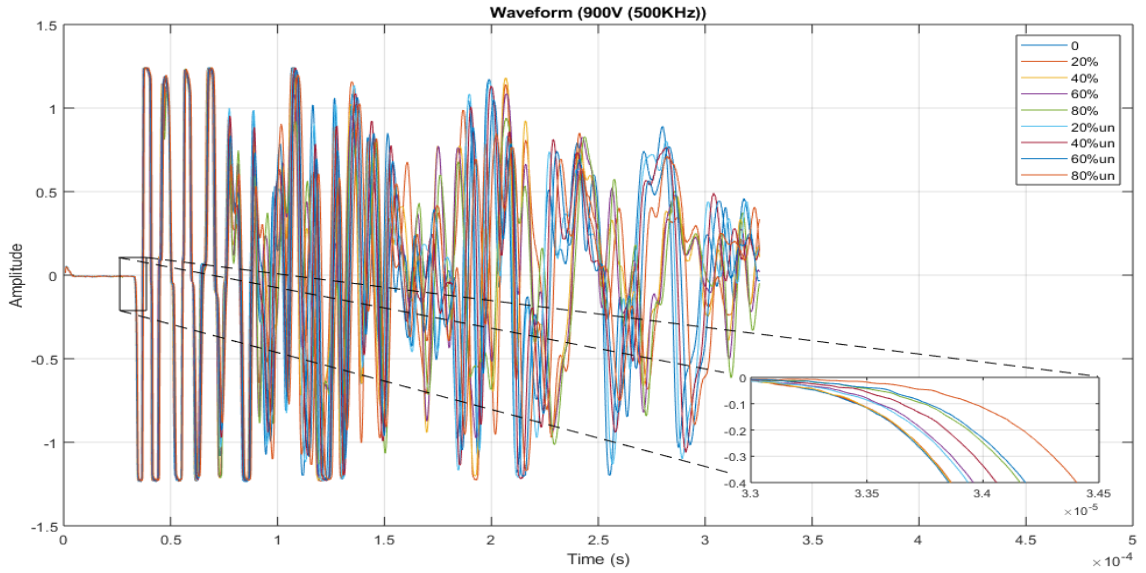

Figure A-3 Specimen 9 wet 900V

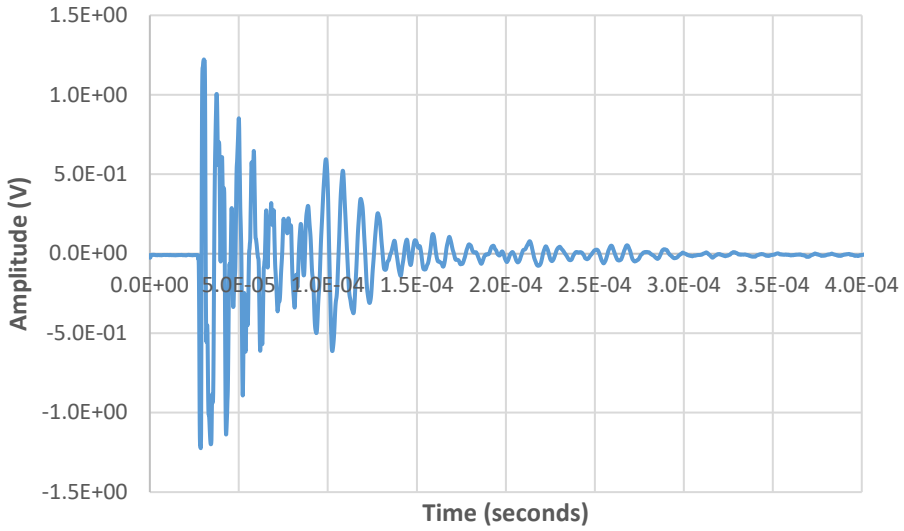

Figure A-4 Unloaded polypropylene reference specimen with 200V amplitude

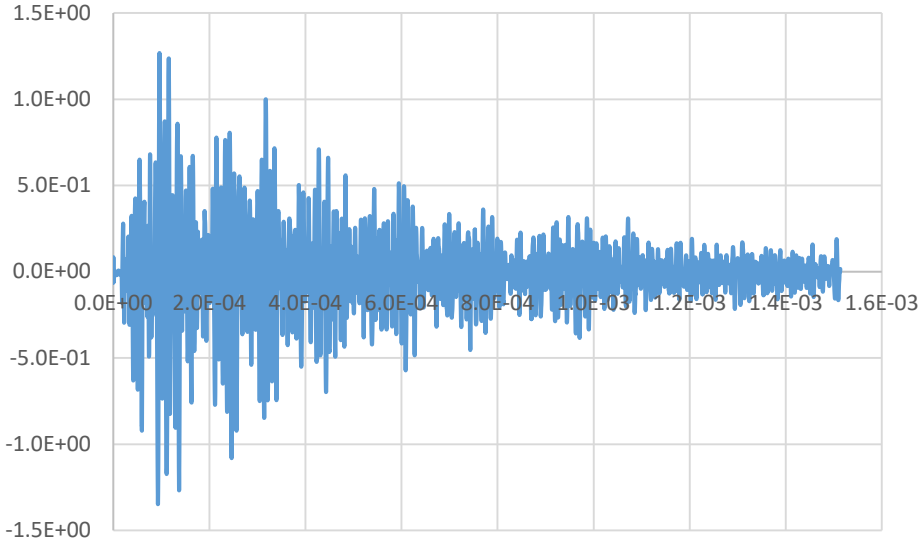

Figure A-5 Unloaded steel reference specimen with 200V amplitude

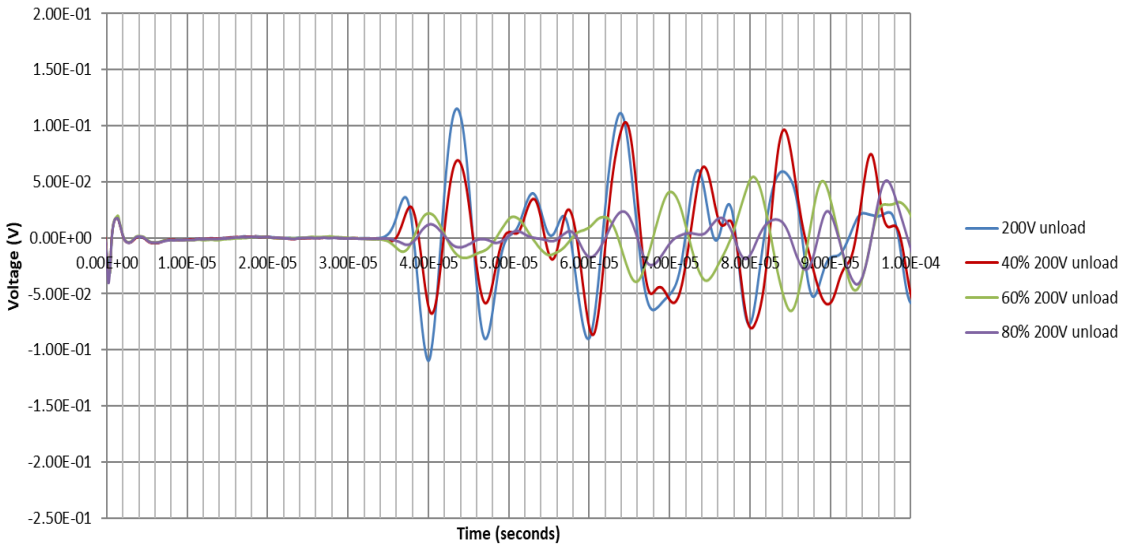

Figure A-6 Specimen 1 unloaded waveform with 200V amplitude

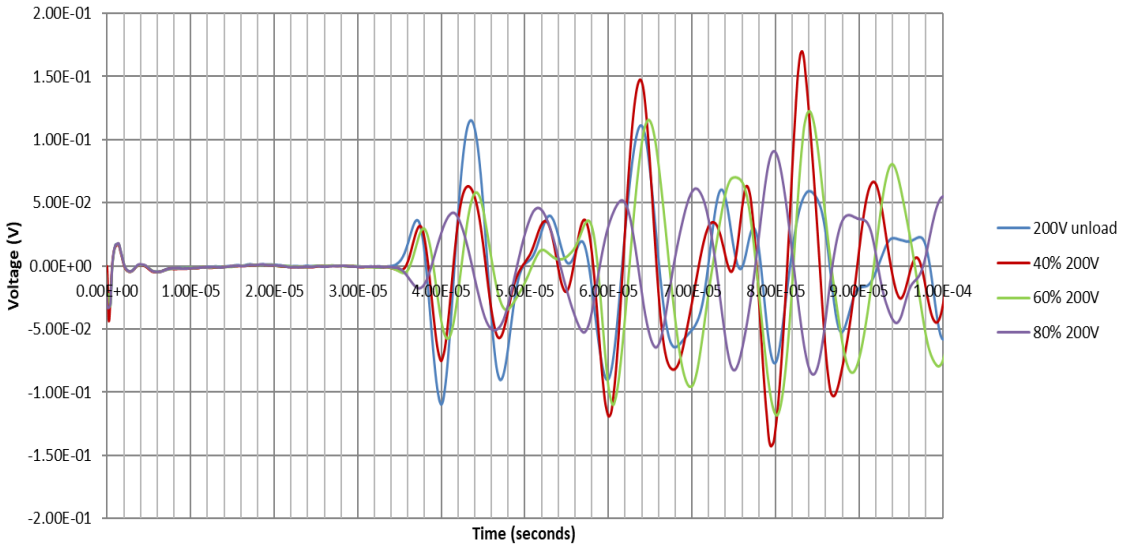

Figure A-7 Specimen 1 1oaded waveform with 200V amplitude

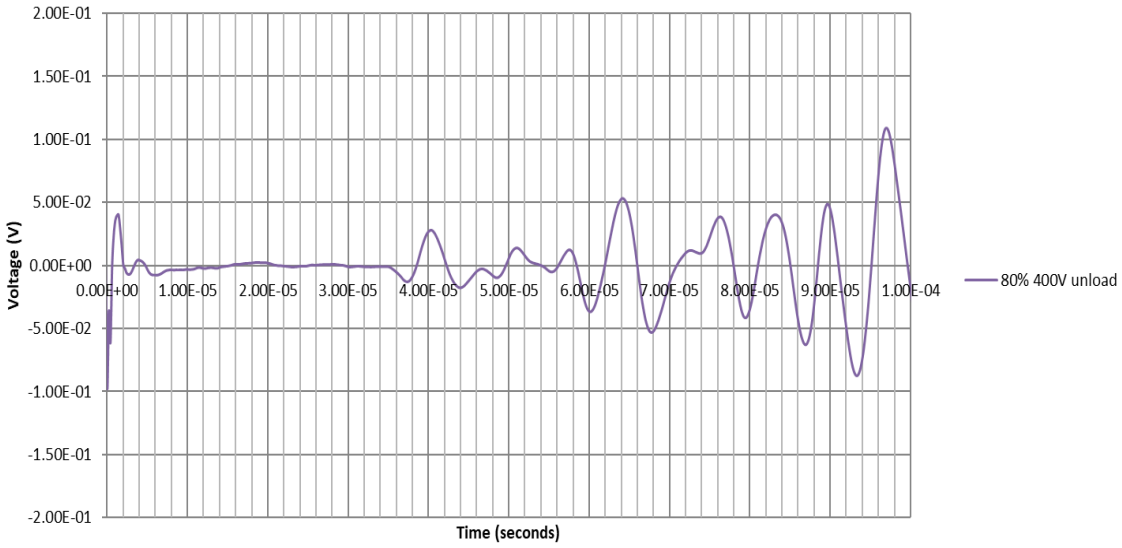

Figure A-8 Specimen 1 unloaded waveform with 400V amplitude

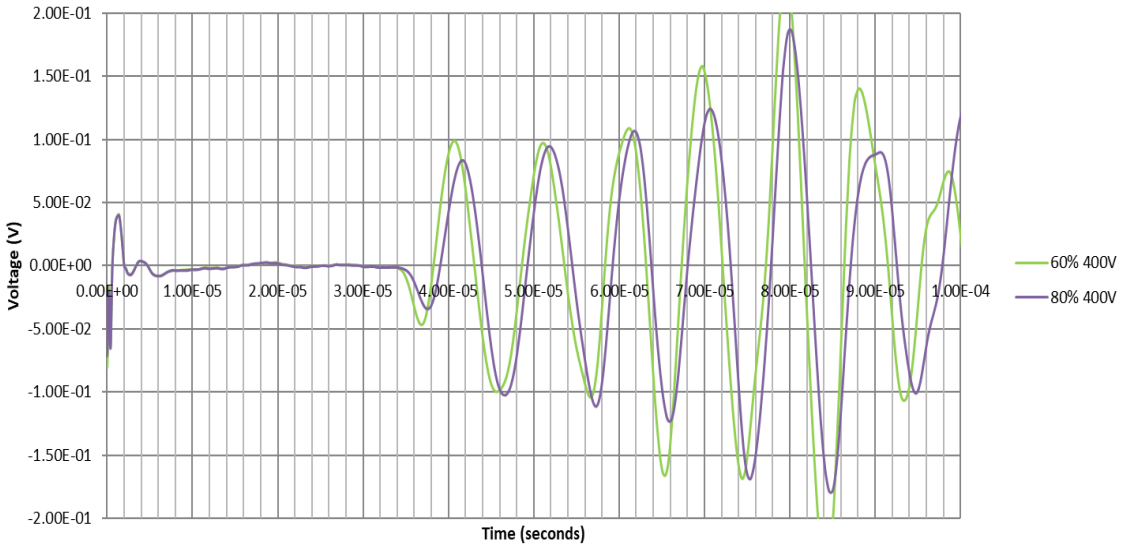

Figure A-9 Specimen 1 loaded waveform with 400V amplitude

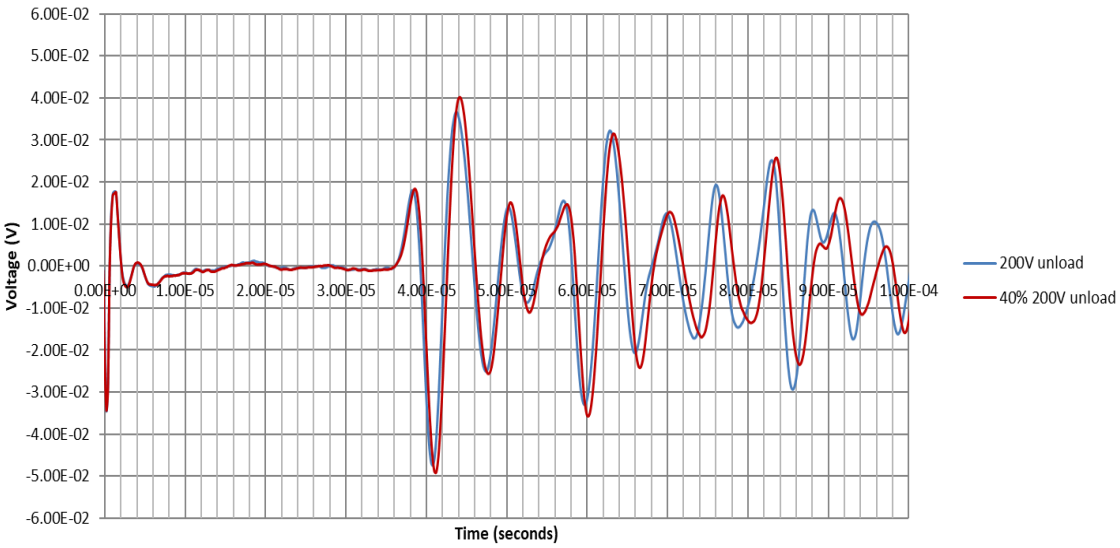

Figure A-10 Specimen 2 unloaded waveform with 200V amplitude

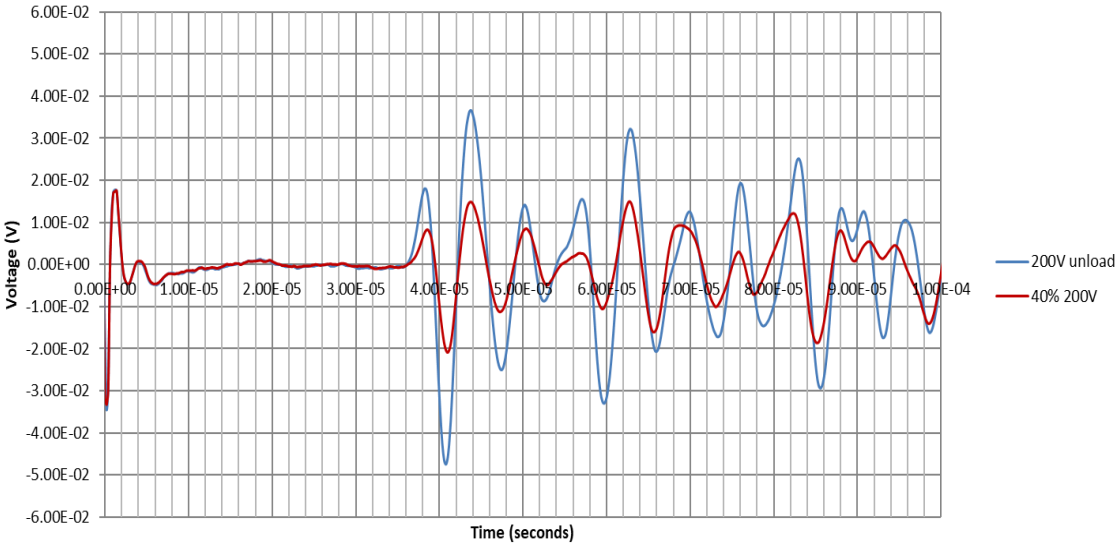

Figure A-11 Specimen 2 1oaded waveform with 200V amplitude

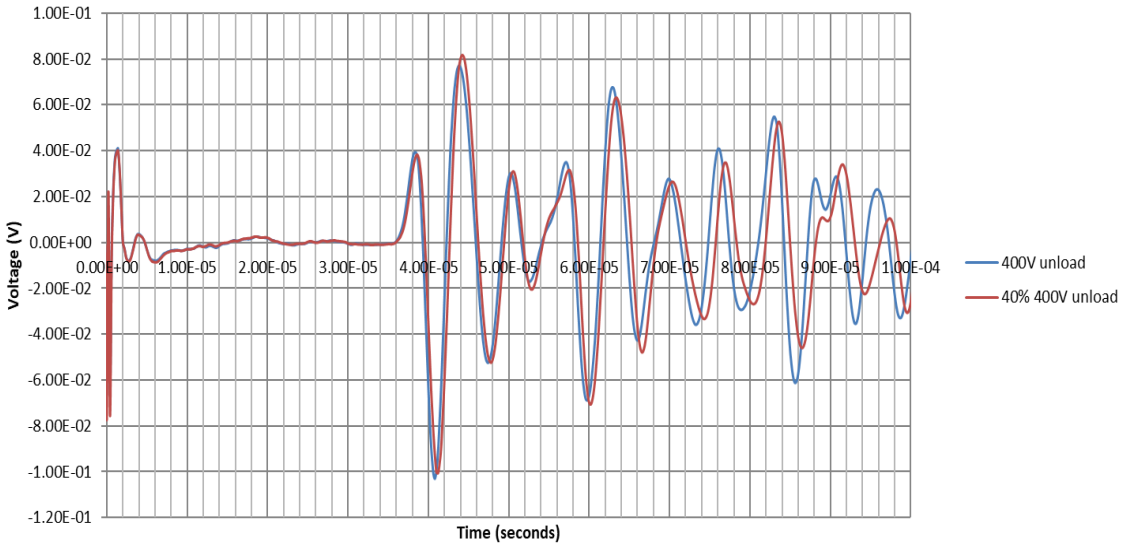

Figure A-12 Specimen 2 unloaded waveform with 400V amplitude

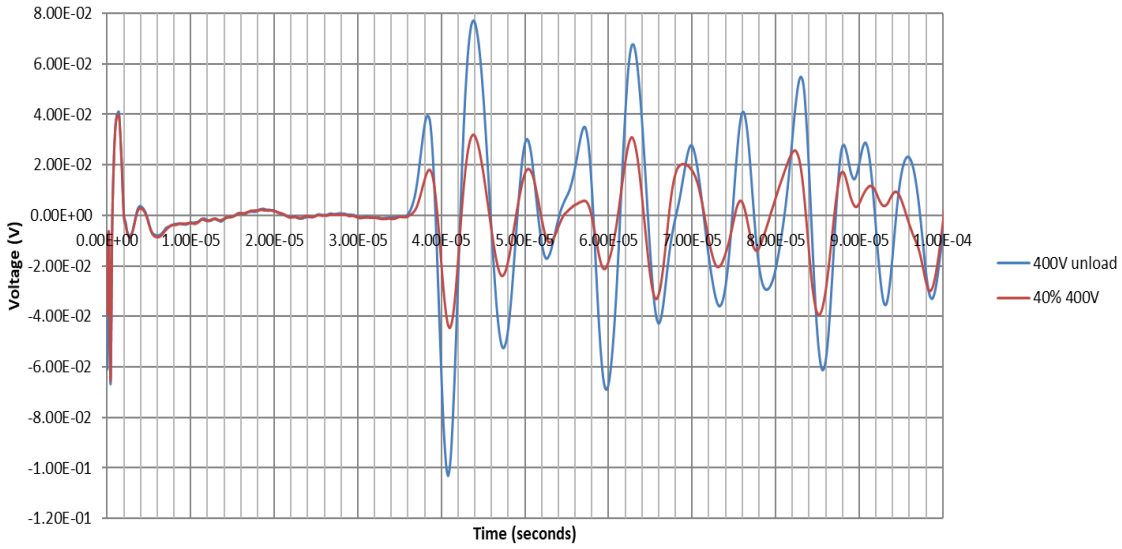

Figure A-13 Specimen 2 loaded waveform with 400V amplitude

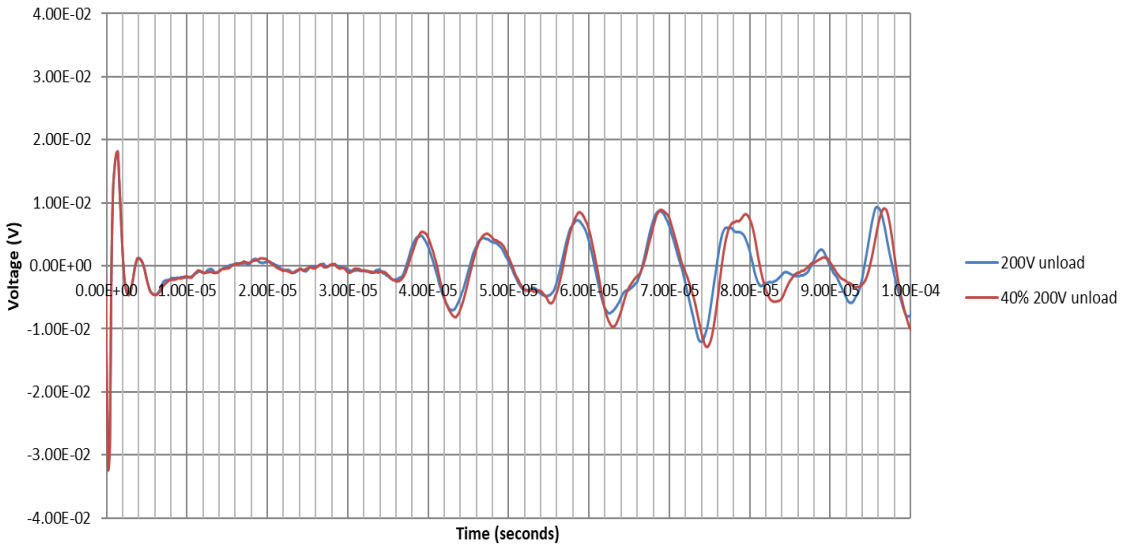

Figure A-14 Specimen 3 unloaded waveform with 200V amplitude

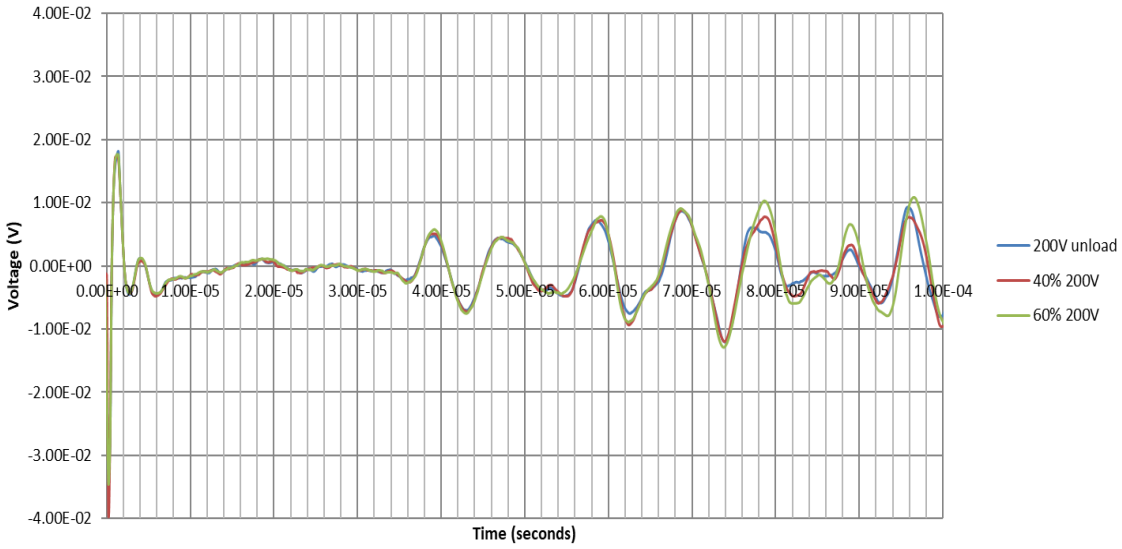

Figure A-15 Specimen 3 1oaded waveform with 200V amplitude

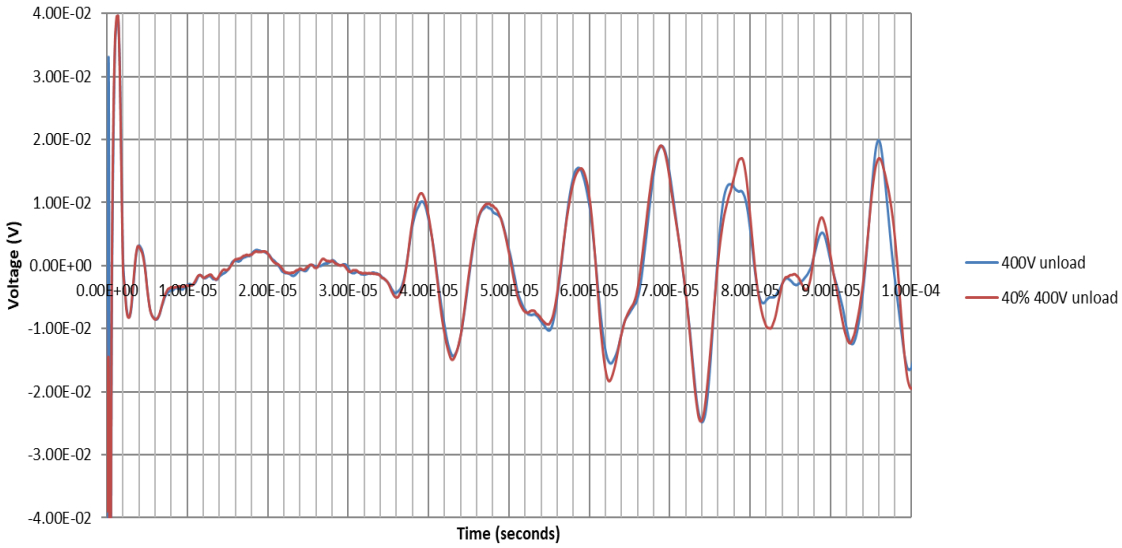

Figure A-16 Specimen 3 unloaded waveform with 400V amplitude

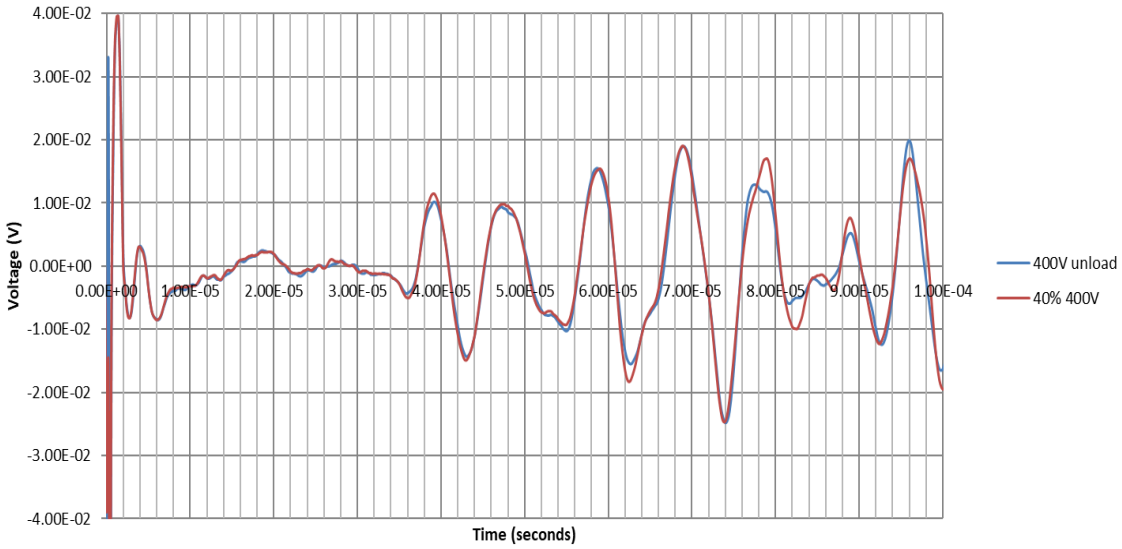

Figure A-17 Specimen 3 loaded waveform with 400V amplitude

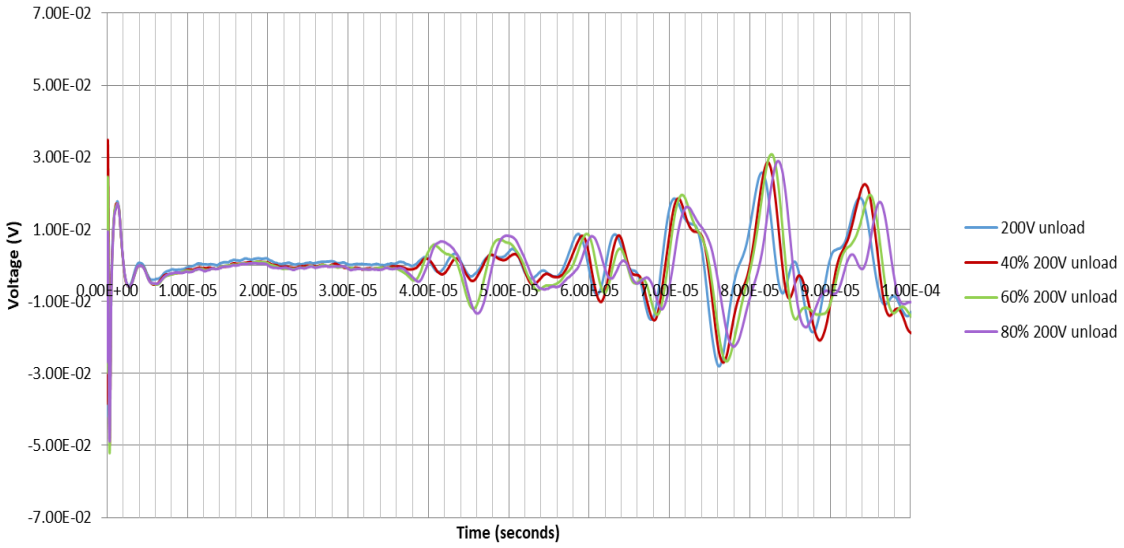

Figure A-18 Specimen 4 unloaded waveform with 200V amplitude

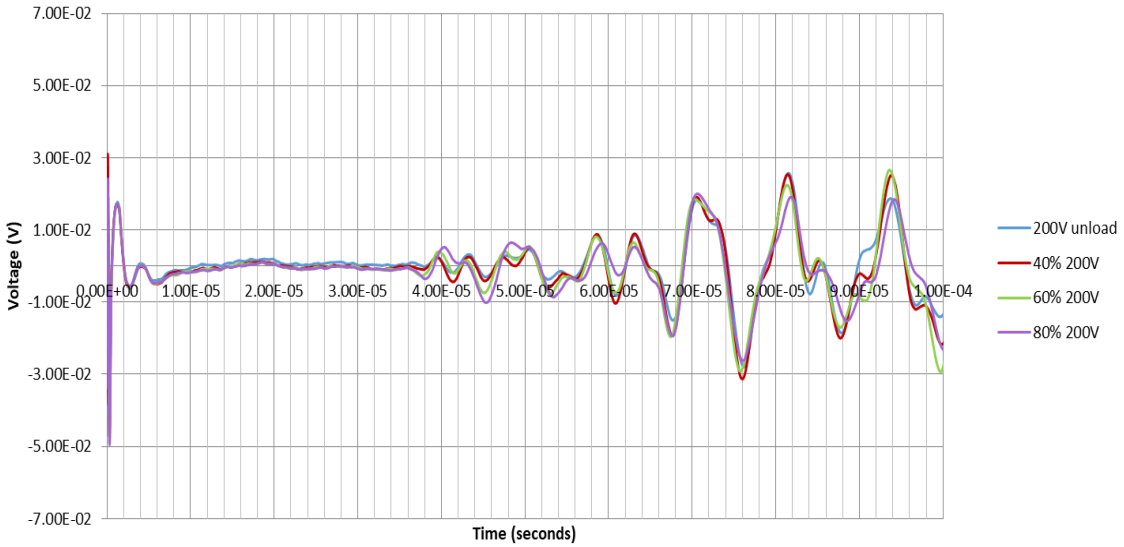

Figure A-19 Specimen 4 1oaded waveform with 200V amplitude

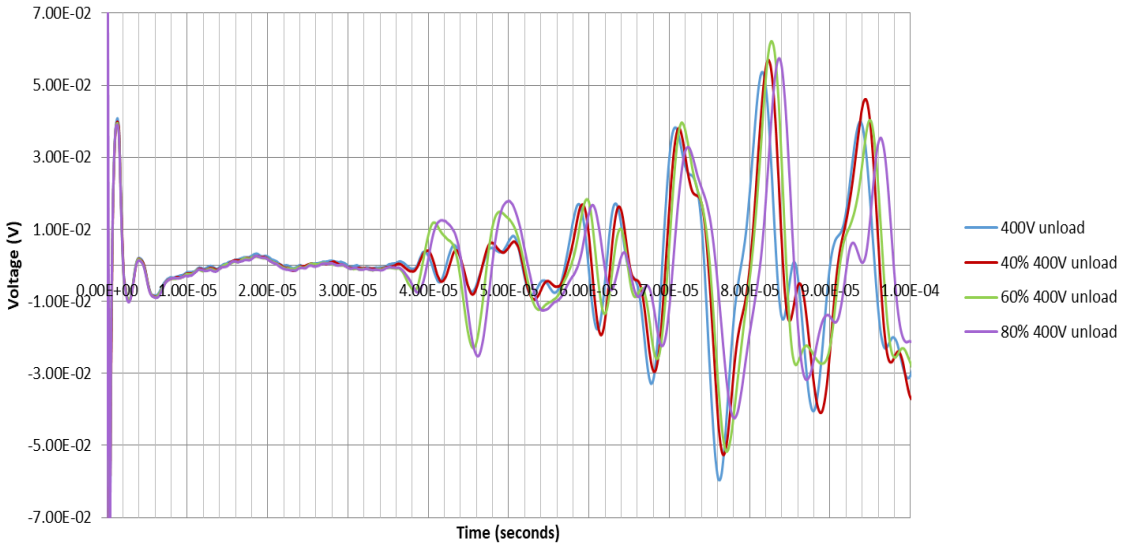

Figure A-20 Specimen 4 unloaded waveform with 400V amplitude

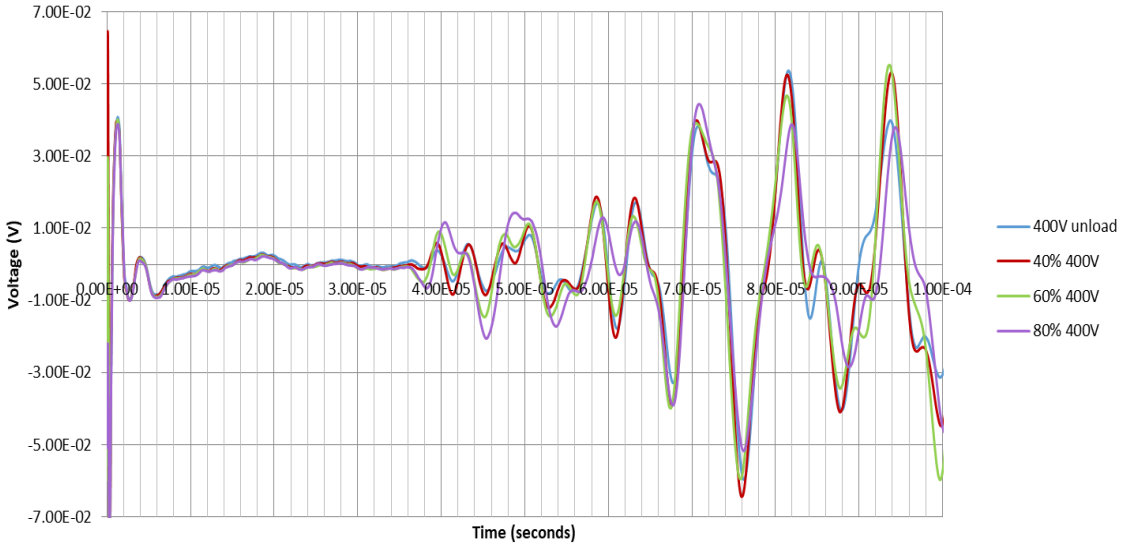

Figure A-21 Specimen 4 loaded waveform with 400V amplitude

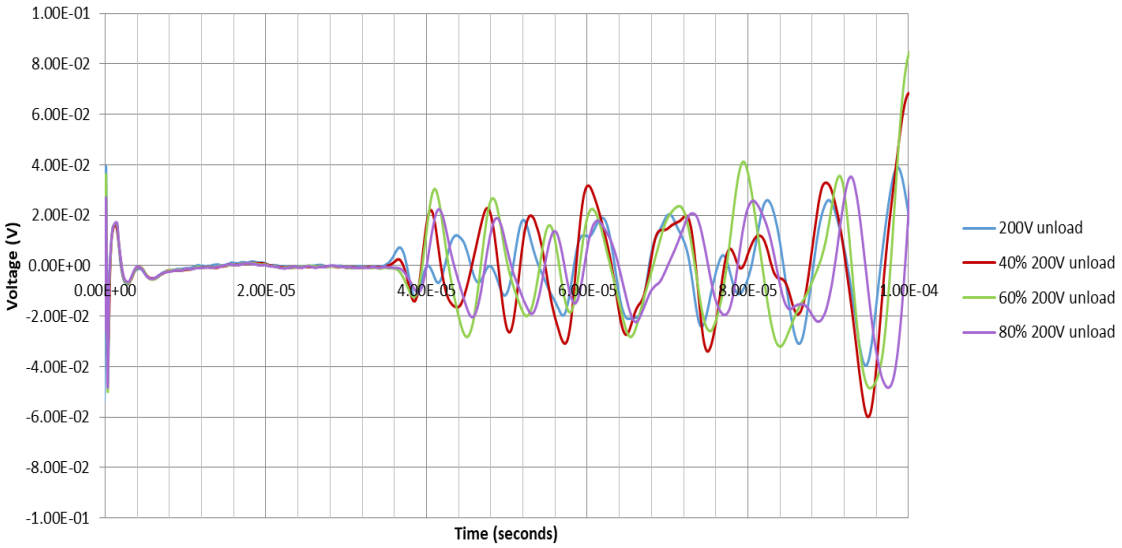

Figure A-22 Specimen 5 unloaded waveform with 200V amplitude

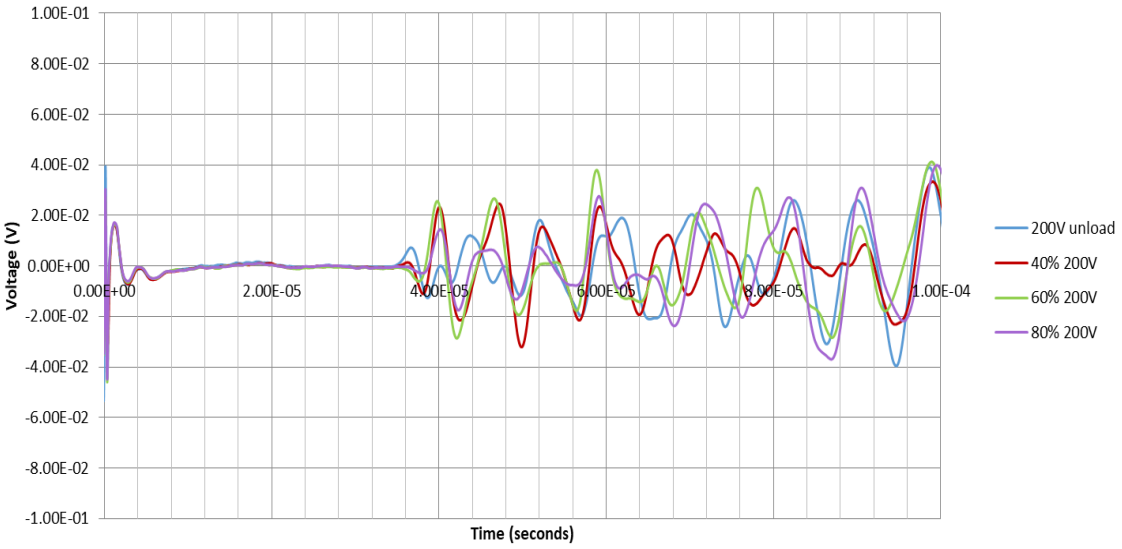

Figure A-23 Specimen 5 1oaded waveform with 200V amplitude

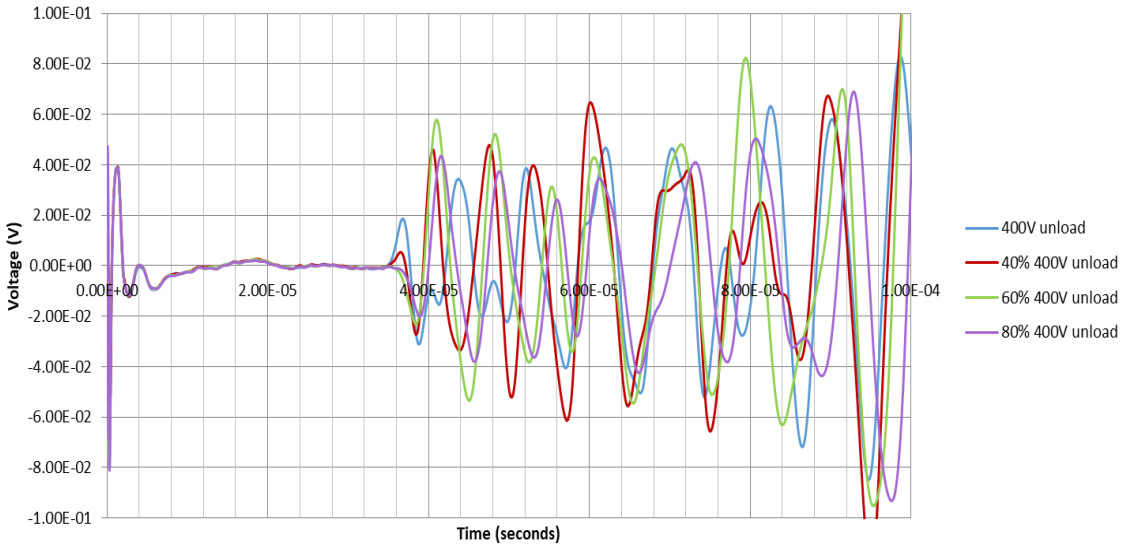

Figure A-24 Specimen 5 unloaded waveform with 400V amplitude

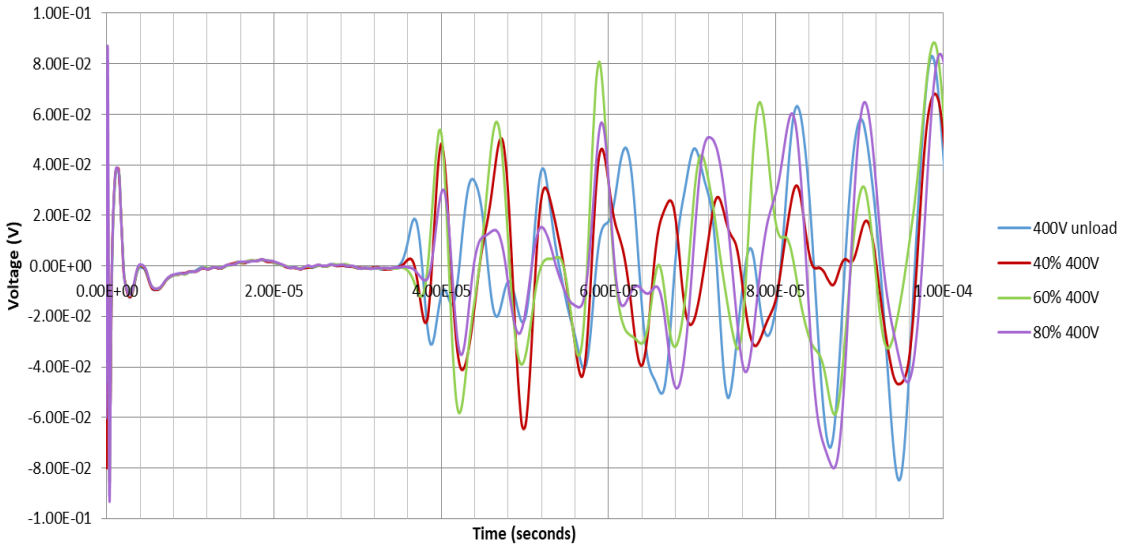

Figure A-25 Specimen 5 loaded waveform with 400V amplitude

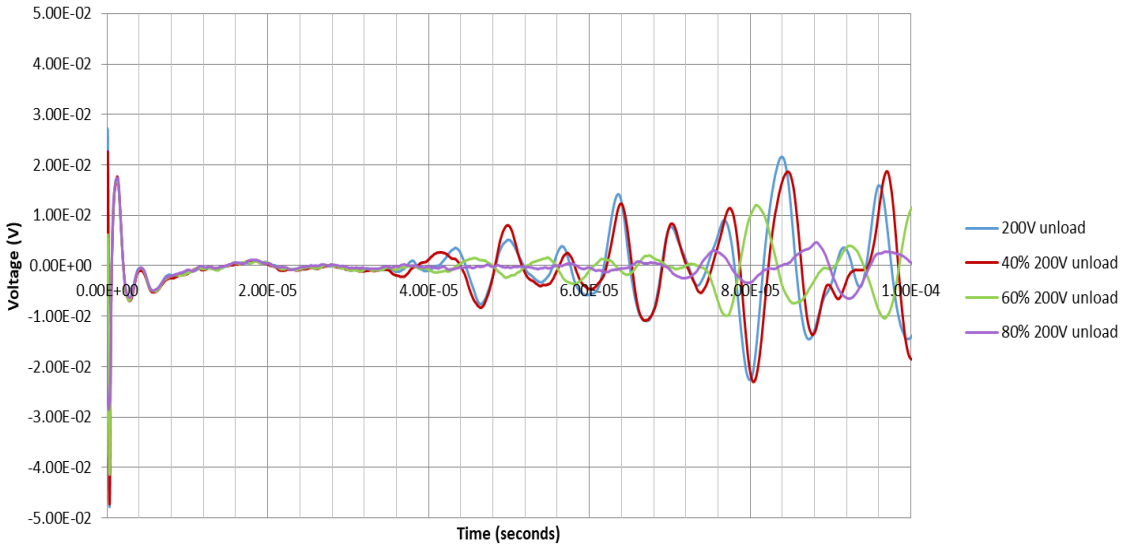

Figure A-26 Specimen 6 unloaded waveform with 200V amplitude

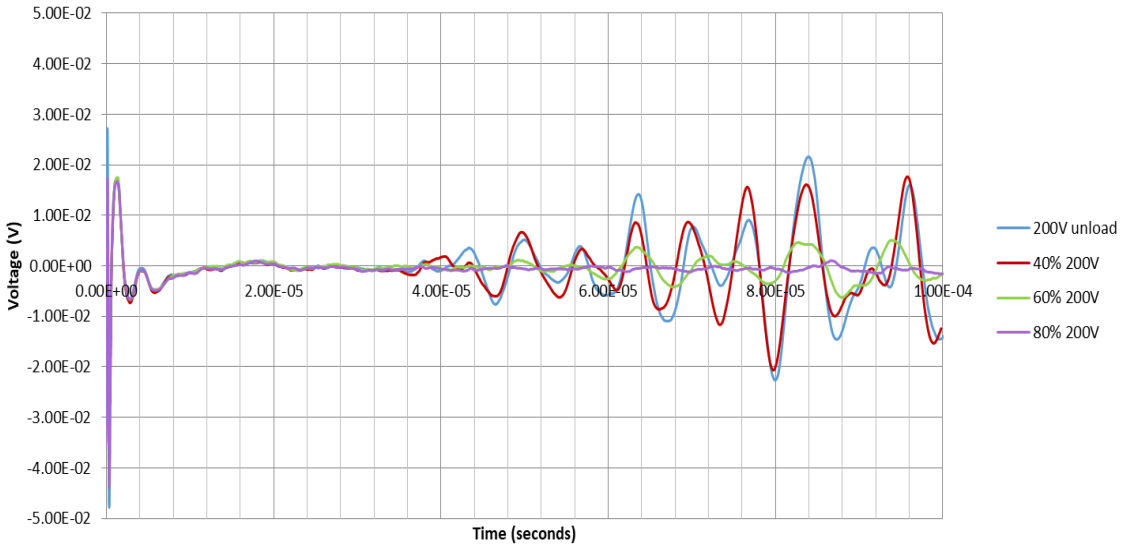

Figure A-27 Specimen 6 1oaded waveform with 200V amplitude

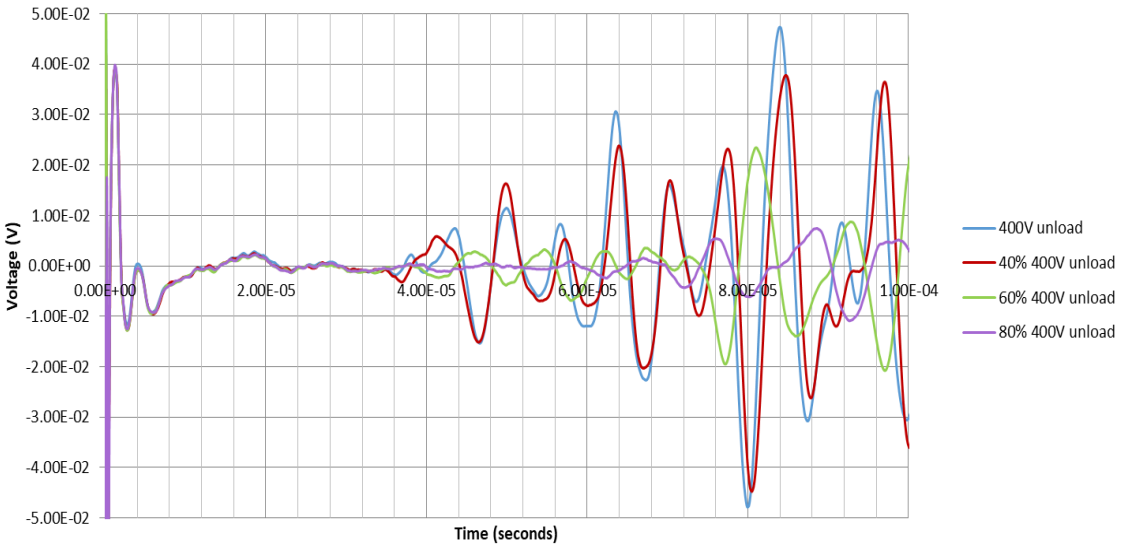

Figure A-28 Specimen 6 unloaded waveform with 400V amplitude

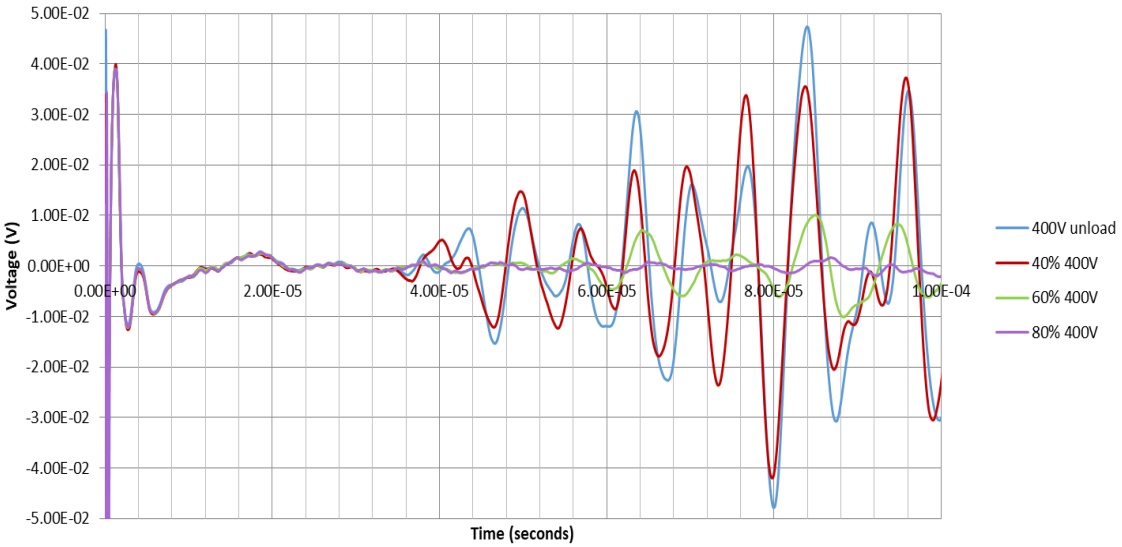

Figure A-29 Specimen 6 loaded waveform with 400V amplitude

Appendix B: Frequency plots

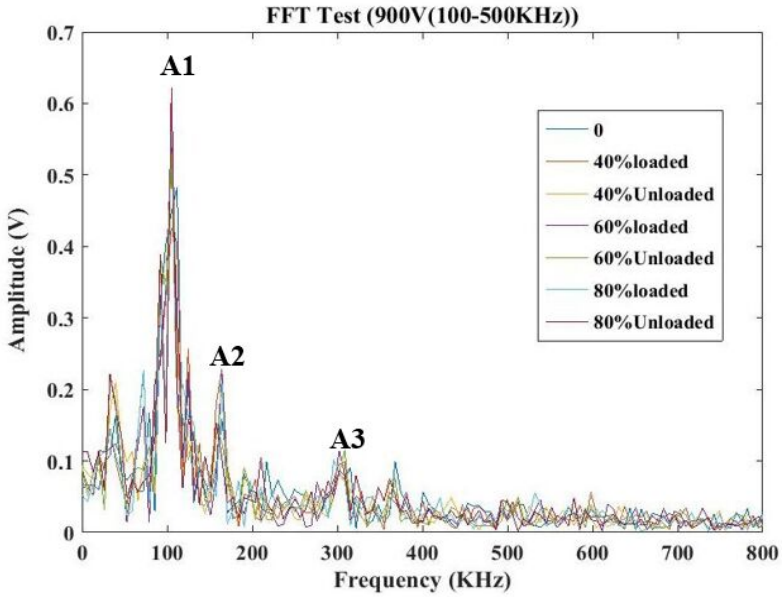

Figure B-1 Specimen 7 wet 900V

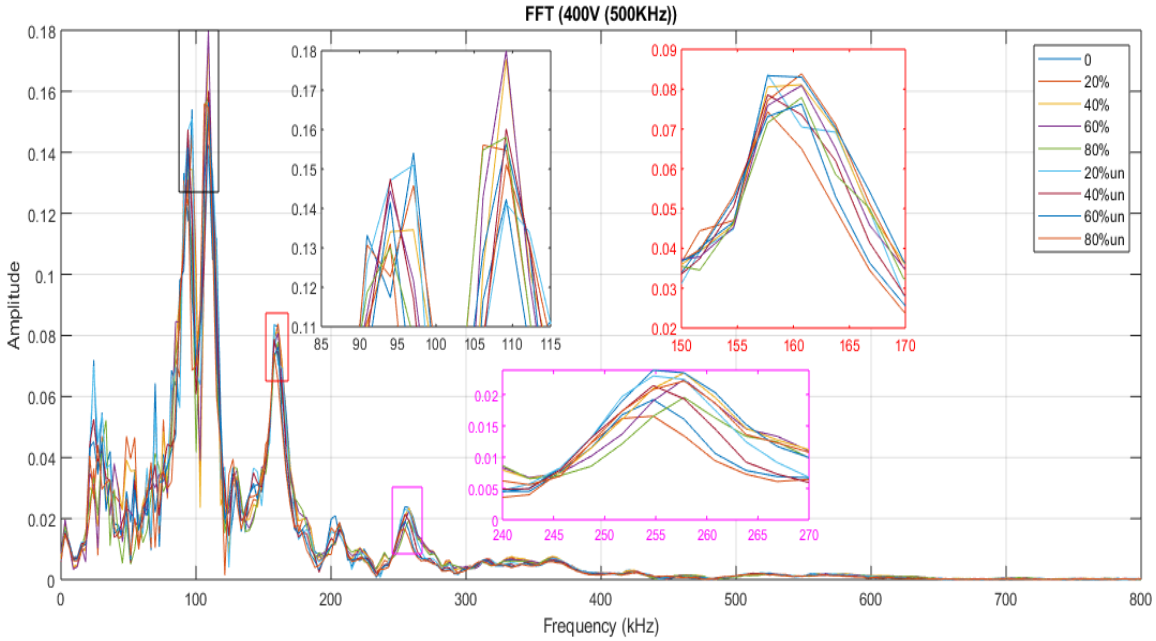

Figure B-2 Specimen 8 wet 400V

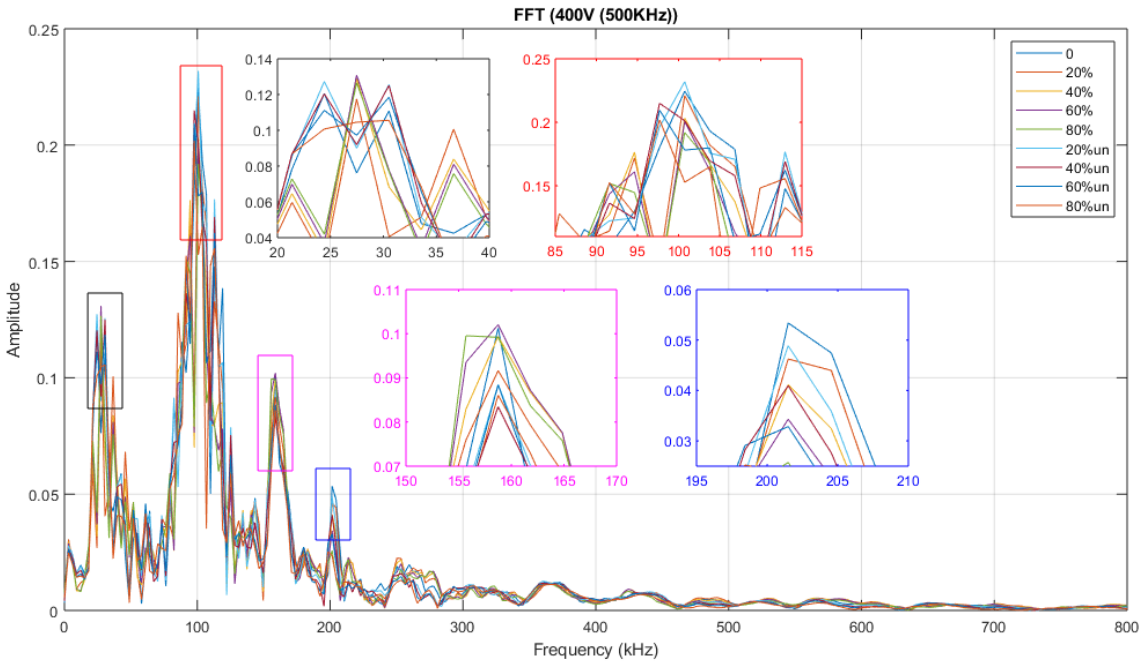

Figure B-3 Specimen 9 wet 400V

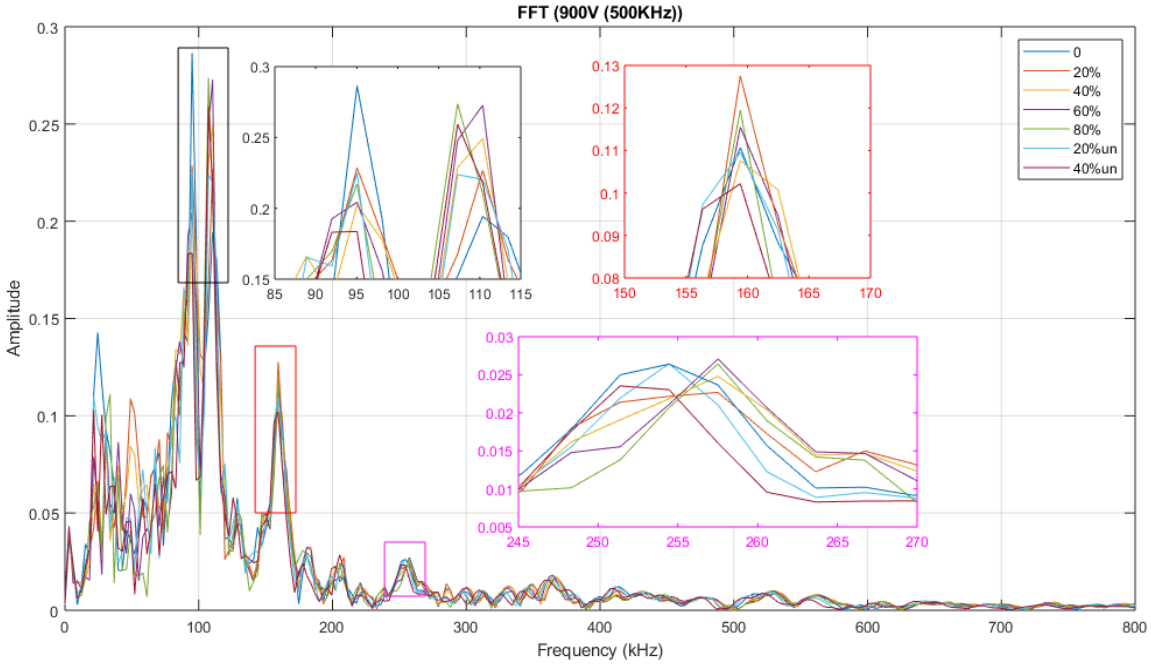

Figure B-4 Specimen 8 wet 900V

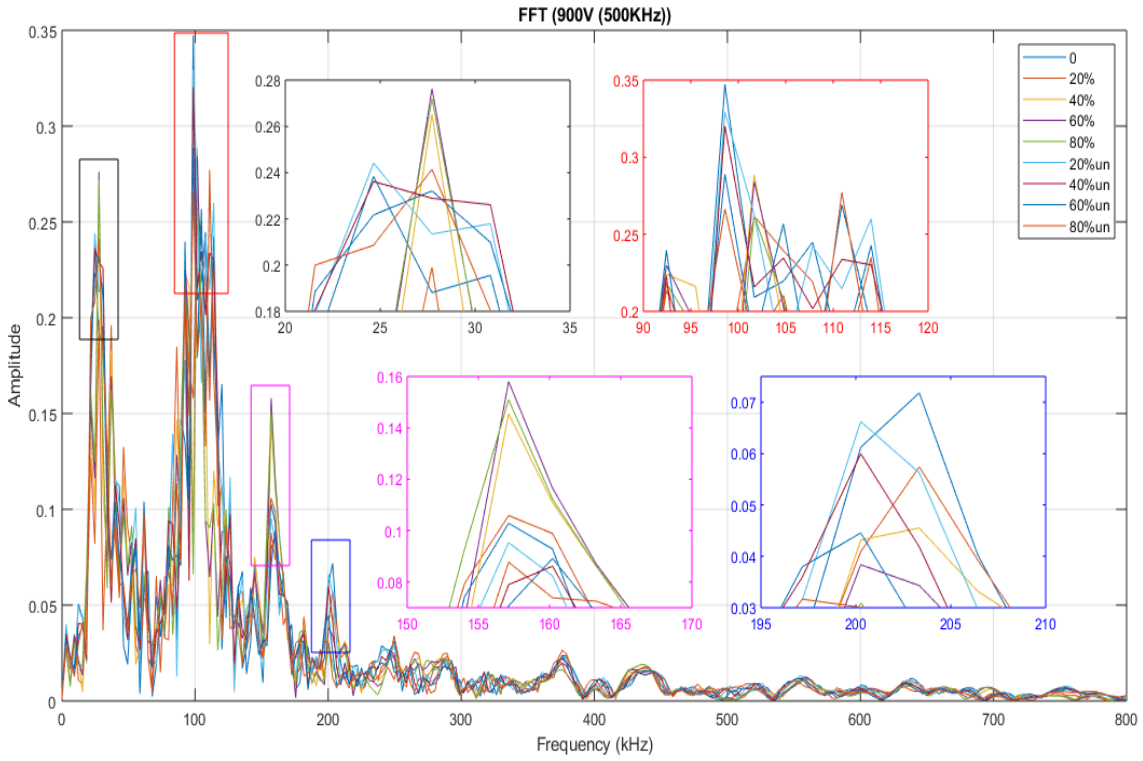

Figure B-5 Specimen 9 wet 900V

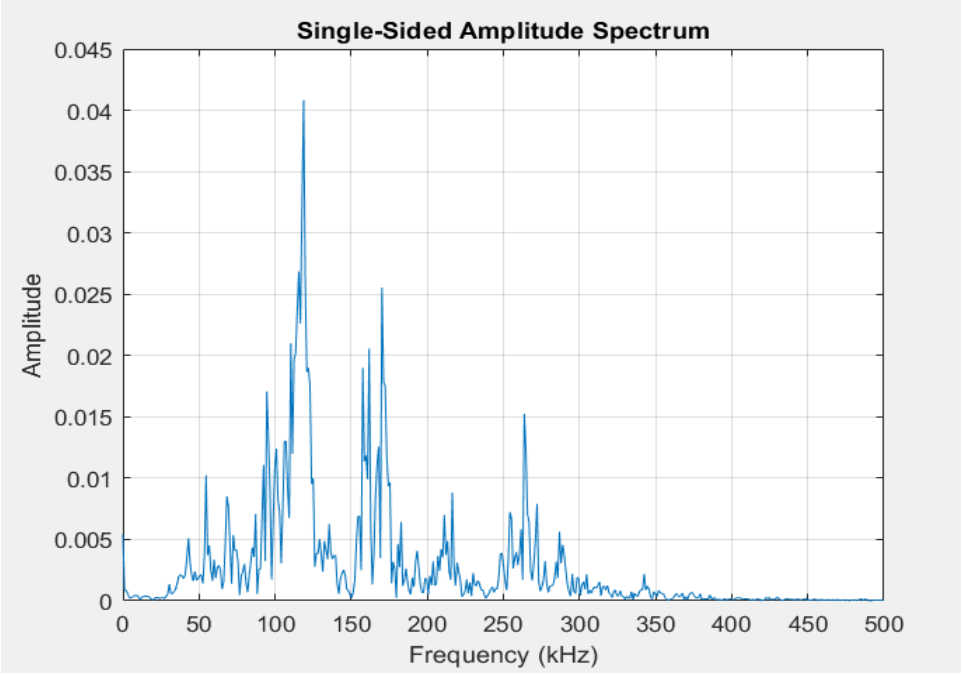

Figure B-6 Unloaded steel reference specimen 200V

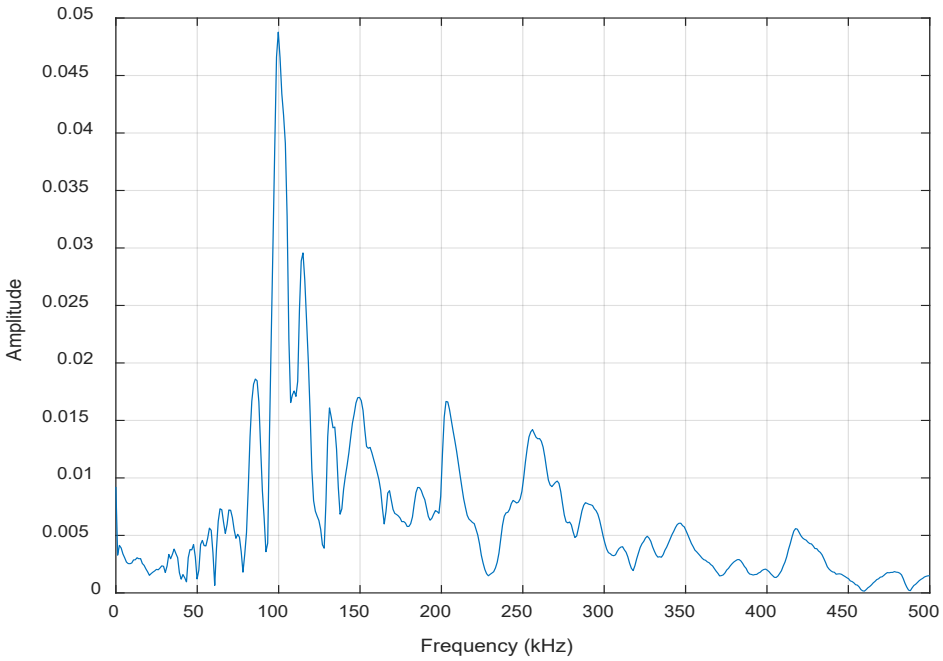

Figure B-7 Unloaded polypropylene reference specimen 200V

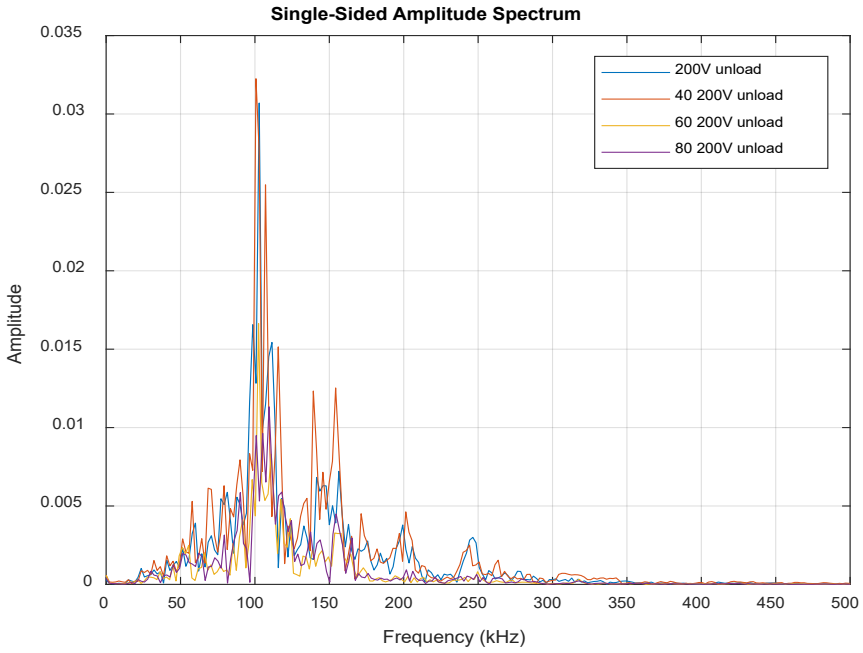

Figure B-8 Specimen 1 200V unloaded amplitude vs frequency

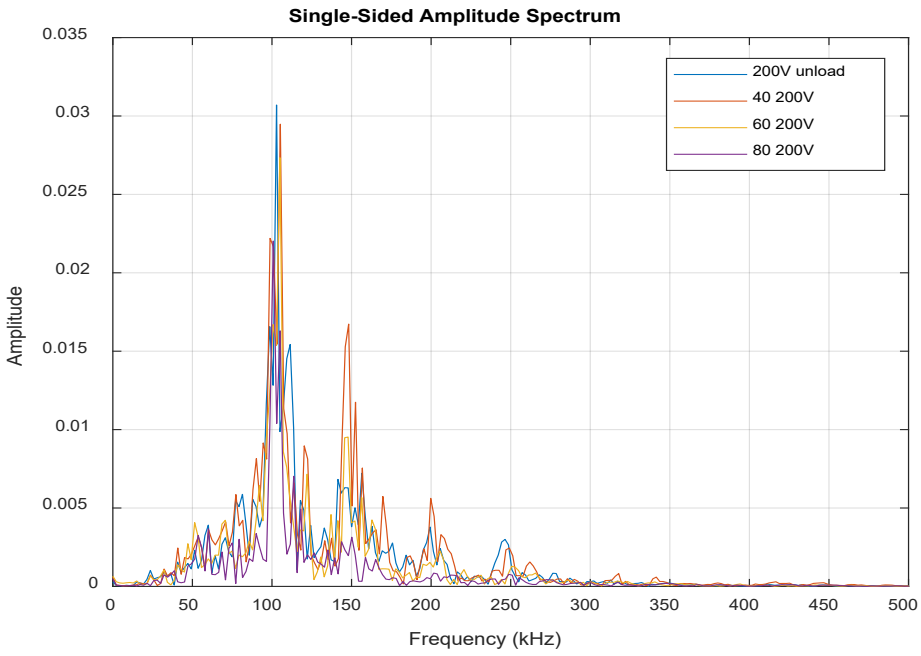

Figure B-9 Specimen 1 200V loaded amplitude vs frequency

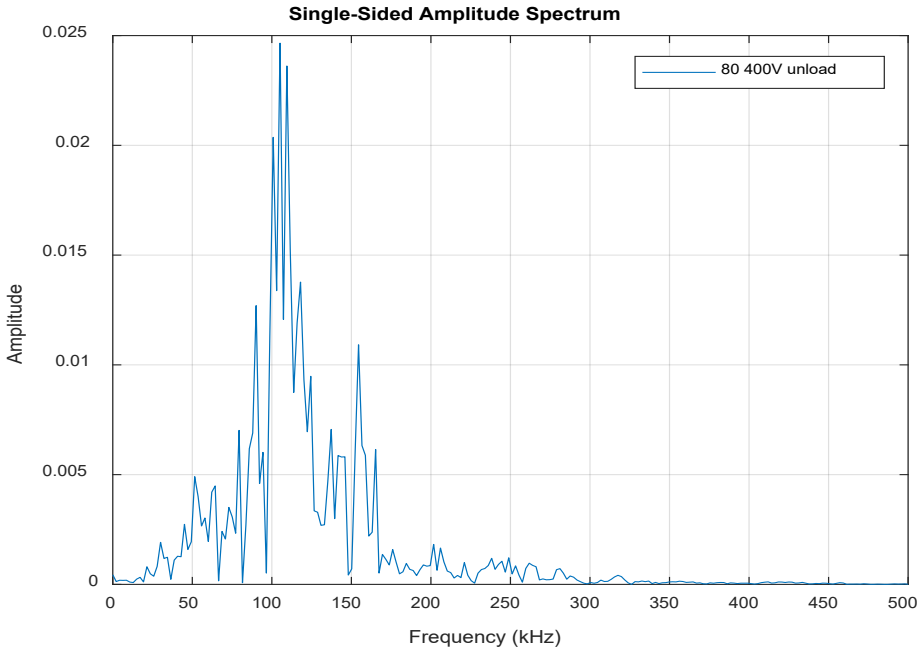

Figure B-10 Specimen 1 400V unloaded amplitude vs frequency

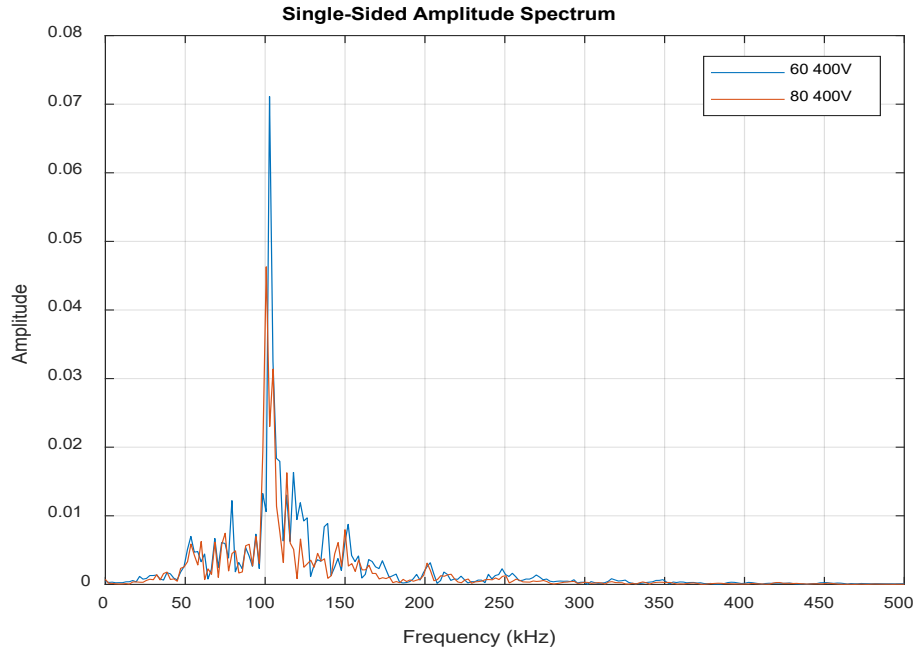

Figure B-11 Specimen 1 400V loaded amplitude vs frequency

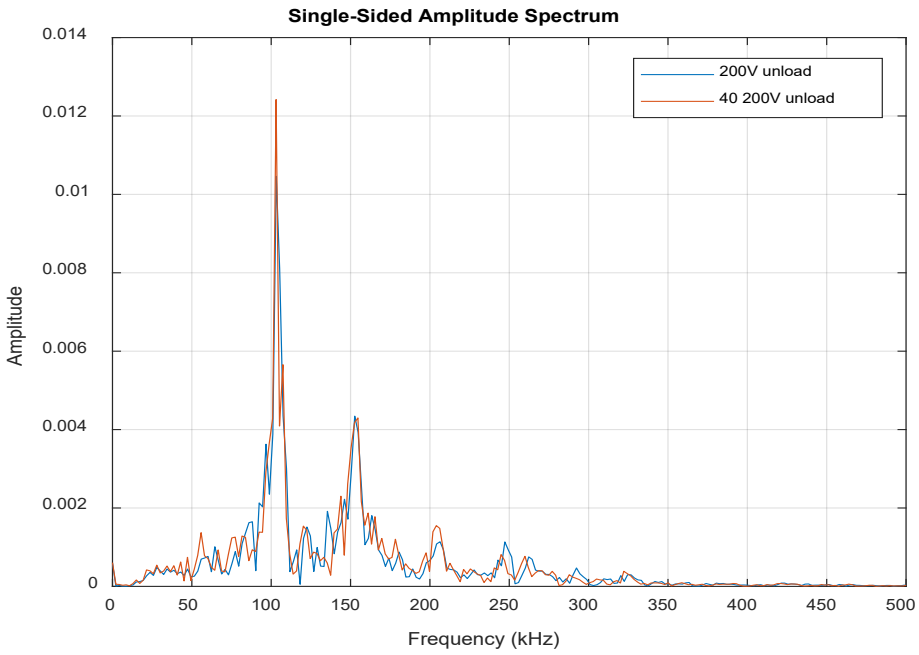

Figure B-12 Specimen 2 200V unloaded amplitude vs frequency

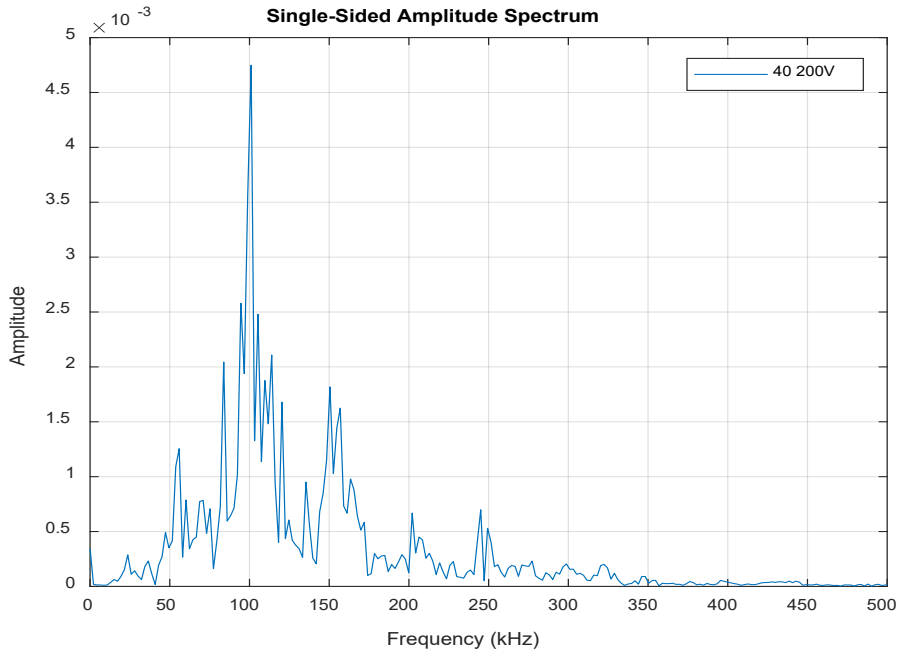

Figure B-13 Specimen 2 Mix 3 200V loaded amplitude vs frequency

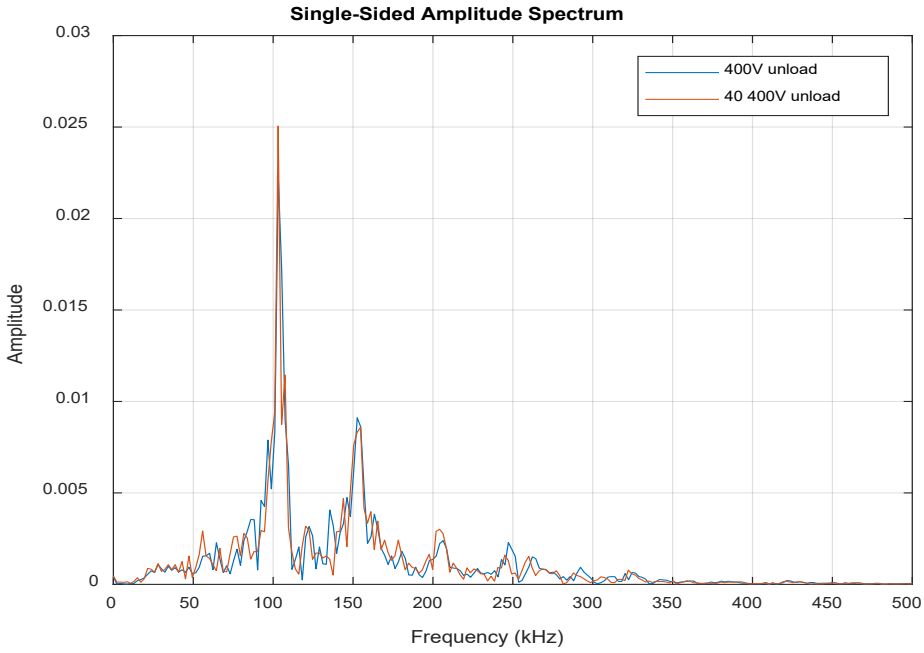

Figure B-14 Specimen 2 400V unloaded amplitude vs frequency

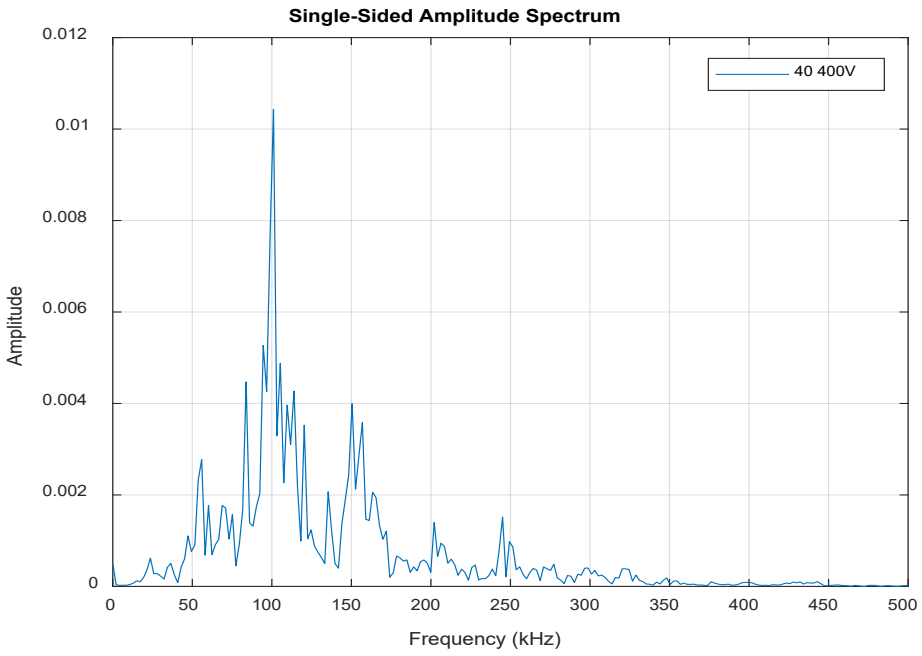

Figure B-15 Specimen 2 400V loaded amplitude vs frequency

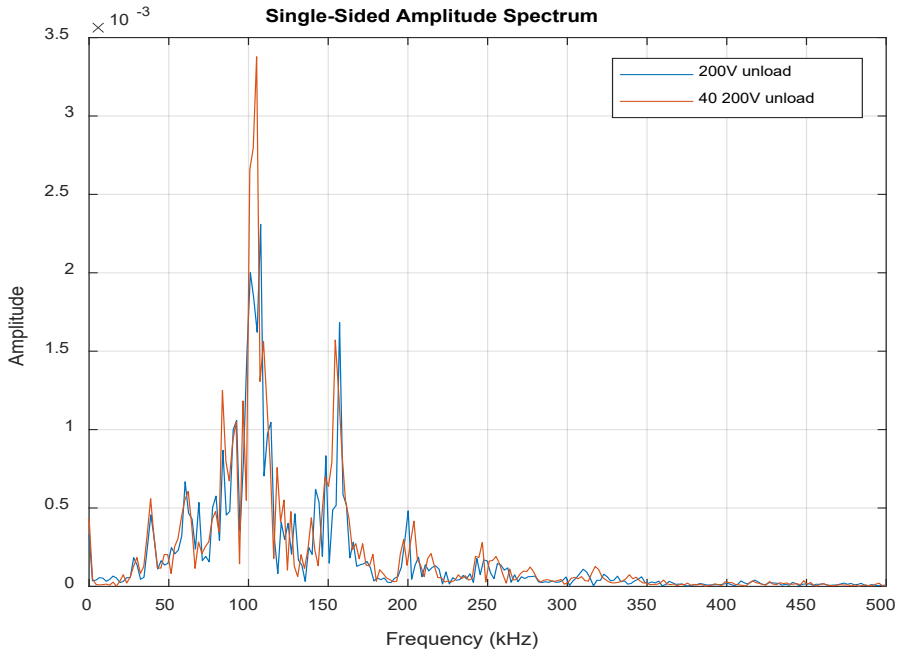

Figure B-16 Specimen 3 200V unloaded amplitude vs frequency

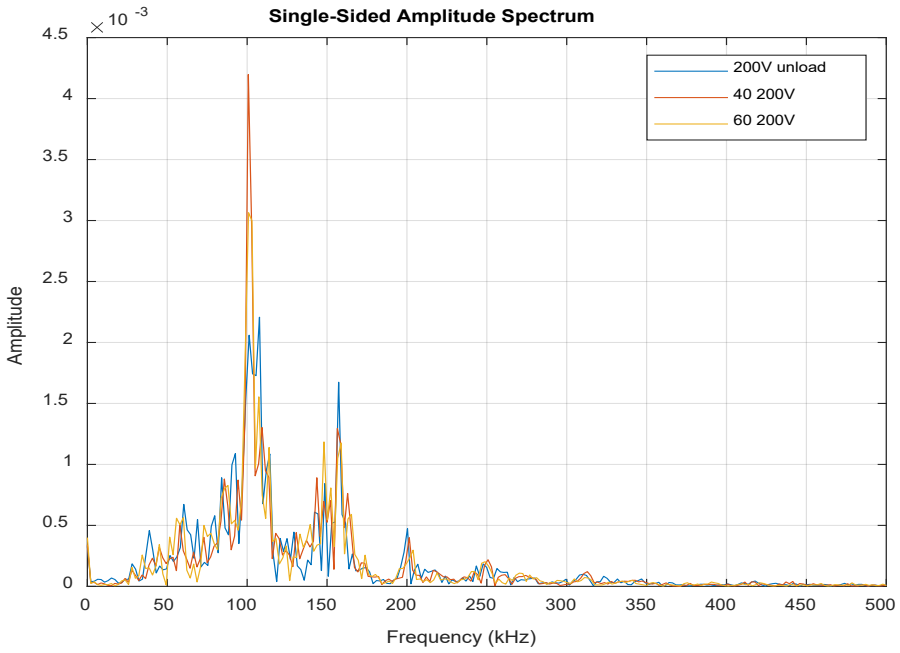

Figure B-17 Specimen 3 200V loaded amplitude vs frequency

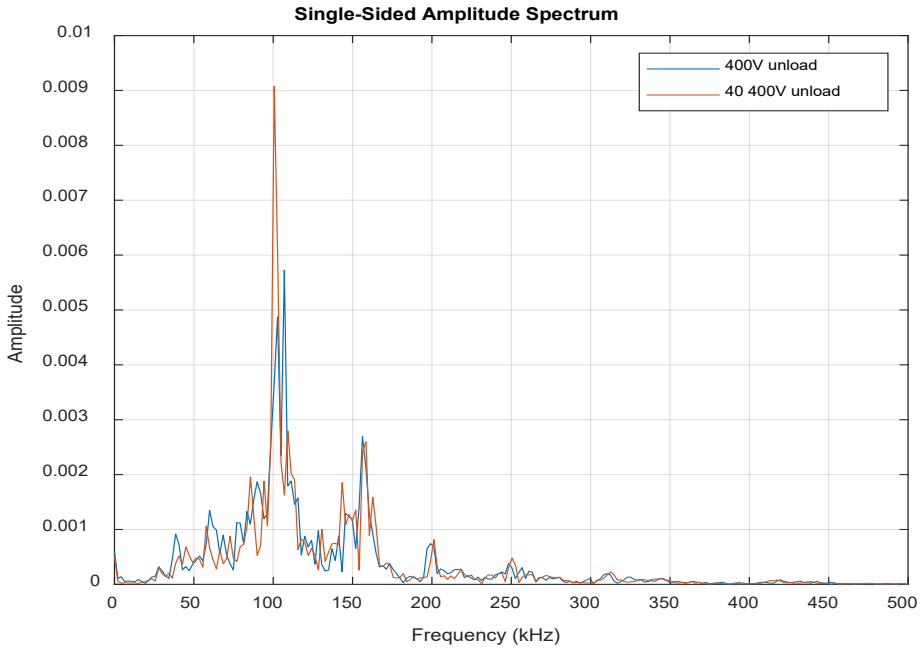

Figure B-18 Specimen 3 400V unloaded amplitude vs frequency

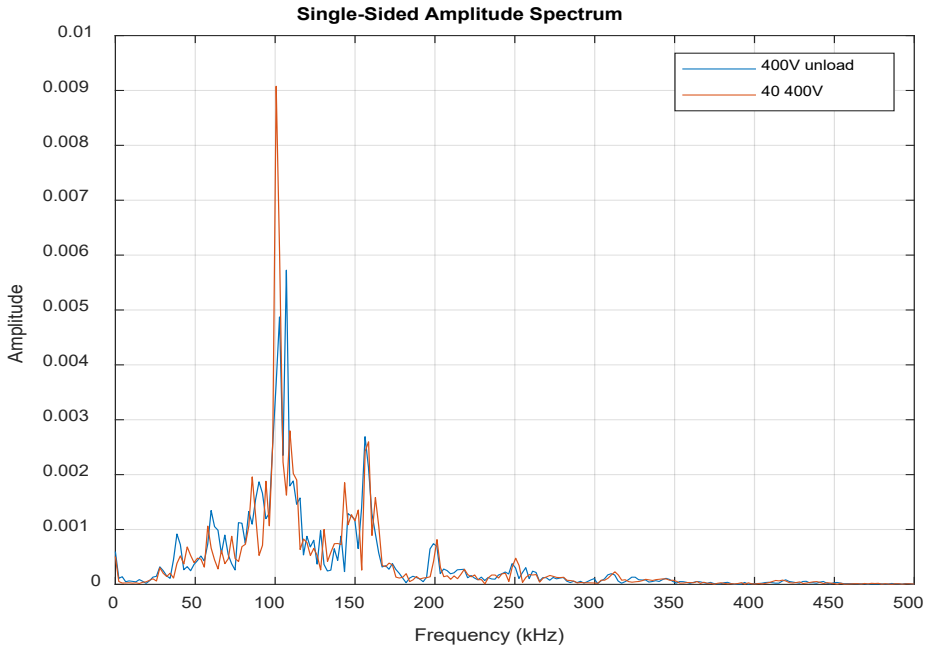

Figure B-19 Specimen 3 400V loaded amplitude vs frequency

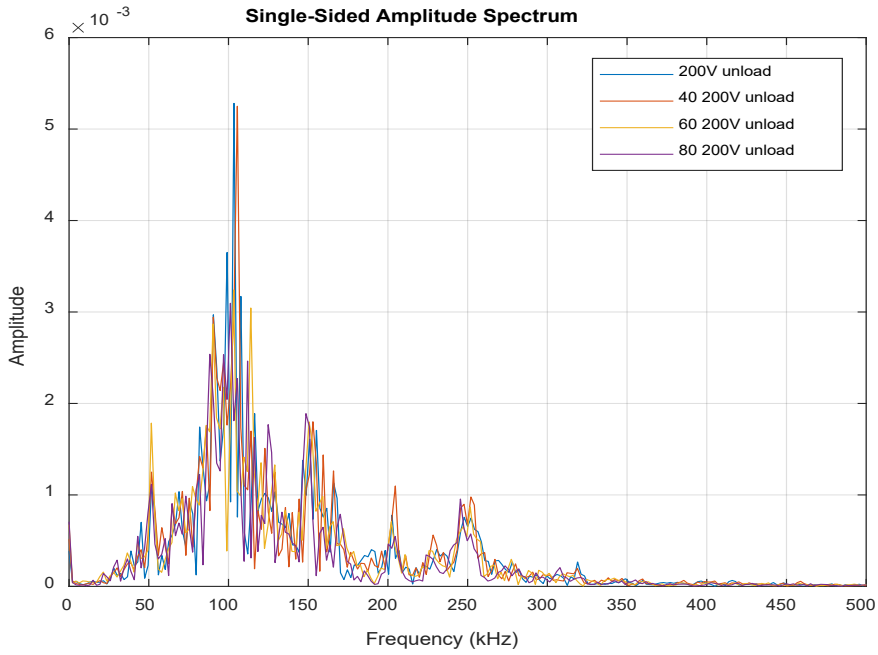

Figure B-20 Specimen 4 200V unloaded amplitude vs frequency

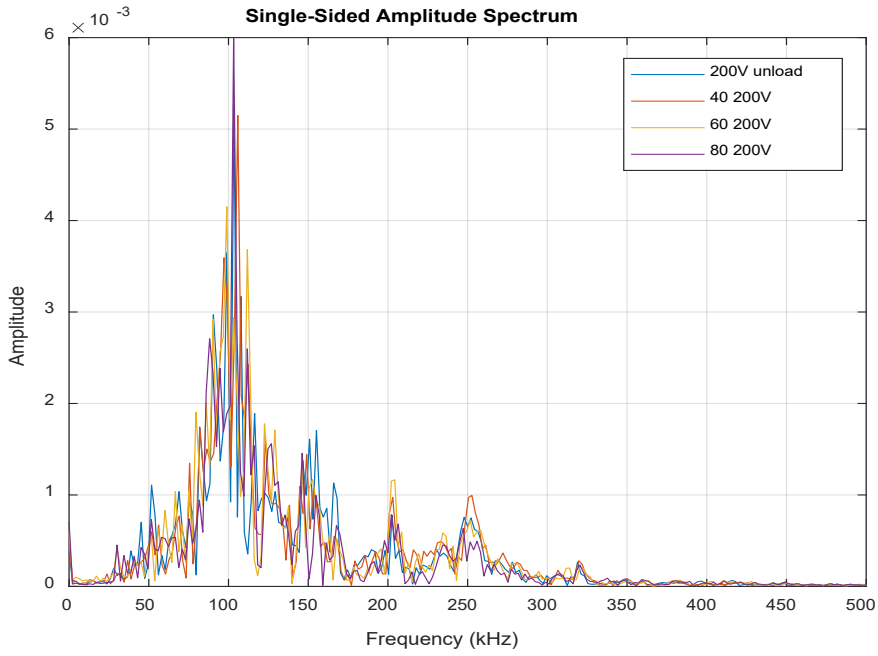

Figure B-21 Specimen 4 200V loaded amplitude vs frequency

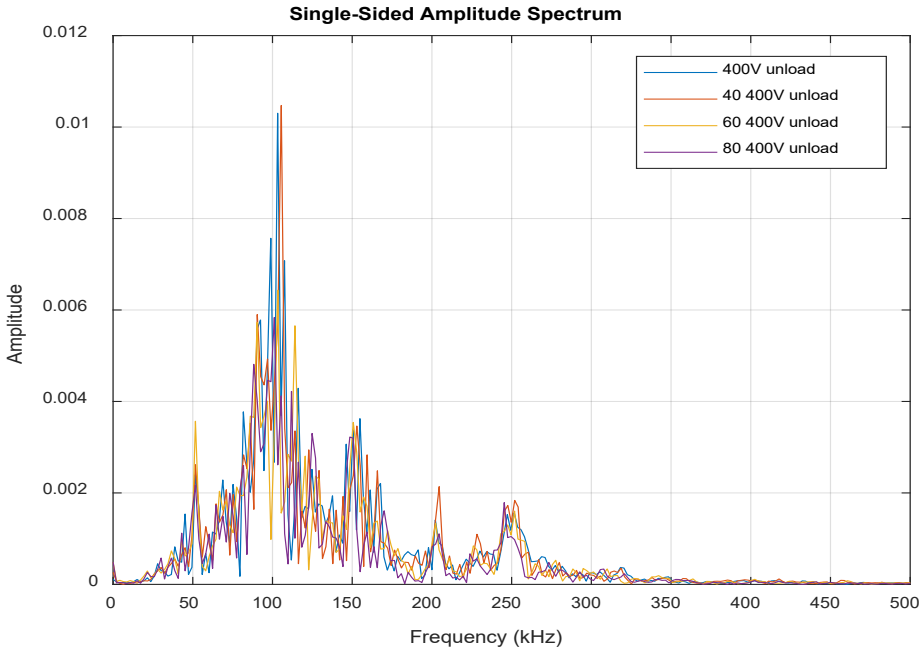

Figure B-22 Specimen 4 400V unloaded amplitude vs frequency

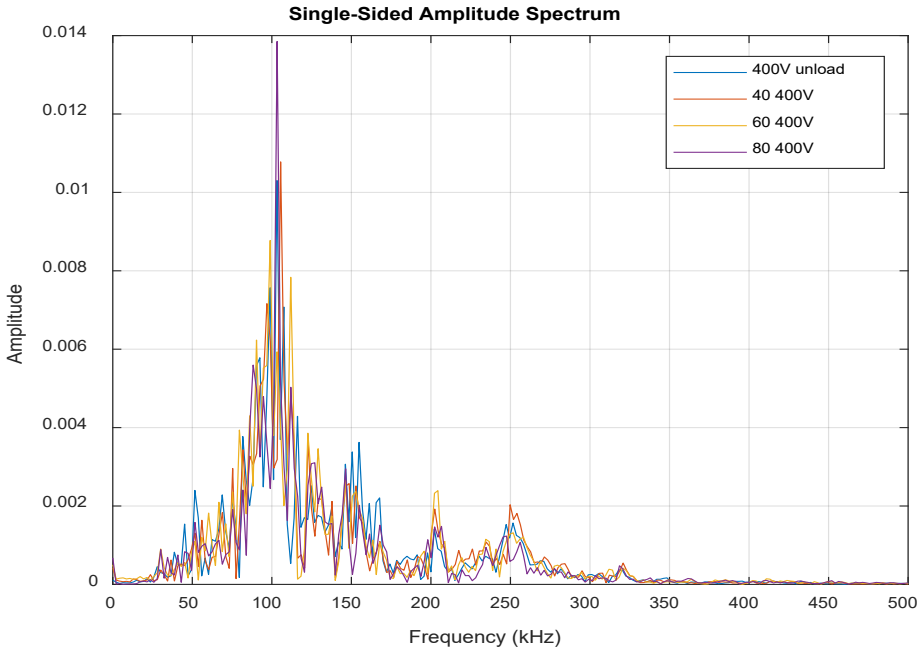

Figure B-23 Specimen 4 400V loaded amplitude vs frequency

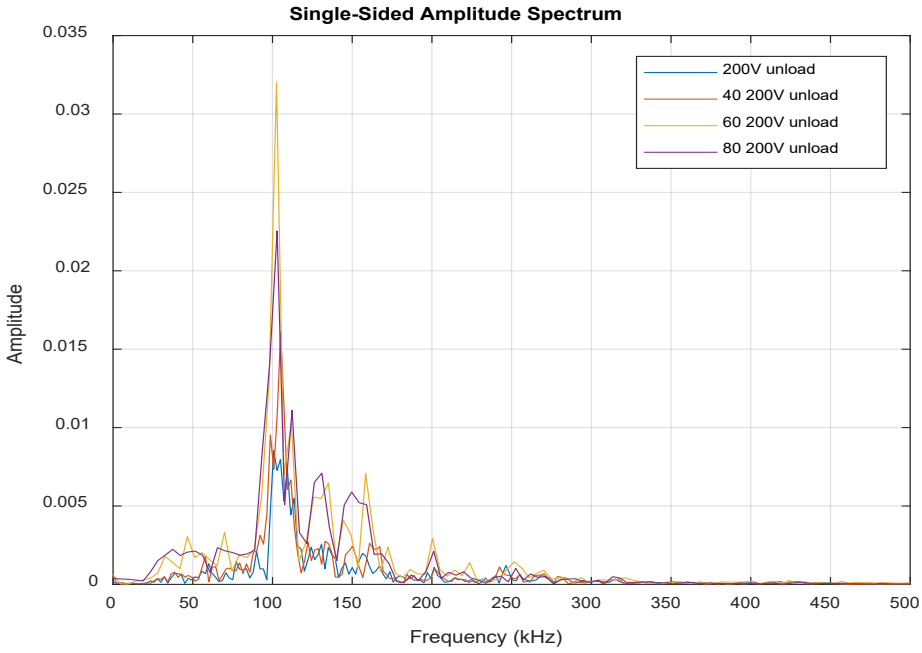

Figure B-24 Specimen 5 200V unloaded amplitude vs frequency

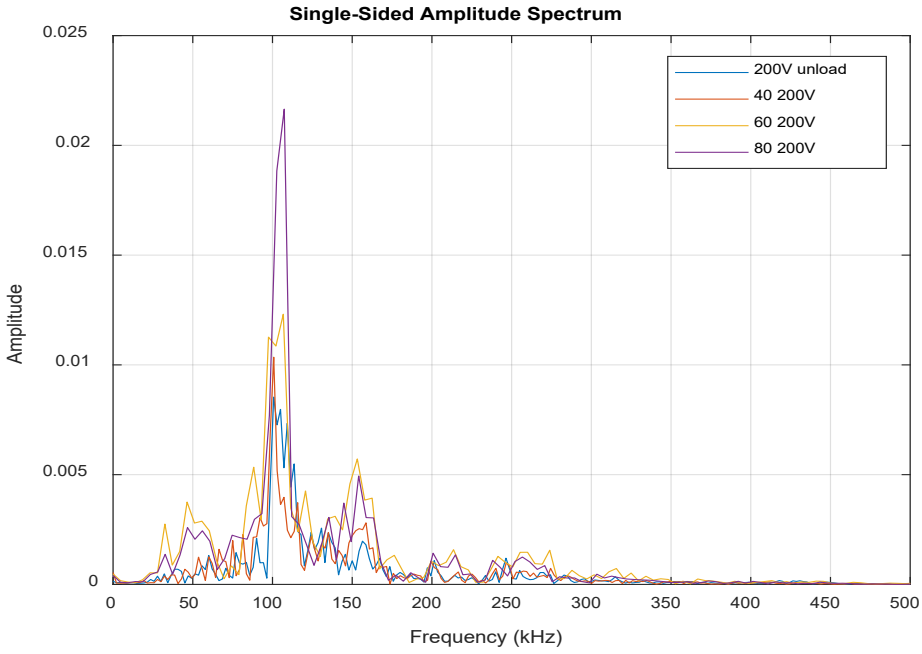

Figure B-25 Specimen 5 200V loaded amplitude vs frequency

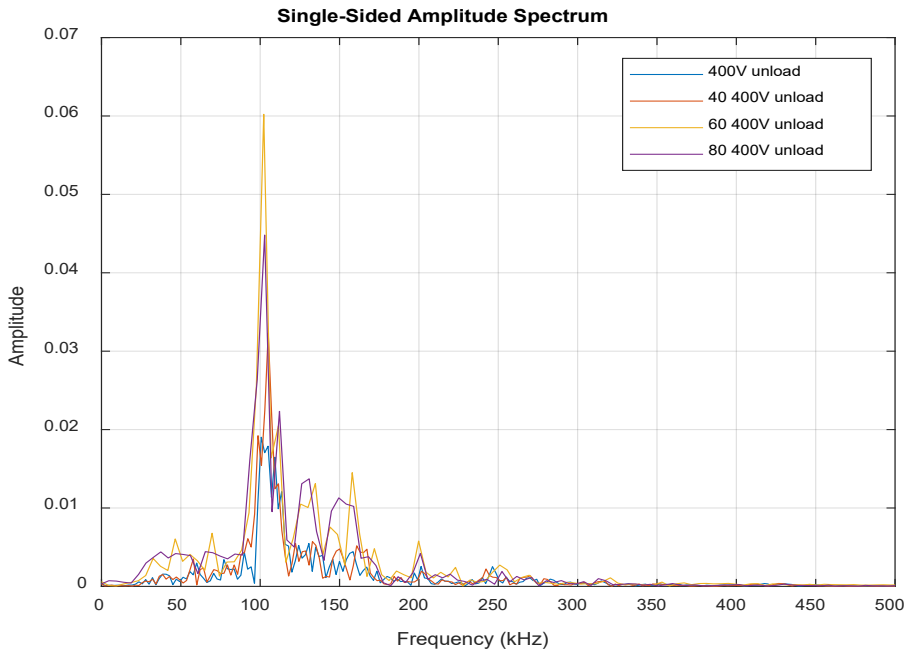

Figure B-26 Specimen 5 400V unloaded amplitude vs frequency

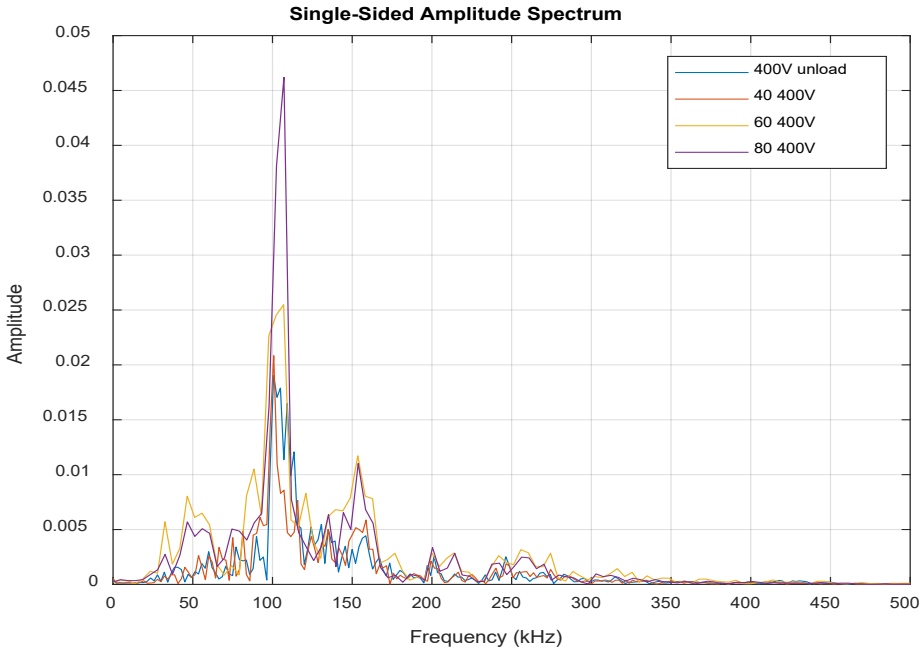

Figure B-27 Specimen 5 400V loaded amplitude vs frequency